ALBERTA INNOVATES

AI PROJECT FINAL REPORT

AI Project Number: 2331

Project Title: Oil-Sands Produced Water Treatment by Electrocoagulation

Project Leader: Dr. Edward P.L. Roberts

Department: Chemical & Petroleum Engineering

Co-Authors: Dr. Milana Trifkovic, Dept. of Chemical & Petroleum Engineering

Dr. Bernhard Mayer, Dept. of Geoscience

Dr. Thomas Oldenburg, Dept. of Geoscience

Institution: University of Calgary

Project Partner: Canadian Natural Resources Ltd.

Report Date: July 24, 2019

ALBERTA INNOVATES

Executive Summary

The project focussed on the treatment of oil-sands produced water by electrocoagulation (EC), to enable increased water recycling while decreasing capital and operating costs. Silica was the key contaminant that was targeted with this technology, but the removal of organics and hardness was also evaluated. The research strategy included a combination of fundamental experimental and modelling studies to investigate the treatment mechanism, bench scale studies of treatment performance under a range of operating conditions, and development and evaluation of novel designs and operating conditions.

EC was found to be effective for the removal of silica from produced water, and silica removal of greater than 95% could be achieved, with a final concentration of a few ppm. The removal performance was found to be a function of the electrical charge passed per unit volume of water treated. EC with Aluminum electrodes (Al-EC) was found to be more effective for silica removal than EC with iron electrodes (Fe-EC). The charge required for 90% silica removal (to meet treatment targets) from produced water was around 800 C/L for Al-EC and 1600 C/L for Fe-EC.

Hardness removal was found to be slower than silica removal. With Al-EC, around 90% calcium removal was achieved after 2500 C/L, and around 50% removal after 1600 C/L. Magnesium was removed more slowly. Around 10-20% organic removal was achieved by EC treatment. Removal of some organics and hardness will reduce the burden on other processes in the treatment train and thus reduce costs. In addition, removal of organics may enhance the silica removal by eliminating complexing effects.

A novel method for mapping pH in-situ during the EC treatment was developed. The results shows that there is a layer of water close to each electrode where the pH is very different from the bulk pH. Acid conditions were observed close to the anode (due to reaction of metal ions with water), and alkaline conditions were observed at the cathode (due to hydroxide production). This pH distribution effects the contaminant removal and electrode fouling processes, since the reactions occurring are pH dependent. The removal performance is not significantly effected, but the morphology of the sludge and the fouling is influenced by the pH distribution.

With both Fe-EC and Al-EC fouling of the electrodes can occur. This can lead to a build up of deposit on the electrode which may affect the operability of the EC process. With Al-EC a hard deposit was formed on the electrodes that was difficult to remove. Also, foaming can occur in the EC system, especially with Al-EC. In Fe-EC system, sulfide passivation of the anode was observed. Periodic polarity reversal was observed to mitigate (but not eliminate) fouling of the electrodes, without effecting treatment performance. Polarity reversal disrupts the pH boundary layer and changes the morphology of the sludge and the deposit on the electrodes. With Al-EC increasing frequency of polarity reversal the particle size of the deposit on the electrodes decreased. This led to a soft layer of fouling (with a reversal period of less than 1 minute) that could easily be removed from the electrode surface. As the frequency increased the particle size of the sludge also decreased, which will affect the solid-liquid separation process. Based on the results, a reversal period of 20s to 1 minute is recommended for Al-EC, to mitigate electrode fouling. With Fe-EC longer reversal frequency of several minutes was found to be suitable.

Other novel operating conditions investigated included electrode oscillation and the use of a magnetic field. With an oscillating anode an enhancement of 20%-30% Si removal in Fe-EC was achieved. For Al-EC system, only the initial stages of EC removal of silica was accelerated by electrode oscillation. The addition of a magnetic field was found to accelerate silica removal at the initial stage of the EC process and assist the reduction of electrode fouling during treatment with Al-EC. The application of a magnetic field to Fe-EC was found to increase fouling and is not recommended. These experiments were performed at very small scale, and further work would be needed to investigate magnetic field effects and to scale up the concept.

ALBERTA INNOVATES

Table of Contents

1. Project Description

The utilisation of water and the disposal of contaminated water is a major challenge for Alberta's oil sands industry. Typically, oil is produced at the surface mixed with water, and the ratio of produced water to oil varies from around 2 to 10 m^3 for each m^3 of oil, with an average ratio of around 3 to 1. In the Alberta's in-situ thermal oil sands operations (e.g., SAGD), produced waters are largely treated using chemical processes such as warm lime softening as produced water is recycled to the steam generators as boiler feed water. The formation of scale in the boilers due to contaminants in the water, including silica and organics, is a significant issue, and around 10-25% of the produced water (boiler blowdown) must be either disposed of or treated and recycled. On average, approximately 27 million m^3 of make-up water per year are currently required for in-situ thermal operations, and the disposal of an associated 16 million m^3 of contaminated water. Although this is an uncertain time for the oil industry, these figures are expected to increase significantly (based on industry forecasts) in the next 10 to 20 years if current practices are not changed. Water is often extracted from and discharged to aquifers with uncertain consequences. It is clear that there is an urgent need to reduce the water intensity of oil production in Canada, driven by environmental concerns and new regulations such as the Athabasca river water management framework.

In order to increase recycle rates and thus reduce water consumption, there is a need to remove contaminants from the produced water (particularly silica, hardness, sulphides and organics) to mitigate boiler scale, which would allow more stable operation with lower blowdown rates. Alternatively, removal of these contaminants from the blowdown could enable increased recycle of the blowdown stream. This project aims to develop new treatment solutions for the removal of contaminants, particularly silica but also organics and some hardness, using electrocoagulation (EC), to enable increased water recycling while decreasing capital and operating costs. Our approach was to investigate the contaminant removal and electrode fouling mechanism during the treatment of SAGD produced water, and use the findings to reduce scale formation while driving innovation in EC design and operation. Novel methods to enhance enhance performance, reduce operating costs, and eliminate operational problems such as electrode fouling were explored. This approach targeted the development of an effective treatment technology for the removal of silica, hardness and organics from the produced water,

with low capital and operating costs. We targeted the EC technology as it is a less chemically intensive operation (in contrast to conventional lime softening) and will enable a significant reduction in make-up water. In summary, the EC technology has the potential to provide a lower cost, high efficiency alternative treatment method for in-situ produced water, which could help unlock the resource in the wake of declining oil prices. However, a much better understanding of the fundamentals of EC relative to in-situ applications is required to make sure appropriate implementation of the technology is employed as failed efforts will result in abandonment of a promising technology.

This project aimed to develop treatment technologies that increase water recycling, reduce treatment costs and sludge production. The amount of make-up water required could be significantly reduced by around 34,000 m^3/day, with >80% reduction in the volume of contaminated water disposed of and 50% reduction in the sludge generated (200 m^3/day). In addition to CNRL, the project will benefit other end-users through technology transfer, dissemination and collaboration.

The savings in water use and reduction in the disposal of contaminated water will help to preserve water resources in Alberta, reducing impact on subsurface water as well as contamination of surface water. The reduction in waste sludge will also reduce the societal impact of contaminated land through reduced disposal in landfill or other facilities. The health impacts of the dispersal of contaminants in the environment, particularly from sludge disposal, will be reduced. These impacts will begin to arise on a 5 to 10 year timescale.

The success of this project will enable Alberta to become a leader in the development and implementation of innovative produced water treatment processes with increased recycle rates, minimal chemical addition, low capital cost and reduced water intensity. This success would lead those involved in conventional and unconventional oil production in the USA and other parts of the world to seek to work with industry, technology developers and researchers in Alberta. It will attract research leaders and technology companies to Alberta and to the University of Calgary. On successful completion of the project, we will work with industry partners to implement a new EC produced water treatment technology developed in Alberta, with demonstrated environmental and economic benefits. We will disseminate this success story through academic, industry and community events, workshops, awards, and social media. This will help to promote community pride among Albertans, by demonstrating the internationally leading research, technology

development at the University of Calgary and its industry collaborators. In addition, finding cost-effective and environmentally sustainable means of treating produced water for recycle will allow regulators to continue to push for more stringent regulations in years to come, furthering Alberta and Canada's place as one of the most responsible global producers of oil and gas.

This project aimed to develop new treatment solutions for the removal of contaminants, particularly silica but also organics and some hardness, using electrocoagulation (EC), to enable increased water recycling while decreasing capital and operating costs. To achieve the overall aims of the project the following research objectives were identified, and each objective had an associated task as follows:

Task A. In-situ visualization of contaminant removal and electrode fouling.

Task B. Bench scale testing of EC treatment, novel cell designs and operating conditions.

Task C. Analysis and modelling of inorganic and organic contaminants in solution, in the flocculated solids and in the electrode fouling layer.

Two other objectives focussing on on-site bench scale and pilot testing were abandoned due to a change in ownership of our industry partner, from Shell Canada to Canadian Natural Resources Ltd. The results obtained, and the key findings for each of the Tasks A, B and C are described in detail in the following sections.

The objective of this task was to directly observe the processes that occur during the electrocoagulation (EC) treatment utilizing spectrophotochemical techniques. During this project, we continue to develop a visualization method of contaminants, i.e. silica and organic bitumen as well as pH variation, based on various techniques of Laser Scanning Confocal Microscopy (LSCM), Raman spectroscopy as well as electrochemical characterisation technologies. The development of the in-situ EC visualisation methodology was challenging especially during the initiation stage of this project; thus, we were behind schedule. Considering a pH mapping within reactor, to the best of our knowledge, there is a very limited research working on this subject, and that this technique has been utilised for the first time to map pH in an EC system. The complexity of the chemistry, the wide range of pH conditions, and the variation of the dye concentration use as florescence detector in the EC cell has made the calibration and the quantification difficult. However, throughout the project, we progressed well that we have developed a unique technique to address these challenges and for the first time quantified the pH distribution in the boundary layer of an EC cell has been monitored.

Methodology and setup of our pH monitoring process has been mentioned in the previous progress reports, briefly, by adding pH sensitive fluorescent dyes, using a ratiometric calibration method and Matlab code to convert fluorescence response of dyes to pH values at each location. Throughout this project, we continued to modify the ratio and the type of sensitive dyes to cover wider range of pH in the EC cell and to monitor the impact of pH on EC performance and the interfacial reaction of electrode/solution phase to understand the formation of fouling layer on the electrodes.

Moreover, to further understand the EC and the fouling process, we had developed a Raman setup to in-situ monitor the fouling layer formation and elimination during treatment using novel EC processes.

Task B. Bench scale testing of EC treatment, novel cell designs and operating conditions

The objective of this task is to develop a bench scale EC system for produced and blow-down water treatment for Canadian oil-sands operations. Progress on this task has been delayed as samples of produced water were not received from Shell / CNRL until April 2017. And also, samples of boiler blowdown water were not received from CNRL until December 2018.

On-going bench scale testing of aluminum EC (Al-EC) and iron EC (Fe-EC) treatment systems for synthetic, real produced water and boiler blowdown treatment indicated that EC was

effective for silica removal. In batch experiments, the silica removal was found to be correlated with the amount of electrical charge passed per liter of water treated, rather than the treatment time or current density. Aluminum electrodes were found to require a lower charge per liter for removal of silica than mild steel. An electrical charge of about 800 C/L was required to remove around 90% of the silica present in the real produced water and about 60% in the real boiler blowdown water using a conventional Al-EC. Whereas for an Fe-EC system only 30% and 18% of the silica was removed from the same respective waters after passing 800 C/L. With a conventional Fe-EC, around 1600 C/L was required to remove 90% of the silica from produced water and never reach the 40% removal from boiler blowdown water when the charge loading reach 5000C/L. Using our innovative cell design of anode oscillation and polarity reversal, this value significantly increased to reach >90% with Fe-EC when the charge loading was 5000C/L. Using the same innovative approaches with Al-EC, significantly speedup the removal process of silica from both produced water and boiler blowdown water. In addition, the use of our innovative approaches of anode oscillation, polarity reversal and the application of magnetic field reduce the fouling layer formation on aluminum electrodes which is beneficial in enabling long run times without plugging, and increased efficiency.

Considering the other inorganic such as calcium was removed more slowly than silica, with around 60 % removal achieved after 1600 C/L from produced water. Magnesium, however, was only partially removed, remaining at about 45-75% of the initial concentration after 2500 C/L of treatment. The removal performance was enhanced for Fe-EC by bubbling air in the reactor due to oxidation of ferrous to ferric ions, however, the foaming was problematic during real produced water treatment. Although aluminum is more expensive than iron, a preliminary economic analysis (study is not included in this report) indicates that the operating cost of Al-EC (including electrode replacement and energy costs) is less cost than that for Fe-EC.

Electrode fouling was also studied, using both the actual EC setup and a small EC reactor to monitor the accumulated materials on the electrode surface following EC treatment (see Task C).

Various innovative approaches to improve EC efficiency were made through; 1) electrode oscillation, 2) applying alternating current, 3) application of magnetic field, or combinations of these systems. The principle of these approaches are either to agitate the solution at the electrode interface or to change the alternatively change the chemistry at the electrode interface so that the

chemical reaction responsible for fouling formation will alter. Brief introductions about the methodology behind the innovative approaches are explained in this report. In general, using an oscillating anode in EC shows a good enhancement in the removal performance. Results shown that with an oscillating anode a total enhancement of about 20%-30% Si removal in Fe-EC was achieved. Whereas, using oscillated Al-EC system, accelerate the initial stages of EC removal of silica.

The impact of magnetic field is to accelerate silica removal at the initial stage of the EC process and assist the reduction of electrode fouling during treatment with Al electrode. We have also provided samples from our experiments with novel EC designs for analysis in Task C, that to investigating the viability of EC to remove organics, which are considered as the cause of fouling in equipment. The range of total organic carbon (TOC) removal using the EC process is about 10-20%. Removal of organics is not an critical target of the treatment process; however removal of organics may enhance the silica removal by eliminating complexing effects. Also, we are experiencing foaming in the EC system, especially with Al-EC. In Fe-EC system, sulfide passivation of the anode was observed.

Task C. Analysis and modelling of inorganic and organic contaminants in solution, in the flocculated solids and in the electrode fouling layer.

The objective of this task is to identify the major and the minor trace inorganic, silica and selected trace elements, as well as a comprehensive analysis of the organics in the produced water and the treated products.

Our preliminarily finding indicates that the produced water as well as blowdown collected from boiler samples from the Peace River Facility is strongly enriched by sulfur containing organic species. Preliminary results also indicate that electro-coagulation treatment contributes to the removal of organic compounds from produced water.

Analysis of produced water sample shows that more than half of all detected compound classes contain at least one sulfur atom per molecule measured either in ESI-N or APPI-P ion mode. The boiler blowdown water is enriched in multi-oxygenated species and is about four times as concentrated than the produced water sample. The boiler blowdown water comprises of higher concentration of higher DBE and higher carbon number containing compounds relative to the produced water sample.

Analysis of the precipitated particles (sludge following treatment) at the bottom of the organic extracts of the electro-coagulation treated produced waters were analyzed for their cationic and anionic composition. The analysis showed that they comprised primarily of sodium sulfate salt, which was getting introduced in the sample due to an experimental step. The experimental protocol for organic analysis was then modified to remove the addition of the salt to the extract. The ion chromatography (IC) and inductively coupled plasma (ICP) of the precipitated particles also showed a high percentage of boron species. Further work is needed to understand this precipitation.

Overall, the electrocoagulation with iron electrodes showed a higher percentage removal of organics from the produced water relative to the aluminum electrode when compared without any of the novel treatment methods.

Within the use of novel techniques for electrocoagulation treatment, the application of magnetic field was shown to increase the removal of few of the organic compound class groups present in the produced water. The use of oscillating electrodes showed no, minor or even hindering effects when used in addition to other novel EC techniques for the removal of organics from produced water. The use of AC current was found to increase the removal of few of the organic compound class groups present in the produced water compared to the DC current, likely caused due to the improved treatment efficiency by reducing fouling.

Over the course of the electrocoagulation, sludge was deposited at the bottom of the electrodes. The sludge was observed to be composed of oil-like organics with high concentration of hydrocarbons and sulfur containing compounds. The sludge comprised of higher carbon number containing organics relative to the produced water.

In addition to the sludge, foam was observed to be formed following treatment with aluminum electrodes. The composition of the organics present in the foam was found to be similar to the treated produced water with the aluminum electrodes, indicating that there is no separation of organic contaminants in the foam.

The analysis of boiler blowdown water treated with electrocoagulation was very challenging due to high inorganic ions in the water interfering with the organic when analyzed in different ion modes using FTICR-MS technology due to ion suppression and clustering effects. However, some overall compositional changes on compound class level were observed to differentiate between iron and aluminum electrodes as well as direct versus alternating current use.

The process or possible reaction systems behind the removal of organics during water treatment with electrocoagulation are not well understood. It could be a side effect of silica removal due to sorption effects of the organics on the silica or the organics themselves are reacting at the electrodes.

In-situ Raman spectroscopy investigation on the fouling products (Task B) was performed, and the results indicated the formation of polysulfur (S_8), polysulfide (S_2^-) and metal sulfide fouling layers on the anode.

Computer modeling of data collected from EC process of real effluent indicate that the causes of the current flow is due to OH^- transport in the cell with Na^+ contributing the least to the current. The reduction of H_4SiO_4 concentration during EC is in a non-identifiable manner with increases in Chrysotile [$Mg_3Si_2O_5(OH)_4$] due to the increase in Mg^{2+} concentration with time.

The pH at the negative and positive electrode surfaces has been successfully modelled in detail. At the positive electrode, the pH decreases with time due to the hydrolysis of $Al(H_2O)_6^{3+}$ to $Al(H_2O)_3(OH)_3$ and H^+. At the negative electrode the reduction of water to $H_{2(gas)}$ and OH^- results in an increase in the pH.

Al^{3+} and Fe^{2+} are generated in narrow bands adjacent to the positive electrode. Diffusion and advection do not disperse these cations within the electrocoagulation cell. However reactions may occur downwind of the electrocoagulation system.

Calcium and magnesium silicates have a high potential of formation in the region around the negative electrode due to the production of OH^- and due to a high concentration of Ca^{2+} and Mg^{2+} in the effluent.

Calcium and magnesium aluminosilicates have a high potential of formation around the positive electrode due to the production of Al^{3+}.The presence of Al^{3+} increases the number of minerals that can form. Whereas, iron silicates and iron calcium magnesium silicates have a high potential of formation around the positive electrode.

The aluminum electrode gives the largest number of potential minerals when compared to the iron electrode.

2. APPROACH AND RESULTS

2.1 TASK A. In-Situ EC Visualisation of contaminant removal and electrode fouling.

Milestone A.1: Developed methodology for visualization of contaminant removal, formation of fouling and pH distributions.

Milestone A. 2: Visualization data with natural convection and flow conditions

Milestone A.3: Visualization data ~~for real samples~~ with novel electrode geometries and operating conditions.

Milestone A.4: Image post-processing and quantification to determine effectiveness of proposed electrode geometries and operating conditions

Objective:

The objective of these milestones is to develop a method to directly observe the processes occur during the EC treatment. This investigation is important to understand the mechanisms of pollutant removal during EC treatment. Particularly, the produced water as well as blowdown effluents containing complex unknown organic of bitumen molecules along with various inorganic contaminant that reacting simultaneously within the EC cell. Hence, the resulting products from EC treatment would be expected to be a mixture of coagulates and electrochemically reacted byproducts with unknown structures that are varied dynamically during the process of treatment, e.g. colloid reactions at non-ideal thermodynamics, and multi-phase flow phenomena. In literature, there is a lack of information or reports on capturing these types of dynamic interactions. Simulating the electrocoagulation procedure in this work for in-situ monitoring the electrode and electrolyte processes can reveal dynamic and kinetic information that may help overcome the limitations and enhance the performance during EC treatment of oil-sands produced water. During this project, we have identified some limiting factors encountered during the EC treatment of oil-sands effluents, include electrode fouling and mass transport effects. The findings reported here to investigate the process for better approaches in our novel developed EC treatment.

Method and Achievements for millstone A.1, A.2, A.3 and A.4

Note:

1- The four milestones are considered together.

2- true time video imaging of the pH mapping during theisprocess are available, however, for size meter these can be provided in separate documents.

Aa laser scanning confocal microscopy system (LSCM) was used for visualization of contaminant removal in an EC cell and for mapping of the pH distribution. Figure [1] shows images of two electrocoagulation cells that are used in this work; a) side view, and b) face view, along with an image of both the EC cell and the objective lens attached to the LSCM system via a periscope arm. The cell volume was reduced to 25 ml compared with the previous 170 mL EC visualization cell. The cells were designed using CAD software and 3D-printed using polycarbonate polymer (PCP) filaments. This PCP material was chosen based on it little noticeable interaction with organics and fluorophores. The three-electrode EC cell was designed with a transparent side covered by a 170 μm thickness borosilicate glass window of 24×60 mm (from Fisher Scientific). This window was facing the electrode to enable visualisation of the electrode surface using the confocal's microscope objective. Identical working and counter electrodes with an effective surface area of 2 cm^2 of either low carbon steel (ASTM A109) or aluminium (grade 1100, McMaster-Carr Inc., Atlanta, GA) were used. The potential of the working electrode was measured relative to an Ag/AgCl reference electrode. The gap between working and counter electrodes was fixed at 2 cm. Electrochemical measurements were performed using a PARSTAT 3000 (Princeton Applied Research, Oak Ridge, TN, USA) potentiostat and VersaStudio software.

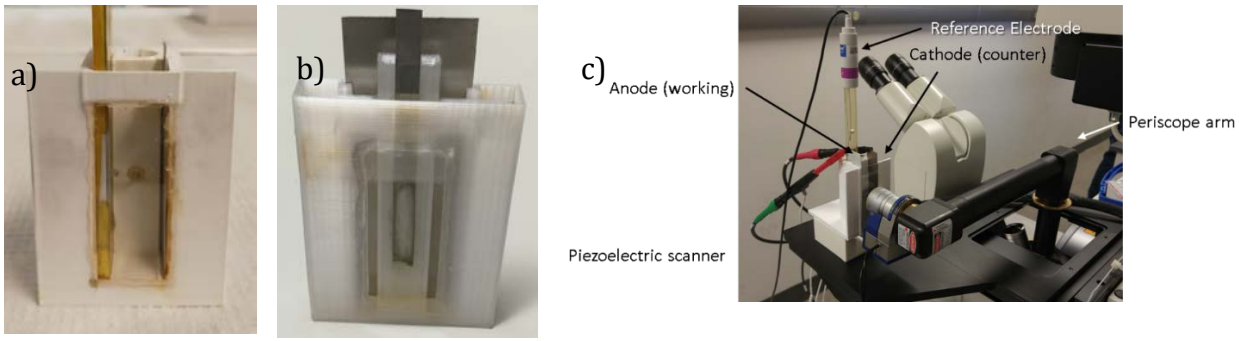

Figure [1]. Photographs of the electrochemical cells: a) side view and b) face view, c) the EC cell and the objective lens used for LSCM imaging.

Images were obtained using a dry objective (HC PL APO CS2 10x/0.40 dry) attached to a piezo scanner and periscope arm. Leica TCS SP8 X (Leica Microsystems, Germany) inverted confocal laser scanning microscope was equipped with a pulsed white light laser source capable of emitting 8 different visible lights in the range of 470-670 nm at 80 MHz. Furthermore, the microscope is

equipped with an acousto-optical beam splitter (AOBS), 12 kHz resonant scanner, three hybrids (Leica HyD™) detector and two photomultiplier tube (PMT) detectors.

We have newly upgraded the LSCM (Leica TCS SP8 X) to excite beam at multiple wavelengths (range 470-670 nm) and simultaneously detect emission at multiple wavelengths (range 400-800 nm). Using the newly upgraded LSCM allow us to use only one single dye as indicator (not mixture), excite at multiple wavelength and detect emission from this dye at multiple wavelength. In this way we can eliminate error related to dye mixture when several dyes are used. However, since one single dye cannot cover a wide range of pH, we use one dye to visualise acidic range and other for basic range. These are, Lysosensor™ Green DND-189 (LSG) was used to visualise the electrolyte at acidic pH range, whereas, 5(6)-Carboxynaphtho fluorescein was used to visualise the basic range. Hence, to evaluate the response of fluorescent probes over a wide range of pH, we measured the intensity of emitted beams at different combination of excitation wavelength and emission bands.

Outcome of the in-Situ EC Visualisation

Figure [2] shows the following: a) the chemical structure of LSG, b) normalized fluorescence intensity of 1 μM LSG in phosphate buffer in range of pH 4.0 to pH 7, c) normalized fluorescence intensity of LSG in phosphate buffer in the range of pH 0.9 to pH 4.0, d) normalized fluorescence intensity of LSG (excited at 470 nm and emission recorded at 500 nm) in different buffer and produced water solutions, e) ratiometric calibration for LSG using 560 and 535 nm emissions (excitation at 470 nm), f) ratiometric calibration for 10 μM CNF in produced water, excitation at 488 nm and emission ratio of 667 nm and 567 nm. Tuning the combination of excitation and emission bands will show variation in band intensities that can be utilised in our experiment to verify the electrolyte pH. For example, the fluorescence intensity at 500 nm reached a maximum at about pH 4 when the probe was excited with 470 nm laser, whereas, the intensity of the emitted light at 560 nm peaked at pH 0.9 using both excitation wavelengths of 470nm and 514nm.

In this task, we have been focusing on obtaining a ratiometric calibration to use this fluorophore in the acidic pH range. Figure [3] shows the calculated ratios of the intensity at two dye concentration of 1 μM and 2 μM of: a) the detected fluorescent light at wavelengths of 508 nm and 572 nm from excitation at 470nm, and b) emitted light detected at a wavelength of 572 nm with excitation at 470 nm and 514 nm.

Thus, by normalizing the responses of Lysosensor, two ratios can be used for ratiometric calibration. Ratio L1 is the ratio of emission intensity at 560 nm with excitation at 514 nm, and emission intensity at 500 nm for excitation at 470 nm. This ratio is sensitive to pH for pH < 4. Ratio L2 is the ratio of emission at 500 nm when the probe is excited at a wavelength 470 nm.

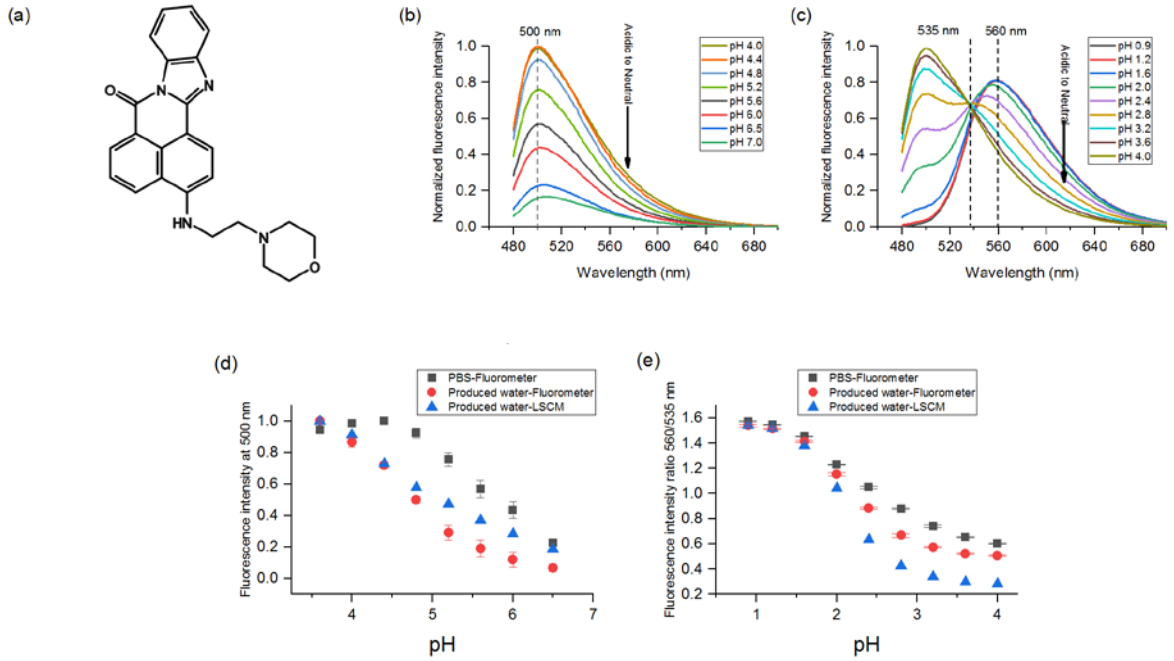

Figure [2]: a) Structure of LSG, b) normalized fluorescence intensity of 1 µM LSG in phosphate buffer in range of pH 4.0 to pH 7, c) normalized fluorescence intensity of LSG in phosphate buffer in range of pH 0.9 to pH 4.0, d) normalized fluorescence intensity of LSG (excited at 470 nm and emission recorded at 500 nm) in buffer and produced water solution, e) ratiometric calibration for LSG using 560 and 535 nm emissions (excitation at 470 nm.

To monitor pH in basic conditions, dye indicator 5(6)-Carboxynaphtho fluorescein (CNF) was found to give a good response. Figure [4] shows the ratiometric calibration for 10 µM CNF in produced water, excitation at 488 nm and emission ratio of 667 nm and 567 nm. This dye indicator was preferred over Carboxynaphtho fluorescein as it has better response in neutral pH and the absorption and emission spectra show shifts in the range of pH from 5 to pH 9.

Varying the combination of excitation and emission bands indicates that the intensity band can be utilised in our experiment to verify the change in pH at the electrode/electrolyte interfaces. It is clear in Figures [2 & 3] that the intensities of emission are completely changed by only varying the pH of the solution. The calibrations obtained at two different dye concentrations are almost

identical. This confirms that the ratio is not dependent on the concentration of dye and can be used in the subsequent experiments for pH monitoring in electrolyte. These results indicate that CNF dye can be used to monitor the pH of electrolyte from pH 5 to 9.

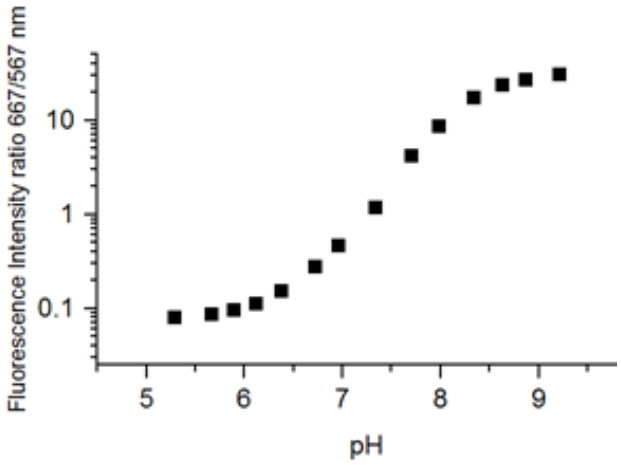

Figure [3]: Ratiometric calibration for 10 μM CNF in produced water, excitation at 488 nm and emission ratio of 667 nm and 567 nm.

The aforementioned calibrations were utilized in our experiments to map the pH in the electrolyte close to the anode (acidic) and cathodic (basic) in the EC reactor. Figures [??-??] show images of pH mapping obtained at the anode and cathode boundary layers at different time interviles of 0, 5, 10, 15, 30, and 60s obtained using LSCM images acquired near electrodes interface from the side view after applying current density of 2mA/cm^2. The evolution of pH boundary layer are presented at both electrodes. As expected, the boundary layer becomes more acidic and more basic at the anode and cathode, respectively.

We also monitored the evolution of interfacial pH using different current densities ranged from 0.5 to 16 mA/cm^2. Figure [4] represents the pH map images for the galvanostatic EC at anode and cathode interfaces after applying different current densities (0.5 to 16 mA/cm^2). As depicted in Figure [4], the boundary pH layer was strongly influenced by the applied current density. Furthermore, gas evolution was also observed with an increased rate upon increasing the applied current density. No gas evolution was observed at anode interface at the very low current densities (< 1 mA/cm^2) indicating that the change in electrolyte pH under these conditions was diffusion driven. However, gas evolution became predominant after applying a current with a density of ≥

2 mA/cm^2 and the thickness of the boundary pH layer was decreased at both anode and cathode interface.

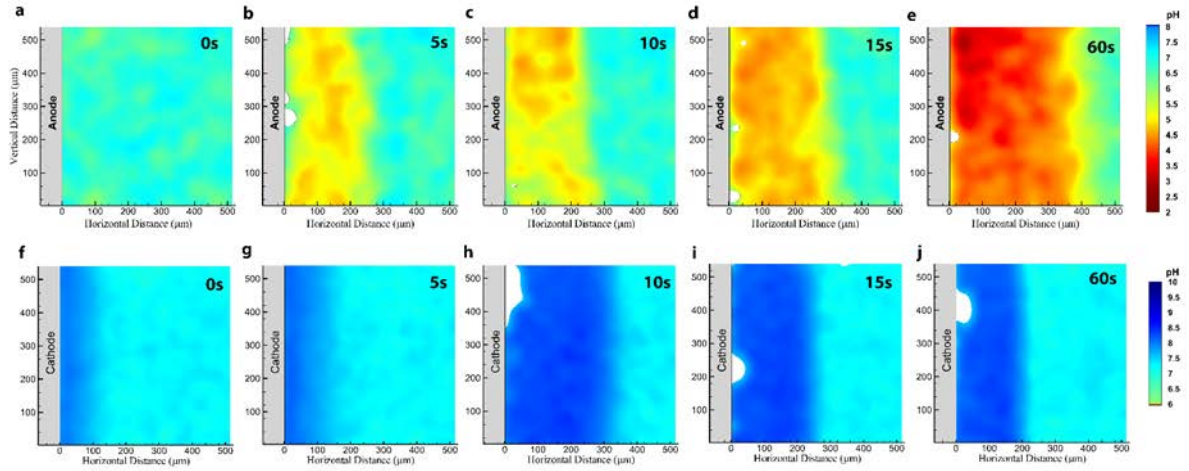

Figure [4]. a) pH map images of anode interface of vertical electrode acquired after 0 seconds, b) 5 seconds, c) 10 seconds, d) 15 seconds and e) 60 seconds after applying current density of 2 mA.cm^{-2}, f) pH mapping images of cathode interface acquired after 0 seconds, g) 5 seconds, h) 10 seconds , i) 15 seconds and j) 60 seconds after applying current density of 2 mA.cm^{-2}. The initial pH was 7.00±0.05 in all experiments. The electrode surfaces were shown as gray areas and the white regions are gas phases. Each frame represents 580 µm across.

The gas evolution at the cathode side is considered to be a function of the applied current. However, the gas evolved at the anode side is commonly hypothesized to be oxygen attributed to a side reaction at large overpotentials, where a small portion of current is consumed to produce gas bubbles. Even the small rate of gas evolution, at the anode side, can alter the interfacial pH value and concentration of cations and protons in the boundary layer. This in turn can influence the dissolution and speciation of the aluminum cations produced.

The pH maps shown in Figure [5] illustrate that pH at the anode-solution interface is higher than that observed in the layers further away. This result indicats that the gas evolving at the anode was likely not oxygen. To gain deeper insights, we complement these findings with an online gas chromatography (GC) characterization and the measurement of anode potential at all applied current densities. A preliminary GC characterization of the evolved gas from the anodic side indicate the formation of hydrogen; not oxygen. This result is in agreement with the literature

{Wang, 2009 #50}, hence we can propose that the protons produced form metal hydrolysis could be converted to hydrogen gas as in the following reaction:

$$6H^+ + 2Al \rightarrow 3H_{2(g)} + 2Al^{3+} \qquad (4)$$

Such anodic polarization could initiate the aluminium dissolution followed by aluminium cations hydrolysis while the protons produced from the hydrolysis reaction can be converted to hydrogen gas.

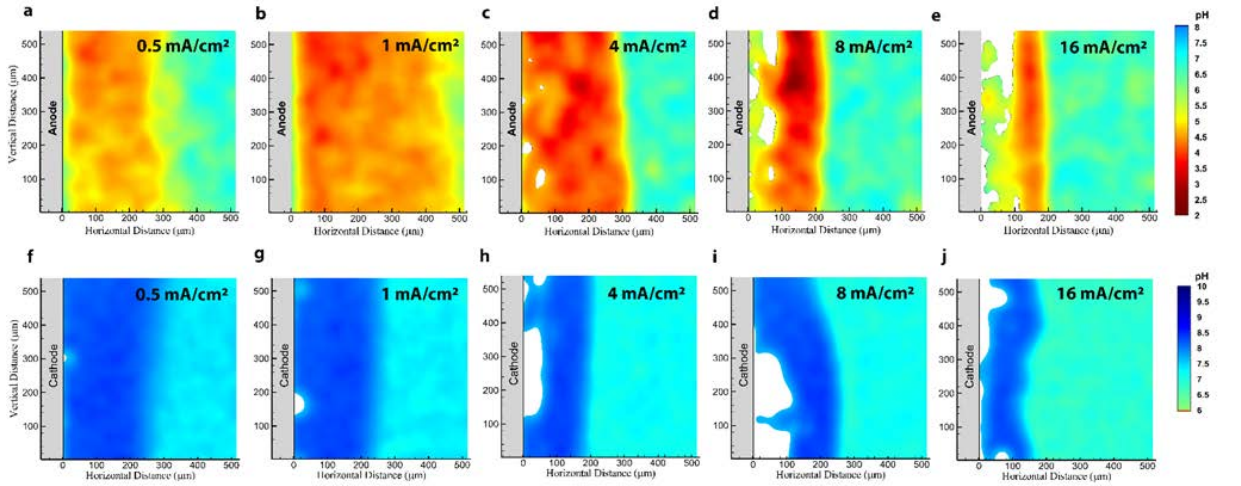

Figure [5]. a) pH mapping of anode interface acquired after applying 0.5 mA/cm^2, b) 1 mA/cm^2, c) 4 mA/cm^2 and d) 8 mA/cm^2, e) 16 mA/cm^2, f) pH mapping of cathode interface acquired after 0.5 mA/cm^2, g) 1 mA/cm^2, h) 4 mA/cm^2, i) 8 mA/cm^2 and j) 16 mA/cm^2. Each frame represents 580 µm across. The initial pH was 7.00±0.05.

Visualization data for real samples with natural convection and flow conditions:

Although our preliminary results from EC treatment of real produced water samples show a positive indication of silica remediation (See Task B), the visualization of the same samples using LSCM was challenging. In the LSCM visualization process, we used dye indicators (LSG for acidic conditions and CNF for alkaline conditions) that change in fluorescence behavior with pH. However, it was found that the real produced water samples provided from the CNRL production site at Peace River indicate the presence of naturally fluorescent species. This fluorescence nature may be due to organic molecules that are present in the produced water. The presence of these fluorescent compounds in samples interfere with the dye indicators (LSG for acidic conditions and CNF for alkaline conditions) that are used to monitor the change in

conditions within the EC cell. This interference prevented us from quantifying the variation of pH within the EC cell using the aforementioned sensitive dyes in the LSCM technique. On the other hand, using pyranine (1µM) as a pH-sensitive dye, found to have less interference with the real produced water when monitored using LSCM at a pH range of 5.5 – 8.5. This pH range was lower than the one showing with the mixed synthetic days of LSG and CNF (1.5 - 6.5 and 6.0 – 9.0). Using 1µM pyranine in a real produced water as electrolyte and varying the combination of excitation and emission bands indicates that the intensity band can be utilized in our experiment to verify the change in pH at the electrode/electrolyte interfaces. For example, Figure [6] shows that the change in the intensities of the emission bands (at 500nm) from both the real produced water and the synthetic produced water at different pH (5.5-8.5) are completely different when the excitation changed from 405 nm to 470nm. Rateometric investigation between the intensities of the emitted band at different excitation (405/470 nm) and pH showed nearly linear trends for both produced and synthetic waters (Figure 6). These linear trends are used as calibrations curves during the pH mapping of the electrode interfaces. It is clear that real produced water and synthetic produced water show almost identical linear calibration curves. This result confirms that the ratio is not dependent on the fluorescent materials presented in the real produced water and that the amount of pyranine dye (1µM) can be used in the subsequent experiments for pH monitoring [see Appendix for an in-situ recorded video]. Also, the results indicate that pyranine dye can be used to monitor the pH of synthetic produced water in the range 5.5 to 8.5 and of the real produced water only in the pH range of 6.0 - 8.0.

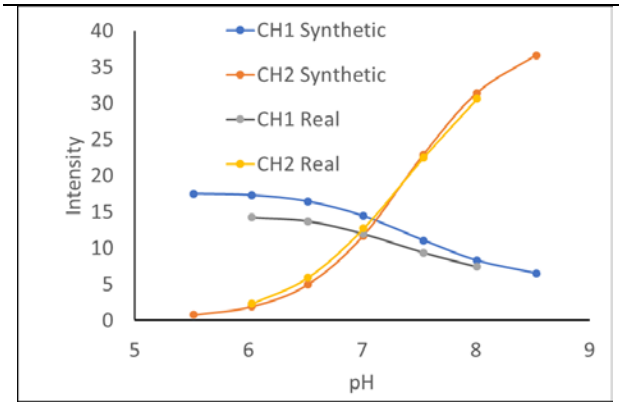

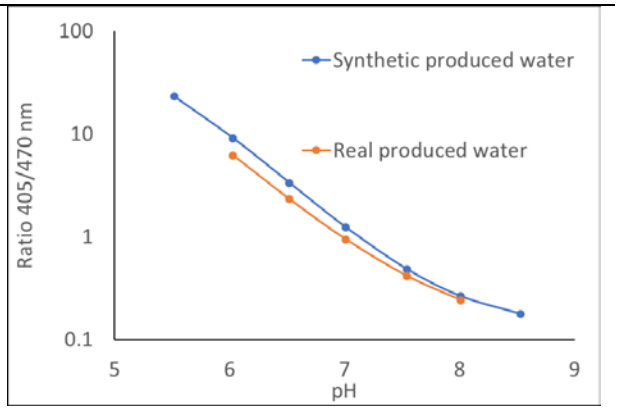

Figure [6]: a) the change in the intensities of the emission bands (at 500nm) from both the real produced water and the synthetic produced water at different pH (5.5-8.5). b) the ratiometric calibration for 1 µM pyranine in real and synthetic produced water. CH1: the excitation at 405 nm CH2: the excitation at 470nm.

Visualization of real produced water during EC treatment

Polarity reversal

The aforementioned calibrations were utilized in our experiments to monitor the pH changes at a constant distance of 60 µm from the electrode. This distance was chosen based on results obtained in the earlier investigation of hydrogen production at an aluminum anode. This distance shows the highest variation in pH at the electrode/electrolyte interface, which expects to be in relation to the hydrogen production reaction at Al anode. Figure [7] shows four different pH variation graphs at an Al electrode/solution interface obtained at various polarity reversal periods of 5, 10, 20 and 30sec using real produced water and applying a current density of 8mA/cm^2.

As part of our investigation to eliminate the formation of fouling layer on anode, a periodic polarity reversal technique was investigated during EC treatment. This study was performed in an attempt to periodically change the chemistry of the electrode/electrolyte interface; hence, eliminating the accumulation of species on the electrode. The implementation of this technique to remediate produced water and blowdown effluents is explained in task B of this report. However, the impact of polarity reversal on the boundary layer thickens was evaluated in this section for both the synthetic and real produced water samples.

Results obtained from using synthetic produced water showed similar results, thus, in this section, we are only presenting results obtained from real produced water. Similar to results obtained from

the mixed LSG and CNF, the pH profile at anode obtained using Pyrinine dye decreased rapidly in all of the experiments (ranged 6.7 - 7.31), however, by reversing the polarity the pH is suddenly increased to a similar value of about 8.0 in all experiments. Reversing the polarity again, the results surprisingly show that the pH will only return to the initial value (ranged 6.7 - 7.31) of the first polarity cycle when the PR is 30 sec or more [see Appendix for an in-situ recorded video]. These results indicate that reversing the polarity of the electrodes will require a certain period for the pH at the interface to restore the same pH conditions. Meaning the amplitude of the pH pulsation will depend on the period of the polarity reversal. Thus, monitoring the period of the polarisation can control the variation of pH at the electrode interface (buffering).

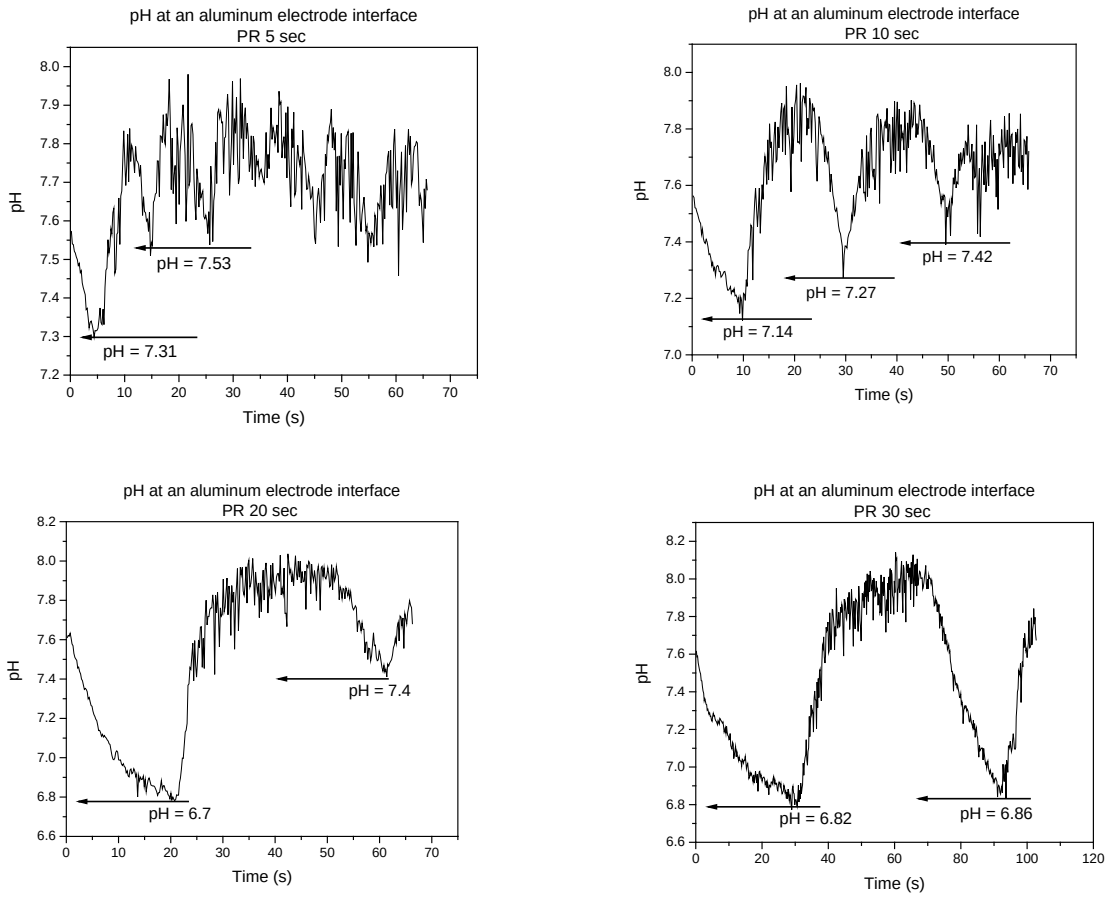

Figure [**7**]: show four different pH variation graphs at an Al electrode/solution interface obtained at various polarity reversal periods of 5, 10, 20 and 30sec. The applied current density is 8mA/cm^2.

Using mild steel electrodes with Pyrinine dye to monitor the change in pH at the interface show similar behaviors with aluminum electrodes (Figure [8]). However, reversing the polarity at a low

PR period of 5sec indicates no changes in the pH that is after the first polarity reversal cycle, with that the pH after 20sec is almost constant at about 8.1. This buffering phenomenon changed to a pH pulsation phenomenon by increasing the PR period. This is similar to an aluminum electrode, the amplitude of the pH pulsation will depend on the period of the polarity reversal. However, careful control of the mild steel electrode with PR, indicate that this electrode requires more time than the aluminum electrode to restore the same pH conditions at the interface. Thus, monitoring the period of the polarisation here, can has more impact on the buffering phenomena than those observed with aluminum electrodes. Further chemical investigations are required at this stage to understand the impact of the pH change on the type of reactions occur at the electrode interface and hence on the fouling layer.

Although it is difficult to draw precise conclusions at this stage, surface pH is expected to influence the fouling processes, since some species may precipitate and adsorb on the electrode under alkaline or acidic conditions. It can be concluded from the data that fast polarity reversal leads to a more stable surface pH which is expected to reduce the rate of fouling associated with precipitated solids,

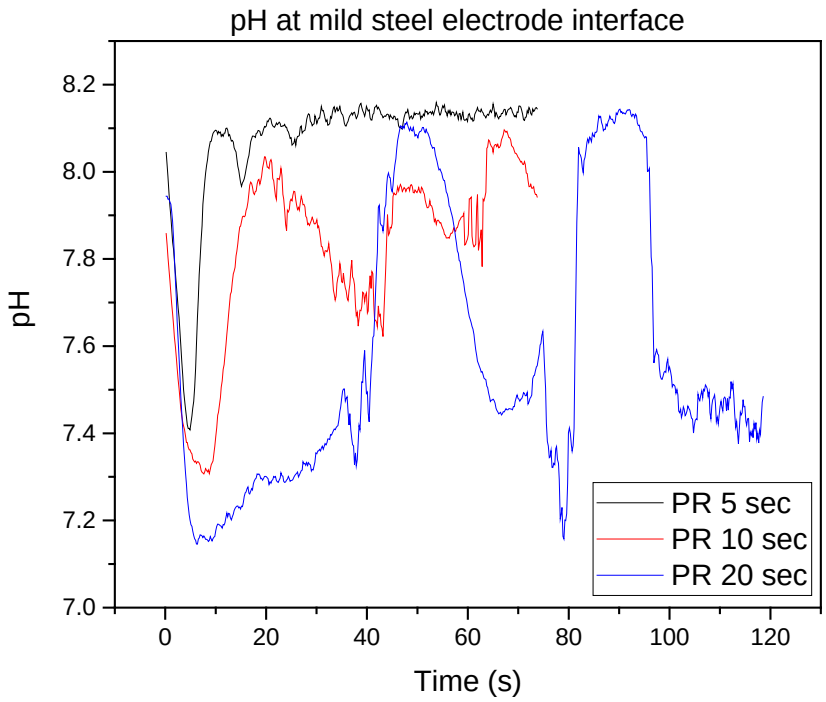

Figure [8]: show three different pH variation graphs at a mild steel electrode/solution interface obtained at various polarity reversal periods of 5, 10, and 20sec. The applied current density is 8mA/cm^2.

Impact of flow rate on pH

To simulate the operating condition of flowing effluent, we also monitored the pH change using Pyrinine dye at a constant distance from the electrode at different flow rates of 30, 60 and 120 mL/min. Figure [9] shows the pH variation at 60 µm distance from both anode and cathode. The results show nearly stable values of pH after about 10sec electrolysis and that increasing the flow rate slightly increases the pH at the anode interface and slight decreases the pH at the cathode interface. For example, after 40 min electrolysis, the pH at the anode interface is about 6.9 and 7.1 when the flow rate was 30 and 120 mL/min, whereas, at the same period of electrolysis the pH at the cathode interface was 7.8 and 7.5 at the same respective flow rate [see also Appendix for an in-situ recorded video]. These results indicate that increasing the flow rate of the electrolyte assist mixing the electrolyte and stabilize the pH at a certain distance from the electrode. This suggests

that increased flow rate will tend to reduce fouling processes due to more a stable pH combined with higher surface shear rates.

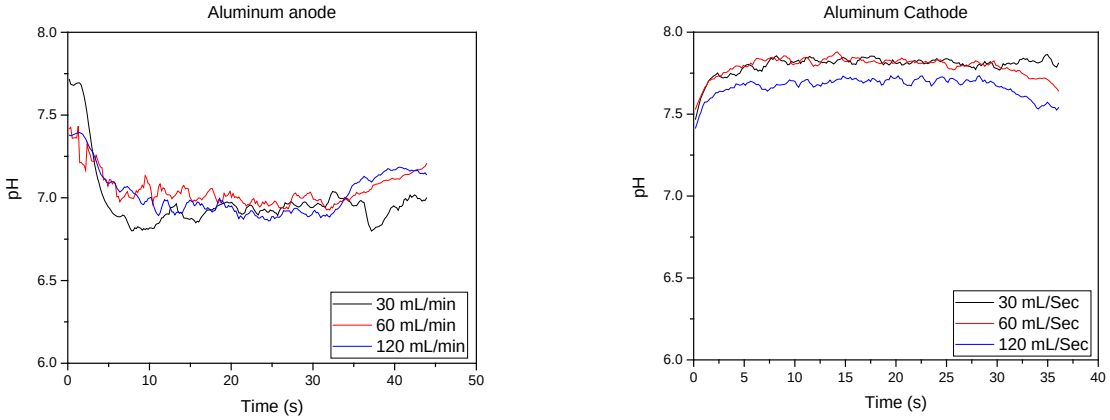

Figure [9]: show three different pH variation graphs at aluminum a) anode and b) cathode interfaces obtained at various electrolyte flow rates of 30, 60, an 120 mL/min. The applied direct current density is $8 mA/cm^2$.

Evaluation of the boundary layer thickness

Polarity reversal system

In addition to the quantification the pH distribution during EC treatment of real samples, it was possible to observe the pH boundary layer close to the electrode. The pH boundary layer thickness was defined as the distance from the electrode surface where the pH approaches teh bulk pH, based on the fluorescent images. Applying polarity reversed current, Figure [10] show images obtained from LSCM at the electrode/solution interface for both anode and cathode in a synthetic and a real produced waters after 60 s of electrolysis (periodic current reversal is 20 s). Monitoring the color near the interface shows a clear variation of pH compared to the bulk, due to building up of the boundary layer. Data on the thickness of the boundary layer after 60 s of the electrolysis at various polarity reversal periods of 10 s (100 mHz), 20 s (50mHz), and 40 s (25 mHz) are presented in Figure [11]. These results show that the thickness of the boundary layer was observed to be lower at a higher frequency. This lower boundary layer thickness can be expected if the time taken for the boundary layer to grow is longer then the half cycle time of the polarity reversal.

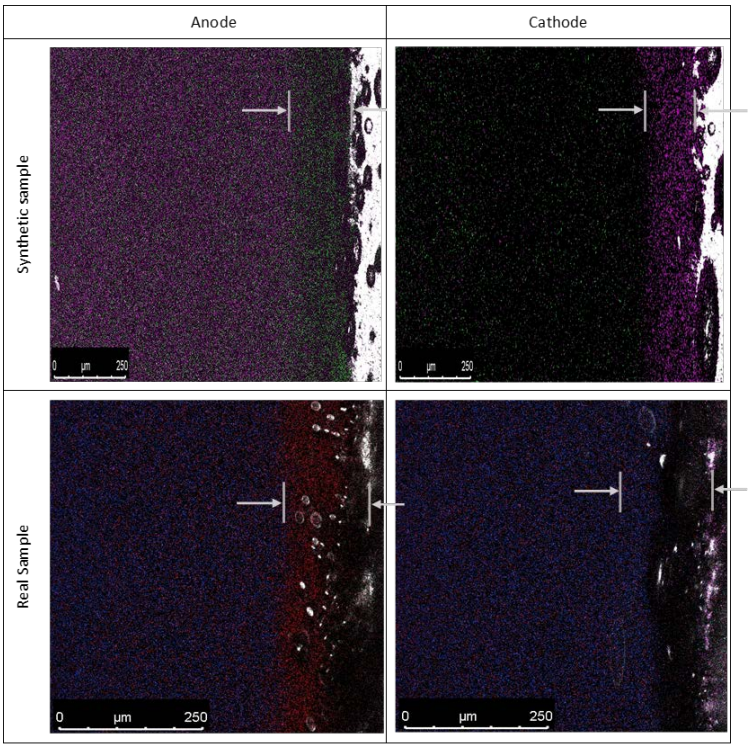

Figure [10]. Images of the electrode/solution interfaces for both of anode and cathode in a synthetic and real PW after 60sec of the electrolysis and periodic reversal period of 20sec.

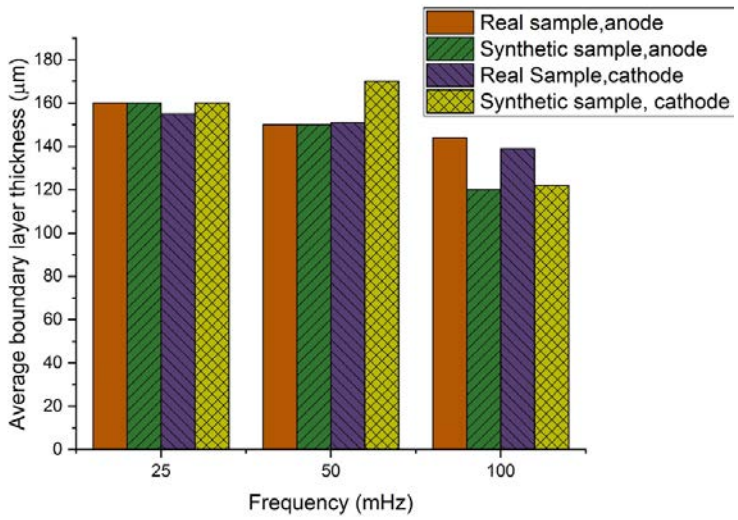

Figure [11]. Boundary layer thickness in AC mode at different frequencies. Aluminum-aluminum electrode, Real and synthetic solution. The applied current density is 8mA/cm^2.

Different flow rate conditions

The thickness of the pH boundary layer close to the electrode at different flow rate was monitored during EC treatment at a different electrolyte flow rate for both real and synthetic PW. Applying direct current, Figures [12 & 13] show images obtained from LSCM at the electrode/solution interface in synthetic and real produced waters after 60 s of electrolysis. Monitoring the color near the interface shows a clear variation of pH compared to the bulk, due to building up of the boundary layer. Data on the thickness of the boundary layer after about 60 s of the electrolysis at a various flow rate of 30, 60 120 mL/min are presented in Figure [14]. These results show that the thickness of the boundary layer was observed to be lower at a higher flow rate [see Appendix for an in-situ recorded video]. This lower boundary layer thickness can be expected when increasing the turbidity of the electrolyte at the electrode interface. Reducing the boundary layer may enhance the treatment performance, due to an improved mass transfer of dissolved coagulants into the bulk solution and thus reduce the fouling layer formation. More detail investigation on the treatment performance with enhanced mass transfer systems is discussed in task B of this report.

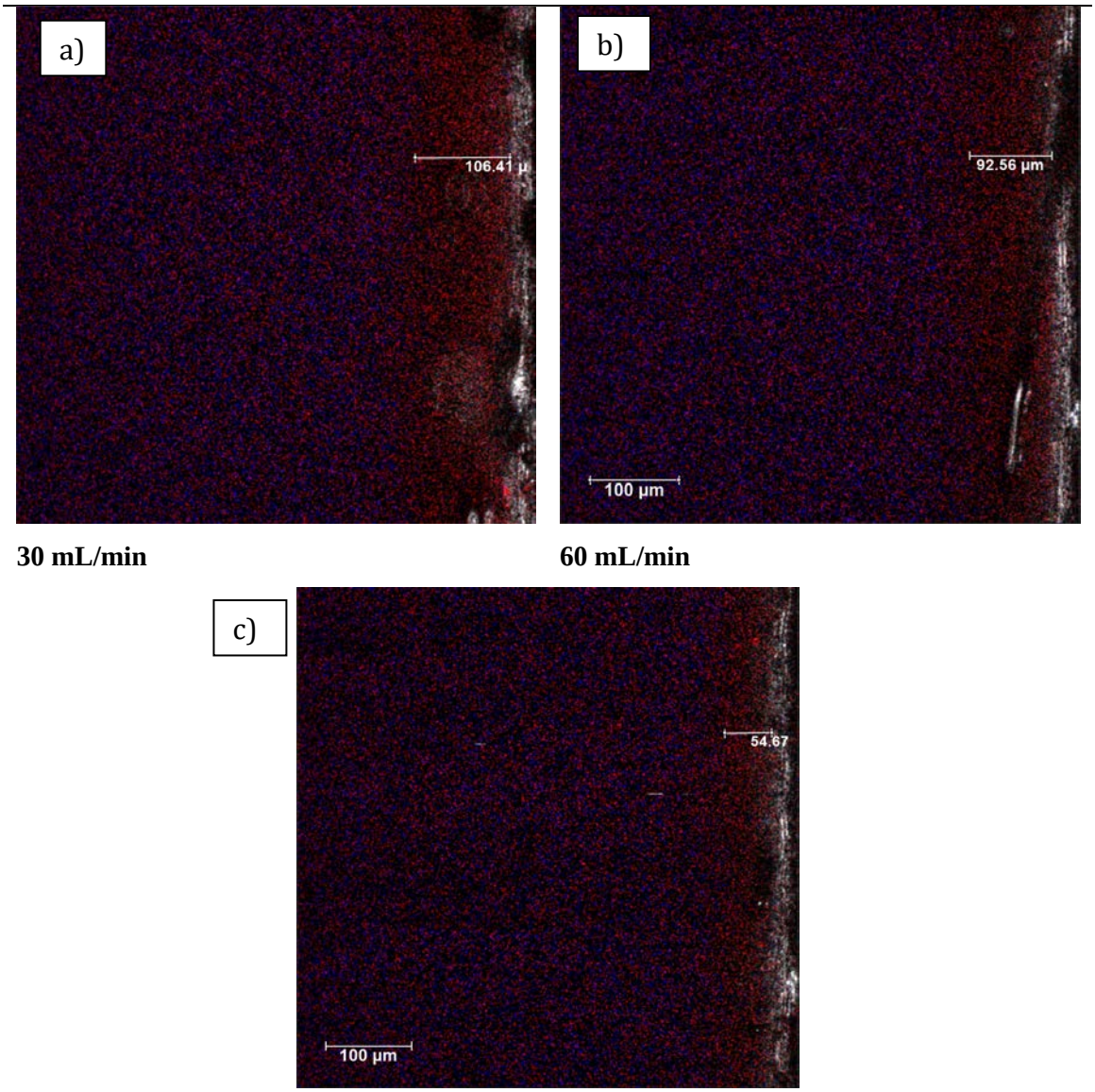

Figure [12]. Images of the anode interface at different synthetic PW flow rates of; a) 30, b) 60, and c) 120 mL/min after 60sec of electrolysis applying direct current density of 8mA/cm^2.

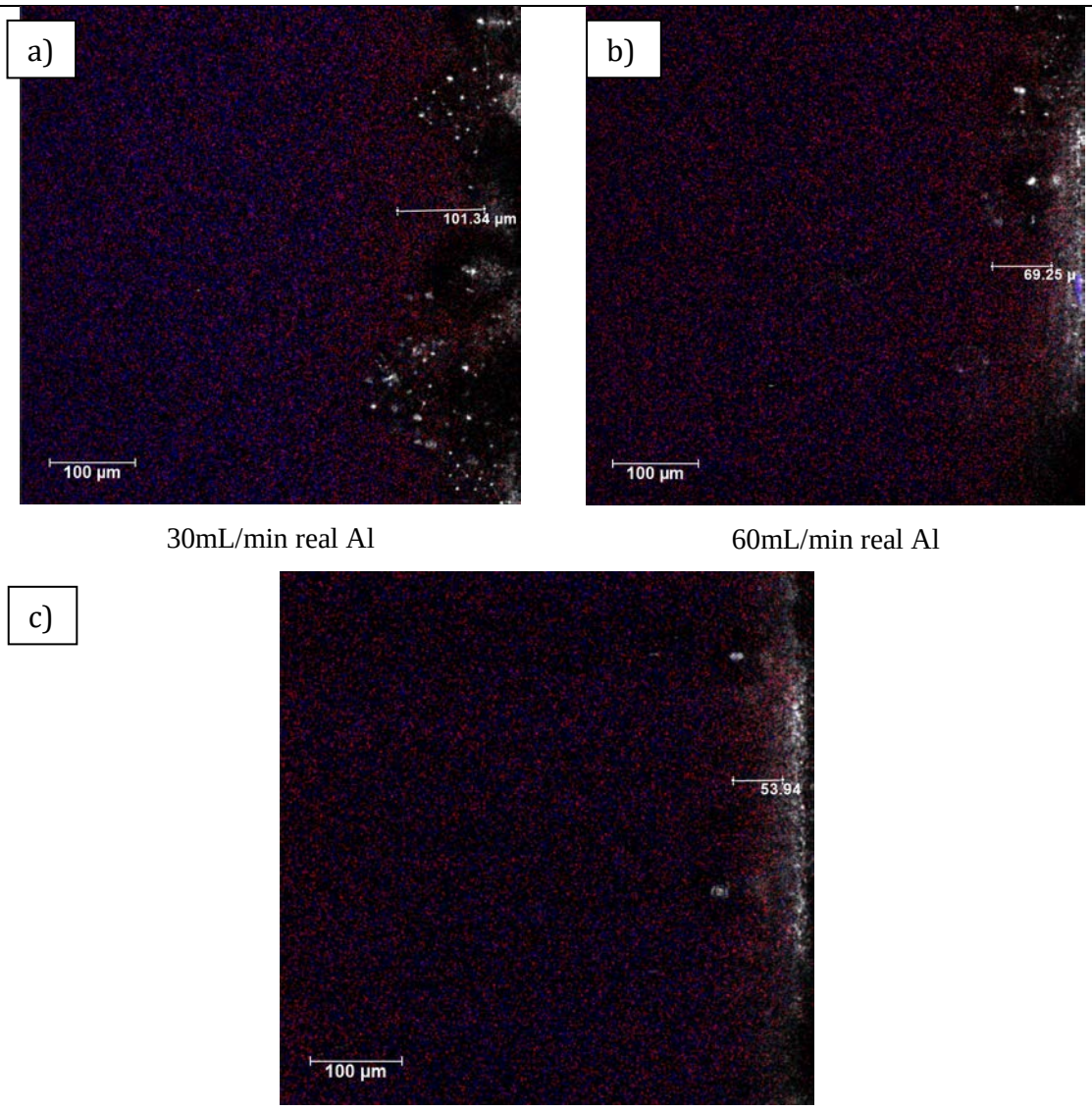

Figure [13]. Images of the anode interface at different real PW flow rates of; a) 30, b) 60, and c) 120 mL/min after 60sec of electrolysis applying direct current density of 8mA/cm^2.

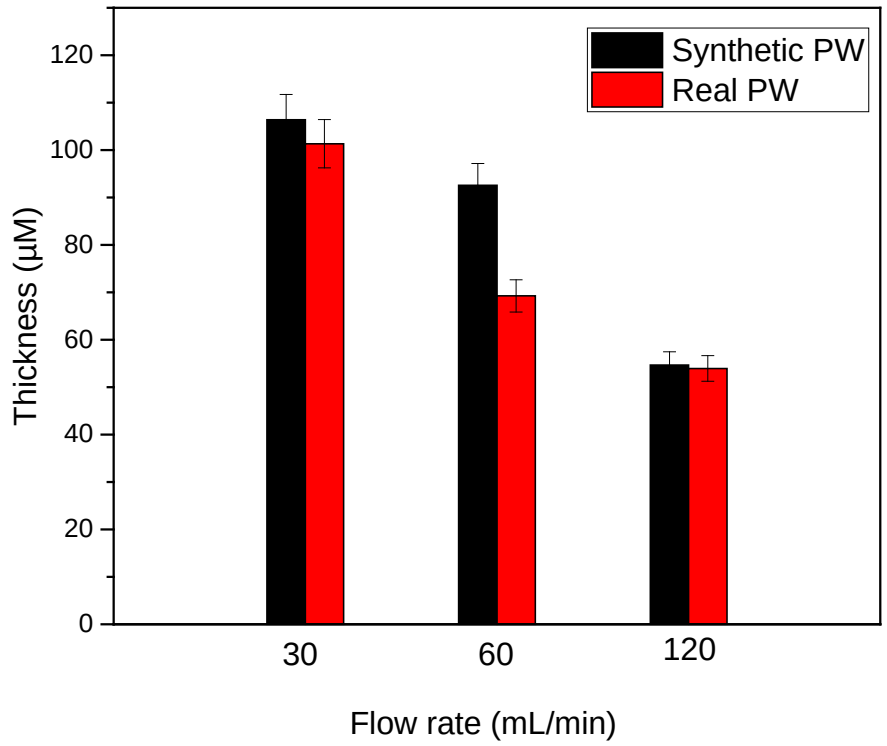

Figure [14]. Boundary layer thickness in DC mode at different electrolyte flow rate. Aluminum-aluminum electrode, Real and synthetic solution. The applied current density is 8mA/cm^2.

Summary of progress on task A

Continued progress has been made on the development of the LSCM imaging for pH distributions within the electrochemical cell. Imaging of pH variation in the range 1 to 11 was possible using two fluorescent dyes: Lysosensor Green DND-189 for low pH ranges at the anode interface and 5(6)-Carboxynaphthofluorescein for high pHs at the cathode interface. The method was optimized by applying a ratiometric calibration method to visualize the pH distribution within the EC cell. A Matlab code was developed to convert fluorescence response of dyes to pH values at each location. In addition, visualization of the pH at the electrode interfaces in real samples of produced water with natural convection and flow conditions was also demonstrated. The impact of flow rate on the pH distribution as well as on the boundary layer thickness was monitored. Increase the mixing by increasing the flow rate shows a dramatical reduction in boundary layer

thickness. On the other hand, monitoring the period of the polarisation can control the variation of pH at the electrode interface and in some cases shows buffering behavior. Thus, the visualization investigation coupled with bench scale investigations of EC process gave some insight knowledge about how we can monitor the thickness of the boundary layer by monitoring the turbidity at the electrode interface or changing the polarity. The thickness of the boundary layer demonstrates the energy required by metal coagulants to cross the interface and react with the contaminant species in the solution. In other words, for coagulation reaction to occur in the bulk of the solutions, the ions must cross the diffusion layer, and hence, the effective thickness of this layer must be small. If the boundary layer thickness is not reduced and the current density is increased beyond that which brings the ion concentration to zero at the electrode surface, then other reactions such as the formation of fouling layer will take place and lower the efficiency of the EC process.

2.2 Task B: Bench scale testing of EC treatment, novel cell designs and operating conditions.

Milestone B.D1: Preliminary samples of treated water, sludge and fouled electrodes for analysis in Task C.

Milestone B.D2: Data on conventional EC treatment for produced water / blowdown.

Milestone B.D3: Samples of treated water, sludge and fouled electrodes from novel EC operating conditions, for analysis in Task C.

Milestone B.D4: Report and performance data for novel EC designs and operating conditions (Dec 2017 to Oct 2018).

Objectives

The objectives of these milestones are to investigate the treatment of synthetic and real produced water as well as blowdown water by electrocoagulation to remove specific contaminants, including silica, hardness (Ca, Mg), colloids, and dissolved organics (e.g., naphthenic acids and other complex organics). Analysis of samples was performed in both the Geoscience and Chemical & Petroleum Engineering departments to provide a detailed composition of the water and sludge, prior, during and after treatment. In addition, any fouling layers that occur were also investigated to determine their composition. This task will enable us to investigate the treatment performance as a function of the operating conditions and to suggest procedures and approaches that will result in improve remediation performance and treatment. This investigation provided us insight understanding of the mechanism of the EC process, and enable us to recommend EC treatment conditions and designs tailored for the target applications.

In the early stage of the project, the performances of electrocoagulation were tested using effluent analogues to that found during oil-sand extraction process and contains inorganic species of Si, Mg and Ca. Fresh samples of produced water from different sites, as well as blowdown samples, were collected during developed phases of the project and test were performed to investigate the performance of different EC designs. Furthermore, samples of fouled electrodes and sludge were also collected from the on-going treatment trials and analysed to provide us more detail understanding of the process. Results for the treatment of produced water by conventional EC process are presented. The treatment of synthetic and real produced water from Peace River Complex and boiler blowdown water samples provided by our partner CNRL are discussed. Characterization of the organic as well as inorganic compositions of both the water samples prior

to and after electrocoagulation treatment are provided in detail throughout the report. Various techniques were utilized, such as ultra-high-resolution mass spectrometry, TOC, ICP, Raman spectroscopy, and potentiodynamic.

Methodology

The performance of the EC process was tested using both synthetic and real water samples. The optimized composition of the synthetic inorganic solution, designed as a model of the produced water, is presented in Table [1]. Treatment of real produced water and boiler blowdown were performed at the optimized conditions obtained from synthetic produced water. Note that, our main concern in this work for both types of water is to remove silica from solution, thus at this stage, no organic additives were used in the synthetic media. Several batch EC treatment experiments were conducted to test the performance of the reactor to remediate this synthetic produced water.

Table [1]: Concentration of components in synthetic produced water (pH= 7.75).

Constituent	Concentration (mg/L)	Concentration mM
HCO_3^-	1700	27.861
SO_4^{2-}	40	0.416
Si	56.2	2
Ca	65	1.622
Sulfide	110	3.228
Mg	20	0.823
Cl	1945	54.861
Na	1900	82.645

To study the impact of the flow type as well as the impact of enhanced mass transferred on the removal of silica from produced waters, different designs of the electrocoagulation cell were used. Moreover, to study the impact of flow type, a comparison study was performed using two cell designs of; 1) “design 1” with a longer pathway destructive turbulent flow, and 2) “design 2” shorter pathway flow through. Figure [15] shows the schematics of the two cell configurations used in this study. For comparison purposes, both cells were designed to have the same sizes, electrode’s surface areas, and cell geometric volumes, whereas, the only differences were the shape and the position of the electrodes within the cell. In the destructive turbulent flow design, the electrocoagulation reactor was constructed using a set of 7 plates of aluminum (grade 6061) or mild carbon steel (grade 1018) as anodes (4 plates) and cathodes (3 plates) with similar effective surface area of 224 cm^2 for each electrode (calculated as double-sided). Electrodes were assembled in parallel (spacing 18mm) into

a rectangular cell (19 x 3.6 x 15 cm) with flow arranged to go sequentially up and down between the plates. In the second design “Design 2”, the EC cell used was the same volume mentioned for the destructive turbulent flow design, however, the two identical cathodes were mounted in the cell parallel to each other on opposite walls of the reactor, at 2.2 cm distance. A rectangular anode (with dimensions 10 cm x 13 cm) of either aluminum (grade 6061) or mild carbon steel (grade 1018) was situated in parallel in the mid-distance between the two cathodes, mounted onto a cam follower above the cell. The mounting cam is designed to promote anode motion, however, the results obtained from this cell when the cam is not moving compared with the results obtained from the destructive turbulent flow cell designed and thus reporting the impact of flow type.

In addition to the study of flow type, the second electrocoagulation cell design “design 2” was used to investigate the impact of the enhanced mass transferred via anode oscillation on the removal of silica from both produced and boiler blowdown waters. To study the impact of an oscillating anode on the enhancement of mass transfer and the efficiency of the EC process, the cam in the flow through design was set at different oscillation conditions. Figure [16] is a schematic diagram of the oscillating plate electrode electrolysis cell that designed to enhance the mass transfer between the electrode surface and the bulk solution. To obtain these conditions, the cam follower was mounted on slide bars so that it could move horizontally between the cathodes. Springs were used to hold the follower against an eccentric cam, driven by a motor so that the follower and anode can oscillate between the cathodes. In principle, the cam offset and the motor speed could be adjusted to vary the amplitude and frequency of the oscillation. In this study, the oscillation conditions were monitored via the oscillatory flow Reynolds number (Re_o) [1]:

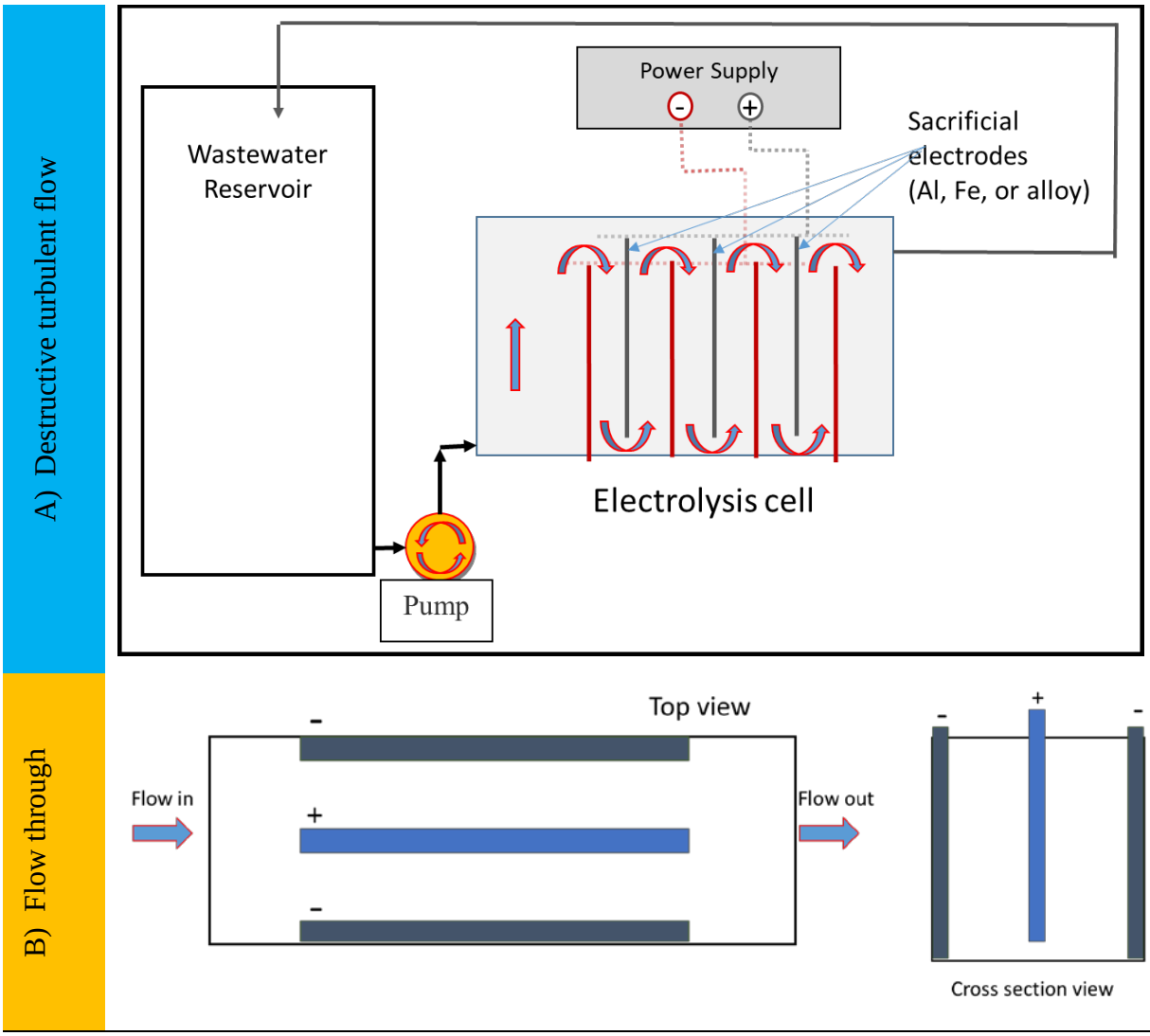

Figure [15]. Schematic diagrams of the two electrocoagulation cells used to study the impact of flow type; a) destructive turbulent flow, and b) flow through.

$$Re_o = \frac{\omega\, x_0\, d_e}{\nu} \qquad \text{(Eq. 1)}$$

where: d_e (cm) the hydraulic diameter, ν (cm^2 s^{-1}) the kinematic viscosity of the solution, ω (s^{-1}) the oscillation frequency, and x_o (cm) the centre-to-peak oscillation amplitude. A change in either the oscillation frequency or the amplitude (centre-to-peak) will alter the oscillatory flow Reynolds number Re_o. In this investigation, we studied the impact of both the oscillation frequency and the amplitude at conditions of constant or various Reynold numbers.

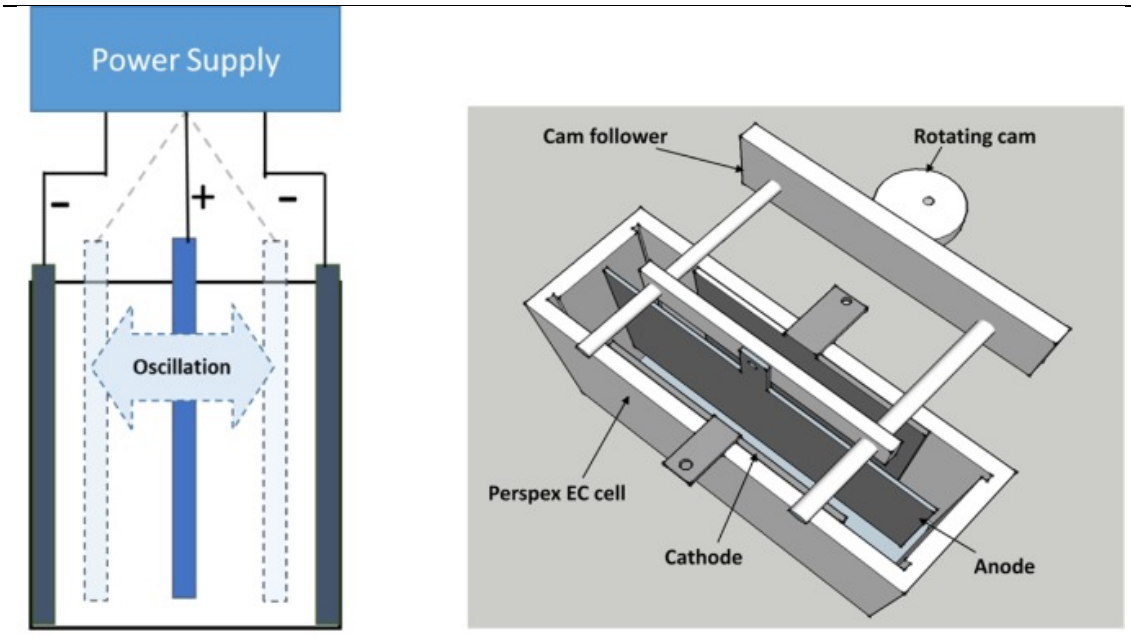

(a) Schematic cross section (b) Perspective drawing

Figure [16]. Schematic diagrams of the oscillating plate electrode electrocoagulation cell.

In all the aforementioned experiments, a current was applied to the electrodes using a direct current power supply (KEYSIGHT, N5766A, 40V/38A, 1520W, USA) with an anodic current density of 8 mA/cm^2 (or otherwise stated). The effluent was recirculated from the feed reservoir tank to the electrocoagulation reactor at a constant flow rate of 170 mL/min with a total volume treated of 1.5 L.

The obtained optimized conditions from synthetic and real produced waters were also applied to treat real boiler blowdown samples and the results is reported hereafter. The inorganic analysis of the as-received real boiler blowdown provided by our partner CNRL and produced waters from Shell's Peace River Complex that are used throughout this research are presented in Table [2].

Results and Discussion

Treatment of produced water

The performances of EC was evaluated using samples of real produced water and a synthetic oil-sands produced water containing inorganic species including Si, Mg and Ca (see Table 1). Samples of treated water, sludge from the treatment of both synthetic and real solutions were collected and analyzed. The performance of EC on the treatment of both synthetic and real SAGD produced water were performed using a bench scale EC cell. The results (Figure [17]) showed that bench scale testing of EC treatment on synthetic and real PW indicated better performance of aluminum electrodes than mild steel. Around 90% of the silica present was removed from real produced water using aluminum electrodes with an electrical charge passed of about 800 C/L. With mild steel electrodes, the only about 30% of the silica was removed afer 800 C/|L was passed, and around 1600 C/L was required to achieve a target of 90% removal. The amount of charge required was significantly lower than in the previous pilot trials carried out at the Peace River facility in 2016, suggesting that the energy consumption can be significantly reduced.

A similar trend was observed with synthetic produced water, but with a faster removal rate. It is apparent that the organic components present in the real produced water reduce the rate of silica removal. Organics with surfactant characteristics may stabilize inorganic nanoclusters, preventing them from aggregating. In addition, molecular organic – inorganic complexes may form, stabilizing the inorganic contaminant and preventing precipitation or adsorption.

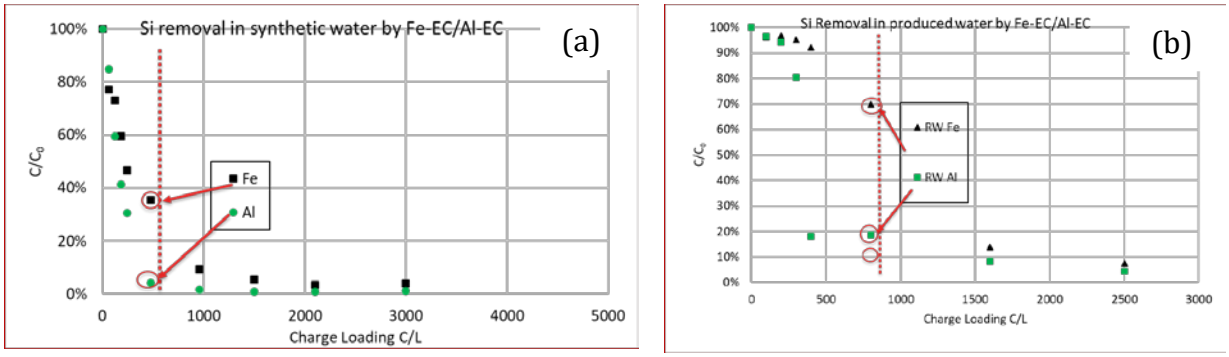

Figure [17] Percentage Si removal in; a) synthetic produced water and in b) real produced water by Fe-EC/Al-EC

After a charge loading of about 2500 C/L, 90% calcium removal was achieved with Al-EC, while a slightly lower calcium removal of 80% was obtained with Fe-EC after the same charge loading. Magnesium, however, was difficult to remove, with the concentration remaining at about 45-75% of the initial concentration after 2500 C/L was passed. Magnesium compounds (carbonate, hydroxide etc) and have higher solubility than the equivalent calcium compounds, thus magnesium removal in softening or coagulation processes are typically lower than those for calcium. Foaming during treatment of real produced water was problematic, which must be considered during scale-up trials and commercial operations.

The impact of air bubbling in the reactor was also studied and representative results on silica removal from produced water using aluminum/or iron electrode with and without air bubbling are shown in Figure [18]. Sparging with air will provide dissolved oxygen and an oxidizing environment, converting the less effective ferrous ion coagulant to the more effective ferric oxidation state. In addition, this oxidizing environment could also reduce the effect of organic contaminants which inhibit the removal of inorganics. As expected, the results showed that the removal performance was enhanced by bubbling air in the reactor.

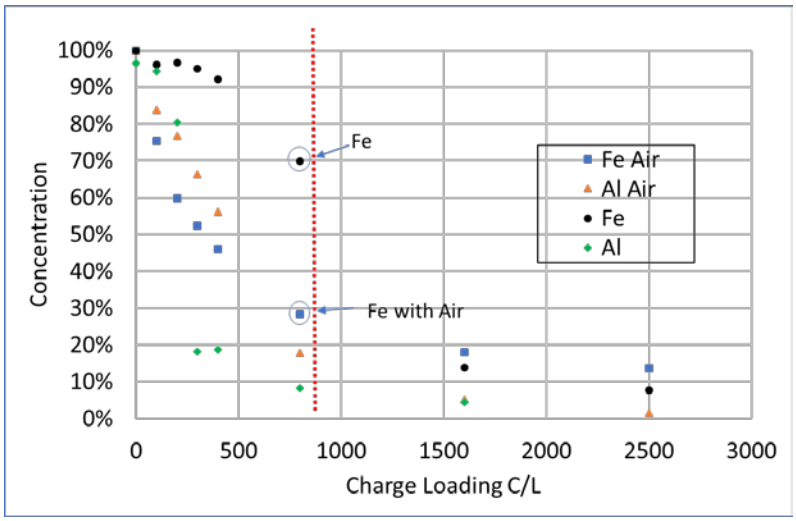

Figure [18]. Percentage Si removal from produced water using aluminum or iron electrodes with or without air bubbling.

The target of the treatment process is silica removal, since this is not easily removed by ion exchange processes. While calcium and magnesium removal is slower, they can be removed by ion exchange to enable recycle of the produced water to the once through steam generator. To

evaluate the economics of the EC treatment, based on information from Shell / CNRL, the treatment required to reduce the silica concentration by 90% was used. Under these conditions, the partial treatment of calcium and magnesium will reduce the burden on the ion-exchange softening process.

Coulombic dissolution efficiencies

In EC process, the amount of dissociated coagulant from the anode is proportional to the charge passed in the electrocoagulation cell and the efficiency of the process is always compared with the actual dissolution rate calculated via Faraday's law [2]. Thus, to determine the coulombic efficiency of the anodic dissolution, we performed an EC batch experiment on synthetic produced water and measure the dissolution rate and the removal rate of silica after loading 400 coul/L and 800 coul/L of charge at different current density of 8 A/m^2 and 16 A/m^2. Figure [19] shows the dissolution efficiency (ϕ, %) at both mild steel and aluminum electrodes, that are calculated based on the theoretic Faradic dissolution rate using Eq. 2 as follow;

Table [2]: Inorganic analysis (mg/L) of the as-received real boiler blowdown provided by our partner CNRL and produced waters from Shell's Peace River Complex

Element	Blowdown water	Produced water
Si^{2+}	122.2 ± 6.3	56.6 ± 2.8
Mg^{2+}	0.32 ± 0.15	56.8 ±2.9
Al^{3+}	0.53 ± 0.20	0.64 ± 0.2
Fe^{2+}	0.89 ± 0.23	12.3 ± 0.6
Ca^{2+}	17.49 ± 0.64	74.5 ± 3.7
Na^{+}	1431 ± 225	3247 ± 162
K^{+}	385 ± 6.5	BDL*
B	226 ± 3.3	16.6 ± 0.8
Mn	0.01 ± 0.01	BDL*
pH	8.2 ± 0.2	8.7 ± 0.2

* Below the detection limit

$$\phi = \frac{z\,F\,C_t\,V}{It} \qquad \text{(Eq. 2)}$$

where: z is the number of moles of electrons transferred per mole of metal ion generated (valence charge for Al is 3 and mild steel is 2), F is Faraday's constant (96485 C/mol), C_t is the concentration of metal ions in solution (mol/L) at time t (sec), V (L) is the total volume of solution, I (Amp) is the applied current, and t (sec) is the duration of electrolysis.

The results in Figure [19] indicate that the dissolution rate with coulombic efficiencies of greater than 100% can be reached with aluminum electrode when a charge of 800C/L is loaded in

the cell. Moreover, a higher efficiency was observed when a lower current density of 8A/m^2 was applied. Decreases in the efficiency at the higher current density of 16 A/m^2 may be attributed to the energy loss in the cell which is due to the increases in the applied potential to values far more than the required overpotential of the metal dissolution. This unnecessary loss of energy can be avoided when a lower current density is applied.

Considering, on the other hand, the efficiency of mild steel electrode, although the z value is taken as +2, a current efficiency of less than 100% was always observed. These results suggesting that the dissolved species from electrodes are in the form of ferrous ions and some portion may react with the sulfide species present in the electrolyte to form insoluble fouling layer of FeS that reduce the efficiency of the EC process when iron anodes are used. Comparing with EC system when aluminum electrode is used, Al_2S_3 may be form during the electrolysis, but it is very unstable compound that is sensitive to moisture and hydrolyzing to hydrated aluminum oxides/hydroxides.

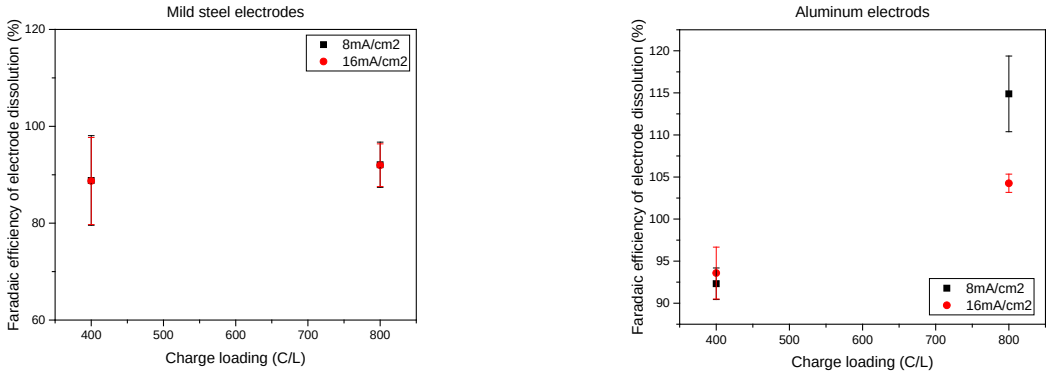

Figure [19]: The coulombic efficiency of the dissolution process of a) mild steel and b) aluminum electrodes, in a synthetic produced water at various current densities of 8.0 and 16 A cm^{-2}. The initial silica concentration was 56 ± 2.6 ppm, initial pH 7.7, and solution flow rate 170 mL/min.

Electrochemical investigation

To further understand the speciation of ions dissolved from the electrode, a cyclic voltammetry investigation can provide some information about electrode/electrolyte interfacial reaction in the produced water environment. Figure [20] shows the potentiodynamic polarization

curves obtained from the aluminum electrode and from iron electrodes. Using Fe-EC, a clear hysteresis loop was observed in the voltammogram indicating passivation which may due to sulfide (S^{2-}) reaction on the anode or iron sulfide formation. These results agree with the aforementioned efficiency results of mild steel anode. Considering, on the other hand, the voltammogram obtained from the aluminum anode in the same produced water electrolyte, clear hysteresis loops were observed in both anodic and cathodic scans. These results indicate that in the anodic scan the pitting continued to occur with increasing potential. The reverse anodic curve exhibited a higher current as compared with the forward scan, with hysteresis loops confirm the formation and the dissolution of hydroxide film. The presence of both anodic and cathodic hysteresis loops with a higher current of the reverse scan indicates that the dissolution of aluminum species requires less energy than the formation of a passivation layer.

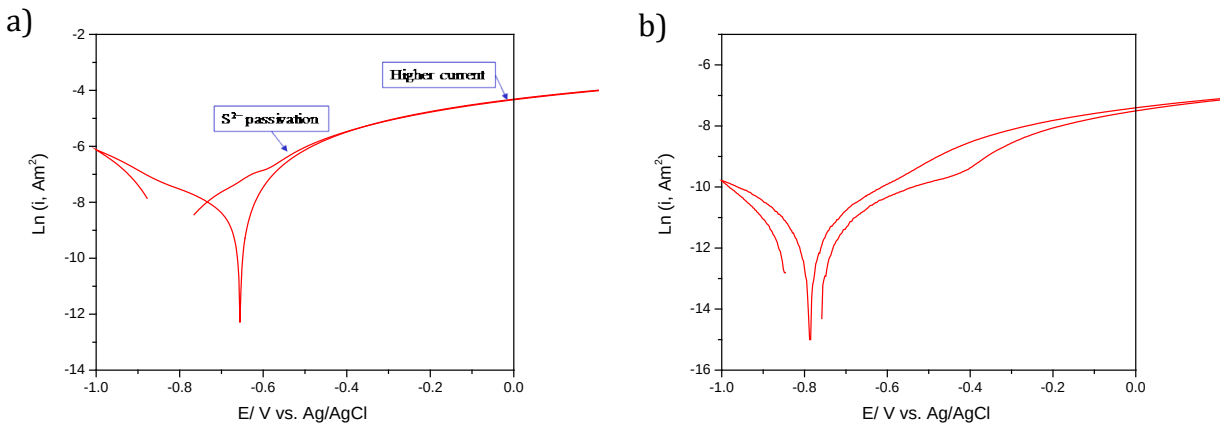

Figure [20]. Polarization curve of a) mild steel and b) aluminium stationary electrodes in synthetic produced water media as supporting electrolyte.

Further investigation on the type of organic/inorganic materials form on the electrode from both produced and boiler blowdown waters on the electrode surfaces are presented in later sections of this report. Moreover, ongoing electrochemical impendent spectroscopy and cyclic voltammetry are still under investigation for more insight understanding of the process.

The performance of EC for real and synthetic produced water treatment

The performances of EC was evaluated using samples of real produced water and a synthetic oil-sands produced water containing inorganic species including Si, Mg and Ca (see Table 1).

Samples of treated water, sludge from the treatment of both synthetic and real solutions were collected and analysed. The performance of EC on the treatment of both synthetic and real SAGD produced water were performed using a bench scale EC cell. The results (Figure 21) showed that bench scale testing of EC treatment on synthetic and real PW indicated better performance of aluminum electrodes than mild steel. Around 90% of the silica present was removed from real produced water using aluminum electrodes with an electrical charge passed of about 800 C/L. With mild steel electrodes, the only about 30% of the silica was removed afer 800 C/|L was passed, and around 1600 C/L was required to achieve a target of 90% removal. A similar trend was observed with synthetic produced but with a faster removal rate. It is apparent that the organic components present in the real produced water reduce the rate of silica removal. The amount of charge required was significantly lower than in the previous pilot trials carried out at the Peace River facility in 2016, suggesting that the energy consumption can be significantly reduced.

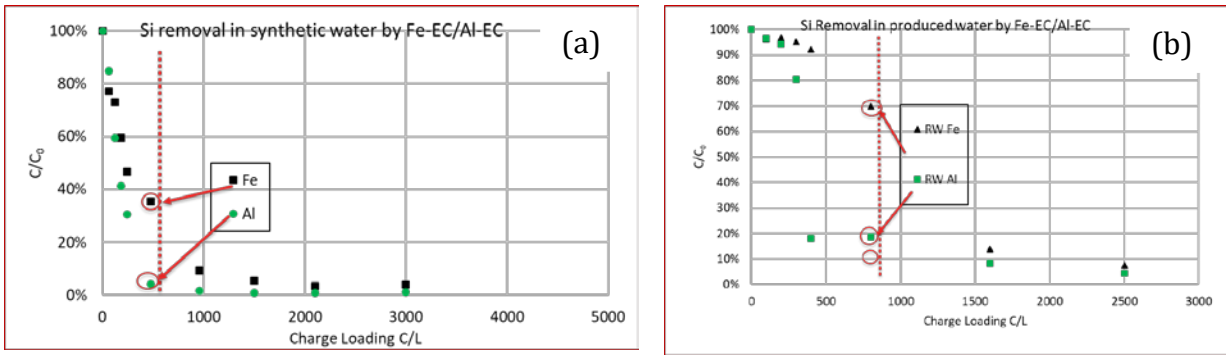

Figure [21]. Percentage Si removal in; a) synthetic produced water and in b) real produced water by Fe-EC/Al-EC

Considering the other cations presented in the produced water, by applying a charge loading of about 2500 C/L, around 90% and 80% of the calcium was removed using Al-EC and Fe-EC respectively. Magnesium, however, was difficult to remove, with the concentration remaining at about 45-75% of the initial concentration after 2500 C/L was passed. Foaming during

treatment of real produced water was problematic, which must be considered during scale-up trials and commercial operations.

The impact of air bubbling in the reactor was also studied and representative results on silica removal from produced water using aluminum/or iron electrode with and without air bubbling are shown in Figure 22. Sparging with air will provide dissolved oxygen and an oxidizing environment, converting the less effective ferrous ion coagulant to the more effective ferric oxidation state. In addition, this oxidizing environment could also reduce the effect of organic contaminants which inhibit the removal of inorganics. As expected, the results showed that the removal performance was enhanced by bubbling air in the reactor.

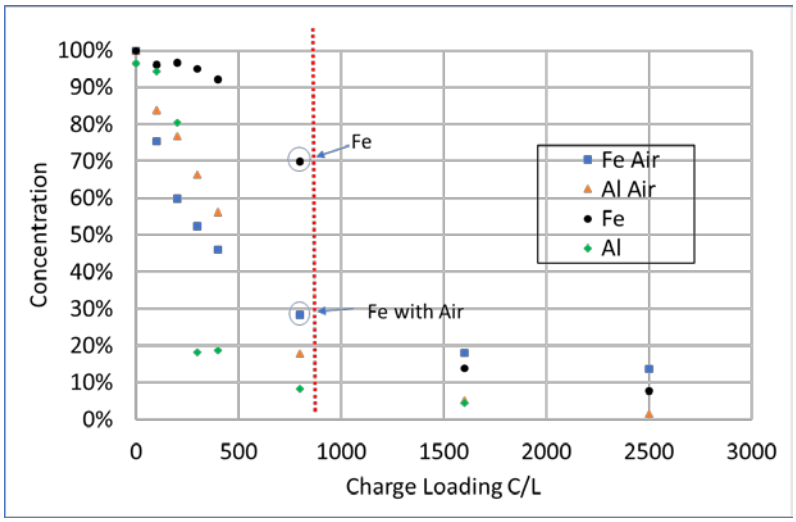

Figure [22]. Percentage Si removal from produced water using aluminum or iron electrodes with or without air bubbling.

Silica removal and the impact of current density

Changing the current density in an EC process can be used to control the rate of the electrode dissolution and hence monitoring the amount of the coagulants in solution [2]. Thus, monitoring the current will coincide with the change in coagulant dose and hence monitor the EC removal process. Previous dissolution results indicated that mild steel electrode is less efficient in dissolution as compared with an aluminum anode, these results are reflected here on the rate of silica removal. Indeed, silica removal with an aluminum electrode is higher during the initiation of the EC process as compared with mild steel anode. For example, after loading of 400 C/L

charges at 4 A/m^2 of current density the removal rate of Si was 56.9% and 6.3% using Al and Fe anodes, respectively. These rates increased by increasing the coagulants dosing with both electrodes to reach the value of >90% removal when the coagulant loading reaches 800 C/L and 1600C/L using the respective electrode. These charge loading values correspond to about 2.76 mmol (74.4 mg/L) and 8.29 mmol (462.9 mg/L) of Al (III) and Fe (II) loading to the solution, respectively.

To test the impact of the same coagulant dosage at various current density, the duration of each experiment was adjusted so that the anodes will dissolve the same amount of total aluminum or iron in each EC experiment. This was done by passing a constant amount of charge (25000 C/L) through the cell at various current densities, by adjusting the treatment duration. Figure [23] shows the Si removal (%) during the EC process at current densities of 4 and 8 A/m^2. In all cases, the aluminum anode showed more rapid Si removal than the mild steel anode, and in all cases, the treatment performance was dependent on the coagulant dose, with little or no influence of the current density. In other words, increasing the current density will not improve the removal rate but reduce the duration of the coagulant loading. On the other hand, considering the fact that when the applied current density is increased the corresponding cell voltage will increase. These increases in both current density and cell voltage will lead to an increase in EC power consumption.

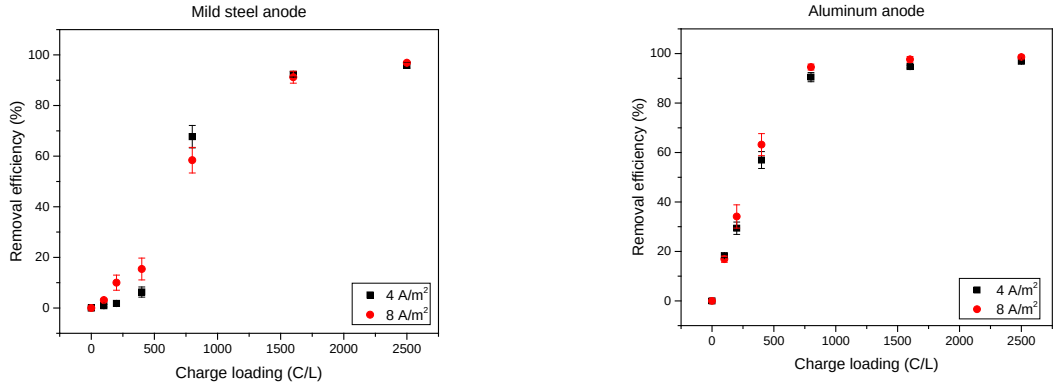

Figure [23]. Silica removal during EC treatment using; a) mild steel and b) aluminum anodes at current densities of 4 mA cm^{-2}, and 8 mA cm^{-2}. The initial silica concentration was 56 ± 2.6 ppm, initial pH 7.7, and solution flow rate 170 mL/min.

Impact of Dissolved Oxygen in EC

The impact of dissolved oxygen on the EC efficiency was also investigated in this study. Generally, the presence of dissolved oxygen help oxidizes both coagulate and coagulant species

to alter the efficiency of the remediation process. In this work, we compare the efficiency of silica removal from synthetic produced water using mild steel and aluminum electrodes in the excess, absence and the presence of dissolved oxygen. The conventional approaches to achieve these conditions were respectively performed at the following three settings; 1) bubbling air in the reservoir to saturate the amount of dissolved oxygen in the electrolyte, 2) bubbling nitrogen to replace the dissolved oxygen in the electrolyte (to obtain an oxygen free electrolyte), and 3) maintaining the dissolved oxygen level at the natural diffusion rate with no bubbling of either air or N_2. The results in Figure [24] show that the level of the dissolved oxygen in the electrolytes has no impact on the removal rate of Si when the aluminum electrode was used. This result may indicate that there is no impact of the level of dissolved oxygen on the modification of the oxidation state of either species; the coagulate (Silica) or coagulant (aluminum ions). However, considering the mild steel electrode, a confined impact of dissolved oxygen can be observed when nitrogen is bubbled in the solution. The removal rate when the solution bubbled with nitrogen (O_2 < 1ppm) reached about 48.7%, whereas, when bubbled with air the removal rate reached a higher value of 58.6%. The dissolved oxygen in the case of mild steel electrode helps oxidizing the dissolved ferrous (II) to ferric (III) ions. Increasing the oxidation state of the hydrated iron species increases the tendency to act as Bronsted acids, thus increase the tendency to lose H^+ ions from the hydrating water molecules bound to them in aqueous solution, Eqs. 3 and 4 [3]. The presence of excess oxygen in solution may thus increase the oxidation phenomena and accelerate the removal process.

$$Fe(H_2O)_6^{3+} \rightarrow Fe(H_2O)_5OH^{2+} + H^+ \rightarrow Fe(H_2O)_4(OH)_2^+ + H^+ \quad \text{(Eq. 3)}$$

$$2[Fe(H_2O)_5OH]^{2+} \rightarrow [Fe_2(H_2O)_8(OH)_2]^{4+} + 2H_2O \quad \text{(Eq. 4)}$$

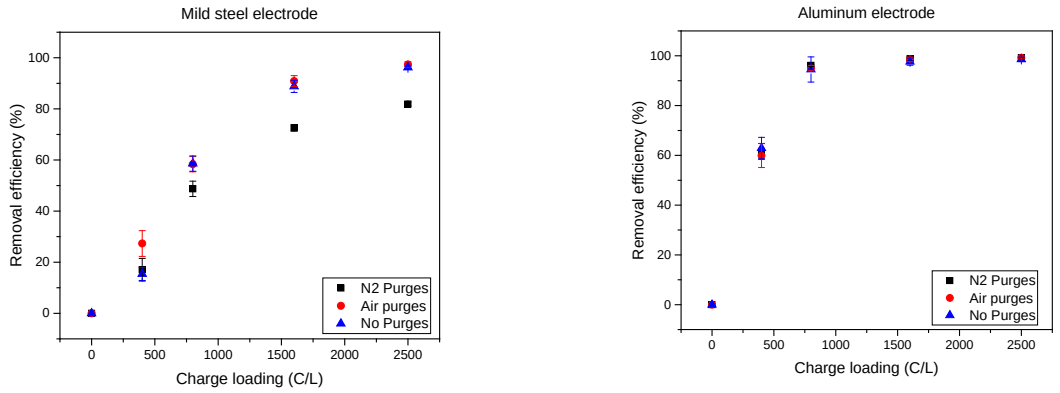

Figure [24]. The impact of dissolved oxygen on the removal rate of Si during EC treatment using; a) mild steel and b) aluminum anodes at current densities of 8 mA cm^{-2}. The initial silica concentration was 56 ± 2.6 ppm, initial pH 7.7, solution flow rate 170 mL/min and the operating current density of 8 mA cm^{-2}.

The impact of cell design and flow type

The impact of the EC cell design was investigated in this study by keeping the electrode surface area constant and lengthen the electrolyte pathway. The conventional approaches to achieve these conditions were to modify the cell so that the electrode positions will be facing the motion of the flow of the electrolyte in the long pathway cell (design 1), whereas positioning the electrodes in parallel with the flow in the short pathway (design 2). Figure [25] in the experimental section shows the schematic of the two cell designs. The shortest pathway of the electrolyte between the inlet and the outlet of the EC cell in the design 1 is about 105 cm whereas in the design 2 is about 16 cm.

Although the two cells have a similar geometric size and electrode surface area, design 1 modifies the flow type to be more turbulent between the electrodes and lengthen the electrolyte pathway. These two factors have a huge impact on the removal process. Indeed, the results in Figure [25] show that the removal rate using longer pathway (design 1) exhibits higher removal rates with both of aluminum and mild steel electrodes as compared with the shorter pathway (design 2) EC cell. In cell design 1, lengthening the pathway will have an impact on increase the mixing and hence the mass transfer or reactants. Loading the same amount of current density should ideally produce the same amount of coagulant and hence should ideally remove a similar amount of silica. However, our finding here confirms the importance of mass transfer pathway within the reactor; i.e. for the same amount of coagulants will results in a different rate of reaction

in the EC process. These results agree with the previous results that obtained when we enhanced the turbine flow of the electrolyte by oscillating the electrodes (oscillation study of the anode will be presented hereafter in this report). Moreover, comparing the removal rate of silica using the two type of electrodes still indicates that aluminum is outperformed mild steel electrodes for silica removal from produced water. The removal rate when an aluminum electrode is used in both designs (1 and 2) reached after loading 800 C/L much higher values (94.5% and 85.2%) with the Al electrode as compared with the Fe electrode (58.5 and 31.6%, respectively).

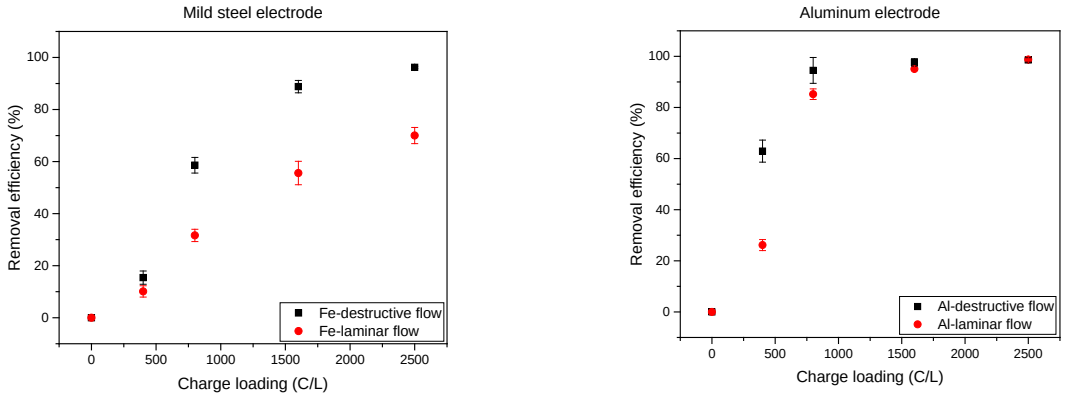

Figure [25]. Silica removal as a function of charge loading during EC treatment using; a) mild steel and b) aluminum anodes for processes operated with different flow design cells. The initial silica concentration was 56 ± 2.6 ppm, initial pH 7.7, solution flow rate 170 mL/min and the operating current density of 8 mA cm^{-2}.

Impact of anode oscillation

The schematic setup diagram of the oscillating cell is illustrated in Figure [16] and summarized in the aforementioned experimental section. In this work, using both aluminum and mild steel electrodes, the silica removal at the initial stage of the EC process increased dramatically when the anode was oscillated compared to the results for a stationary anode (Figure 26). For example, the percentage of silica removal using an oscillating anode of aluminum or mild steel at 1.75 Hz frequency and 12 mm amplitudes were 73.7% and 32.2% after loading 400C/L, whereas with a stationary anode the silica removal reached only 51.3% and 17.8%, respectively.

Typically, the flow conditions inside a reactor are characterized by the Reynolds number, which is characteristic of the ratio of inertial forces to viscous forces. For an oscillating system, the flow

conditions can be characterized by the oscillatory flow Reynolds number (Re_o) (see equation 1). A change in either the oscillation frequency or the amplitude (center-to-peak) will alter the oscillatory flow Reynolds number Re_o. Figure 26, shows the percentage of silica removal from solution using both aluminum and mild steel anodes at different oscillation conditions of amplitude and frequency. Indeed, increasing the frequency in the range of 0.6–1.75 s^{-1} with a fixed amplitude (12 mm) indicates an increase in the removal rate. The increase in the performance in these cases can be attributed to the increases in Reynold's number (Eq. 1), corresponding to an increase in the rate of mass transfer and mixing. However, at this stage, it is interesting to monitor the variation of both amplitude and frequency at constant Reynold's number, i.e. keeping the multiplication of $\omega \times x_0$ in Eq. (1) constant. This investigation may shed light on whether the oscillating current density plays a role in the enhancement in EC performance (See our previous publication for a full explanation about the current pulsation [4]). Figure 26 shows a comparison of the silica removal performance using both aluminum and mild steel electrodes at two different oscillation conditions keeping Reynold number constant ($\omega \times x_0$ = 0.6 Hz x 12 mm = 0.9 Hz x 8 mm). With a low amplitude oscillation (8 mm) at the same oscillatory Reynolds number, the silica removal is slightly higher. This suggests that the enhancement of silica removal with oscillating anodes is due to only the increased mass transport/mixing, and no impact of the pulsed current. These results require more investigation. Previously, we established that the pulsing of the current will lead to periodic addition of metal ions at a higher concentration relative to a constant current. This addition of coagulant would seem to enhance the contaminant removal process, perhaps by leading to an earlier onset of the sweep coagulation due to the increased local concentration of metal ions. Further work is needed to explore the effect of current pulsation on the removal performance.

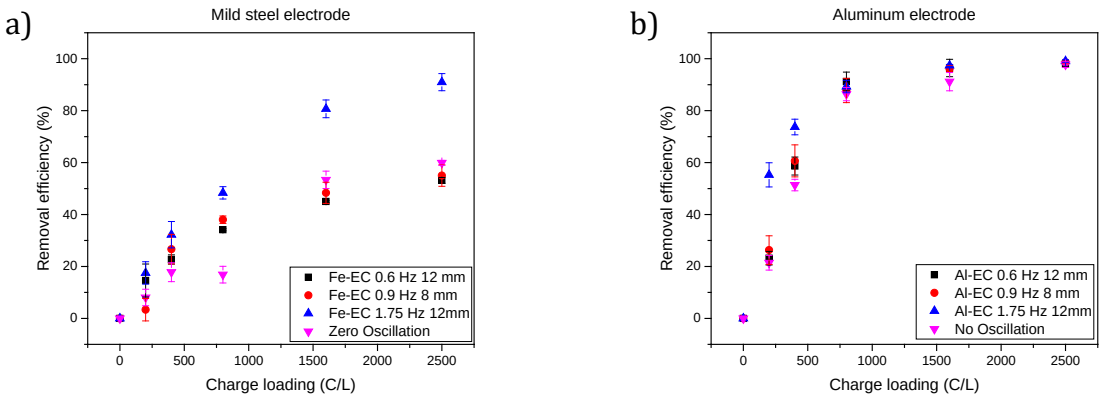

Figure [26]. Silica removal as a function of charge loading during EC treatment using; a) mild steel and b) aluminum anodes for processes operated with different anode oscillation frequencies and amplitudes. The initial silica concentration was 56 ± 2.6 ppm, initial pH 7.7, solution flow rate 170 mL/min and the operating current density of 8 mA cm^{-2}.

Silica removal from real produced water with an oscillating anode

The impact of the electrode's type of either stationary aluminium or mild steel on the removal rate of silica from real produced water provided by our partner CNRL was investigated using design 2 EC cell. The anode oscillation were performed at two different frequencies of 1 Hz and 1.7 Hz. The results in Figure [27] indicate, similar to synthetic produced water, that the percentage of total silica removal increased with increasing the frequency when a mild steel electrode was used. Whereas using aluminium anode, oscillation does not affect the final Si removal, but it helps reaching the equilibrium more rapidly. The enhancement can be due to several reasons, one is oscillation enhances the diffusion of oxygen, which can speed up the oxidation process of the poor coagulant ferrous ions (Fe^{2+}) to the more effective ferric ions (Fe^{3+}); the other reason is oscillation enhances the mass transport of metal ions toward the bulk solution where they coagulate the contaminants.

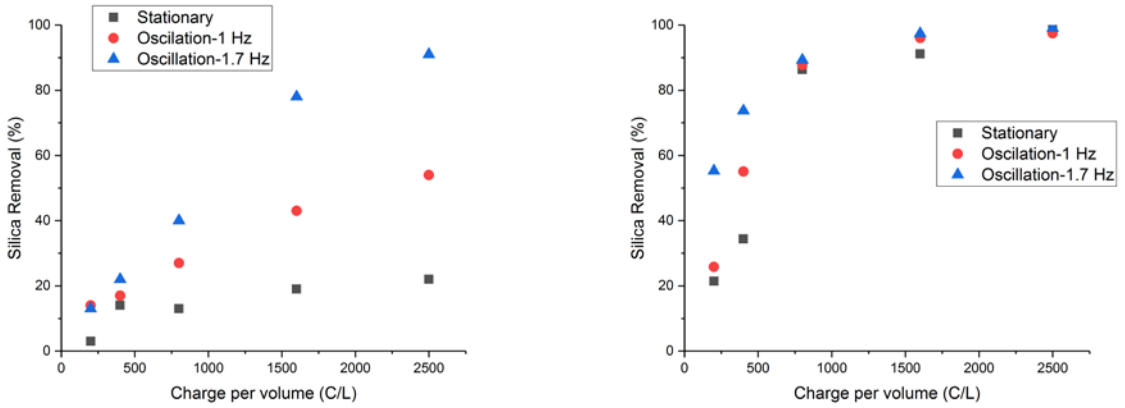

Figure [27]. Removal of silica from real produced water using; a) mild steel electrode with and without oscillation b) aluminum electrode with and without oscillation. The initial silica concentration was 56 ppm, initial pH 7.7, solution flow rate 170 mL/min and the operating current density of 8 mA cm^{-2}.

Applying a magnetic field on the EC cell

Monitoring the fouling formation in the presence or absent of magnetic field was possible by using small EC cell (25 mL) with small electrode (2 cm^2). However, monitoring the fouling using oscillated electrode require further optimisation of the reactor.

Electrochemical production of fouling on the electrodes were investigated using small Fe-EC/Al-EC cells with synthetic produced water. The impact of magnetic field on the formation of fouling layers during EC treatment of synthetic PW was tested at various strengths of magnetic fielcfield of 0.158, 0.316 and 0.474 tesla. Figure [28] show images of iron and aluminum electrodes following 2 h EC treatment and compared with bare electrodes. The images indicate less fouling layers are formed on aluminum electrode by increasing the magnetic field strength. However, using iron electrode, the implementation of magnetic field enhanced fouling formation.

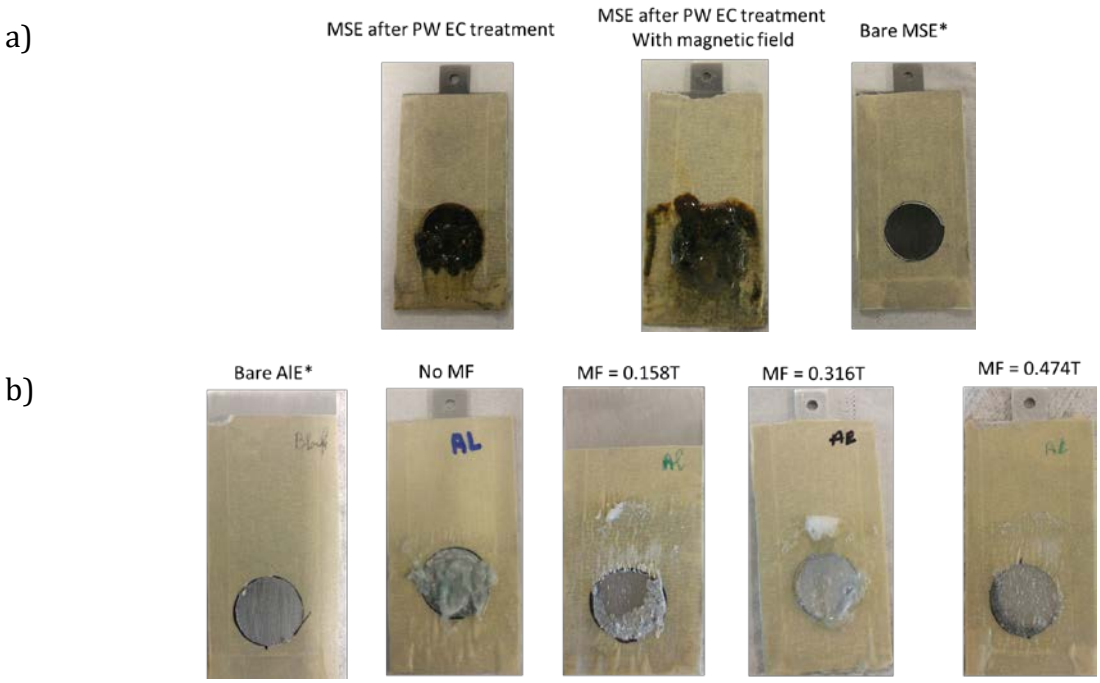

Figure [28]. Images of; a) mild steel electrodes (MSE) and b) aluminum electrodes (AlE) following EC of synthetic PW at various strengths of magnetic fields (MF).

These observations indicate that in the case of iron electrode, the applied magnetic field may enhance the magnetization process of both iron electrode surface as well as the precipitated iron species to resulting in enhancing attraction of ferromagnetic particles to the electrode surface. Aluminum is a non-magnetic metal, so the magnetic field will not have any direct influence on the precipitated particles or the aluminum electrode. Hence the application of magnetic field enhances the implementation of Lorentz force to accelerate mass transfer of the freshly dissolved cations from electrode toward electrolyte.

Electrochemical monitoring of the fouling formation in the presence or absent of magnetic field was possible through recording the chronoamperometric curve at constant voltage (0.5 mV vs. Ag/AgCl) using a small EC cell (25 mL) with aluminum or iron working electrode of 2 cm^2 surface area. A drop in the current during the chronoamperometric application indicates a building of resistance on the electrode surface, due to the formation of a fouling layer. Figure [29] shows the chronoamperometric response of Fe (a) and Al (b) electrodes in the presence of various magnetic field strengths. The Fe-EC and Al-EC show reduction in the chronoamperometric curves due to fouling after about 76 min and 92 min, respectively. Complete electrode fouling occurs after

about 104 min when Fe-EC system was used and after about 113 min when Al-EC system was used. The longer time required for the electrode fouling in the case of Al-EC electrode indicates less fouling as compare with Fe-EC for treatment of synthetic produced water.

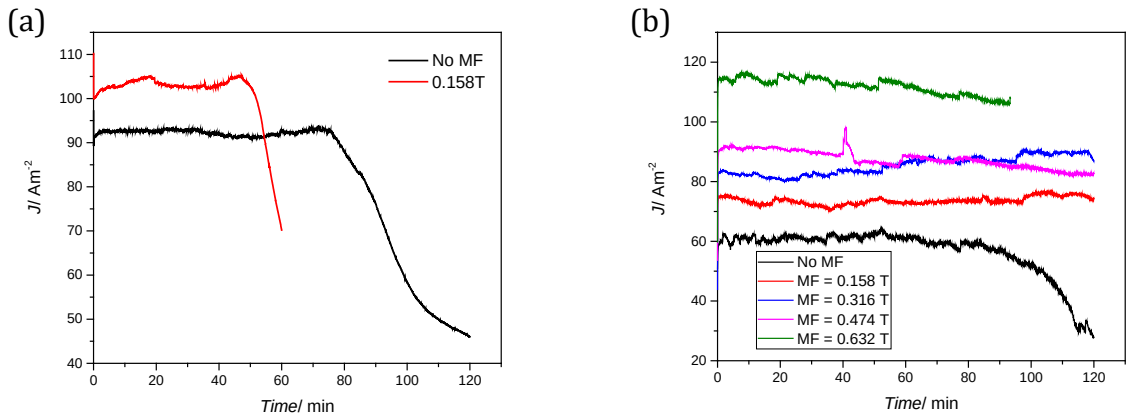

Figure [29]. Chronoamperometric responses of a) mild steel and b) aluminium electrodes in synthetic produced water in the presence of magnetic fields at various strength.

The impact of magnetic field (of 0.158, 0.316 and 0.474 Tesla) on the chronoamperometric responses during EC treatment of synthetic PW shows contrasting results with Fe or Al electrodes. Both electrodes show higher current when applying magnetic field. However, the presence of magnetic field accelerates the fouling formation on the mild steel (Fe) electrode, whereas, it delays it on Al electrode. As discussed above, in the case of iron electrode, a magnetic field is induced in the mild steel electrode, which may lead to the attraction of ferromagnetic particles to the electrode surface. However, in the case of non-magnetic aluminum electrode, there will be no such attraction. Hence the application of magnetic field with an aluminum electrode simply causes a Lorentz force to enhance mass transfer of the dissolved cations from the electrode to the bulk solution.

These observations indicate that the implementation of magnetic field may enhance performance and reduce fouling for an aluminum electrode, but leads to increased fouling rates in the case of iron electrode. Further investigation of the impact of a magnetic field on the removal performance of contaminants from synthetic and real PW effluent in EC system was carried out. Electrochemical treatment was performed in batch experiments using the same flow through EC

system used in conventional EC studies, but with a magnet of 0.13 Tesla mounted on one side or two magnets of the same magnetic strength on the both sides of the EC reactor. The EC setup with magnetic field is illustrated in Figure [30]. The magnet was mounted in a position so that the magnetic field will be parallel to the electrodes in the EC cell. In this way, the magnetic field and the current flow between electrodes will be perpendicular.

The impact of magnetic field on the total amount of aluminum cation generated in the system and the amount dissolved (not coagulated) are showing in Figure [31]. We can distinguish that the amount of total aluminum dissolved in the system is higher than the expected theoretical amount calculated from the Faraday's law of electrolysis. In addition, the total amount of dissolved aluminum in the presence of magnetic field is higher than the amount without magnet. Thus, current efficiencies of slightly greater than 100% were observed, suggesting that some non-Faradaic corrosion occurs during the EC treatment and this non-Faradaic corrosion phenomena increases in the presence of magnetic field.

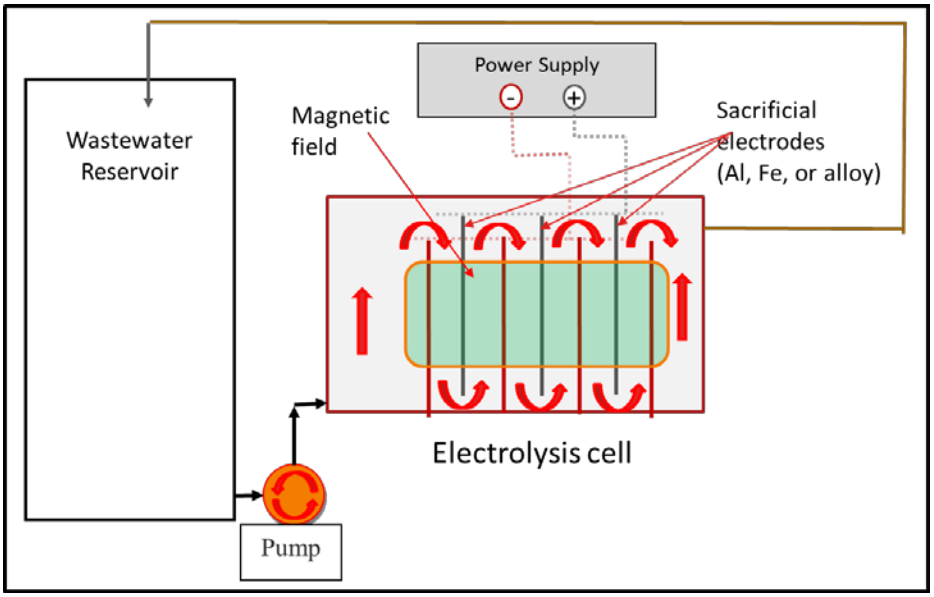

Figure [30]. Schematic diagram of the EC system with magnet.

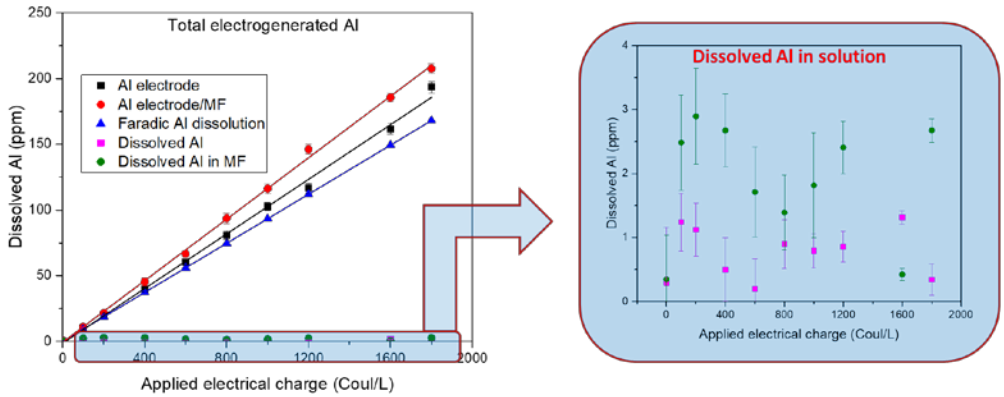

Figure [31]. Theoretical dissolution of aluminium in Al-EC cell as compare with the experimental amount in the present and absent of magnetic field.

During treatment of synthetic produced water using aluminum electrodes, the contaminants (SiO_2, Ca^{2+}, Mg^{2+} and S^{2-}) removal increased slightly in an applied magnetic field compared to the results obtained from EC without magnetic field or EC with air bubbling in the reactor (Figure [32]). Thus, sparging with air will provide dissolved oxygen and an oxidizing environment, that help to reduce the effect of organic contaminants which inhibit the removal of inorganics. As expected, the results showed that the removal performance was slightly enhanced by bubbling air in the reactor. However, the presence of magnet in EC system with Al electrode, further increases the removal rate of contaminants, especially at the initial stage of the removal processes.

Moreover, investigation on silica removal during EC treatment using real produced water indicates similar behavior with those found in synthetic produced water. The application of magnetic field enhances the removal performance of silica in EC system with Al electrode (Figure [32]). By applying 0.13 tesla magnetic field strength the percentage removal of silica reached 86.5% with charge loading of 400 Coul/L, that is about 2-fold higher than the percentage removed without magnet (45.6%). The increase in removal rate of contaminants (SiO_2, Ca^{2+}, Mg^{2+} and S^{2-}) in the present of magnetic field (Figure [32]) can be considered important for both reduced treatment time, and a reduction in the fouling formation thus reducing energy cost and operational issues. Applying two magnets (0.13 tesla) from each side of the reactor, was found to reduce the rate of silica removal compared to a single magnet, but still higher than the removal rate without

a magnet field (Figure [33]). The reduction in the percentage removal of silica with an increase in the magnetic field strength requires further investigation.

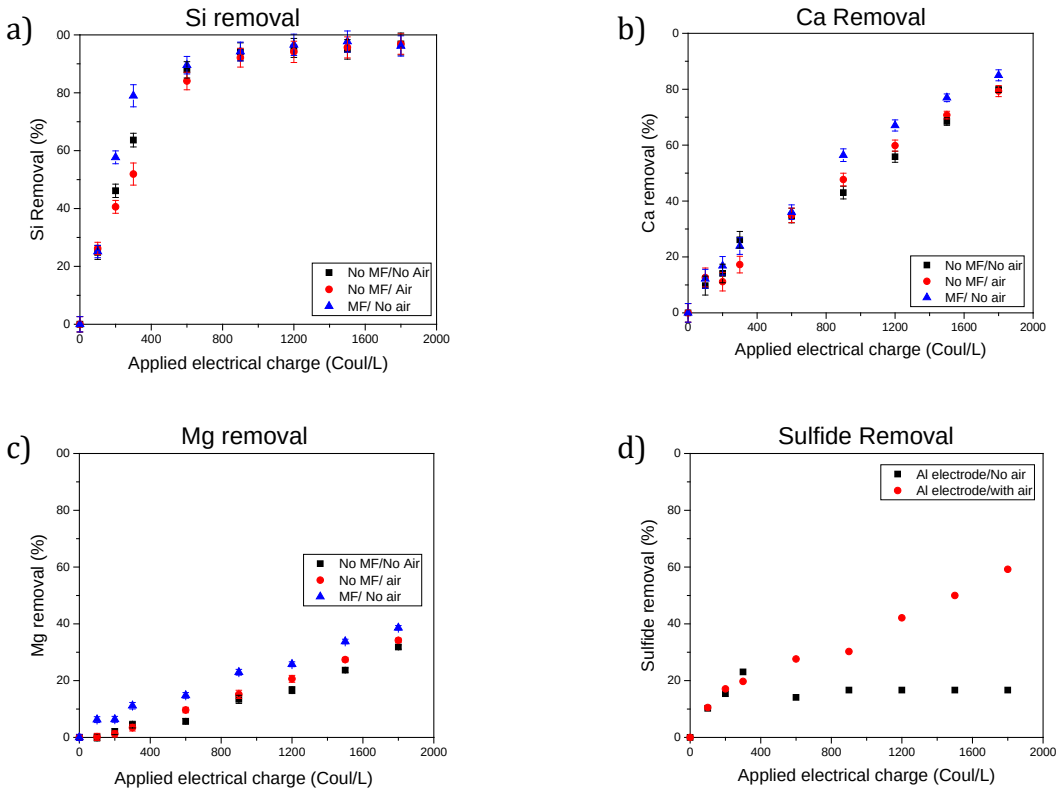

Figure [32]. Metal and Sulfide removal from Synthetic produced water. EC with/ or without a magnetic field (MF)

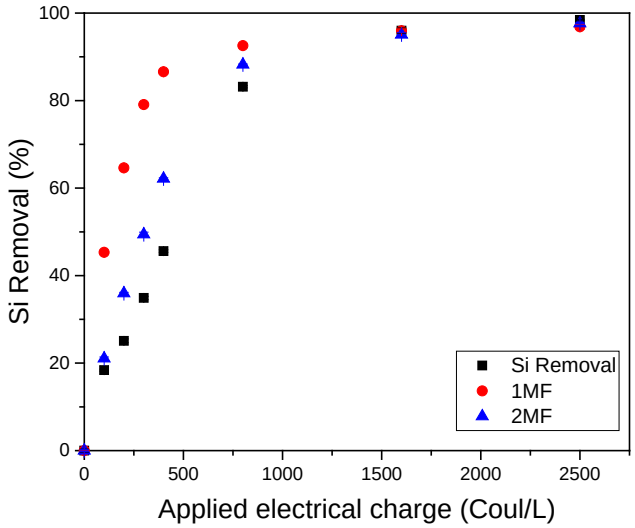

Figure [33]. Silica removal from produced water with magnetic field (MF) on one and both sides of the cell.

Treatment of blowdown water

The impact of the electrode's type of either stationary aluminum or mild steel on the removal rate of various elements present in the real blowdown water was investigated using design 2 EC cell, and representative results are showing in Table 3. It is clear from Table 3 that both anodes remove to certain extent silica and calcium from real blowdown water. Observing the anode surface following treatment indicate accumulation of fouling material following treatment. Figure [34] shows the anodes following the EC treatment.

The accumulated materials on electrodes after treatment as well as sludge precipitated in the EC reactor were collected for analysis. The analysis of the accumulated materials on the electrodes and the sludge were performed via ICP-OES (ICP-OES Vista Pro Axial, Varian, Australia). A proper adjustment was taken to meet the standard ICP-OES analytical requirement for sulfur (see supplementary information). Samples (100mg) were digested by adding 1.5 mL of HNO_3 (70%) and 3.5 mL of H_2O_2 (30%) and heating to 50^{o}C for 4 hours, the final volume was then adjusted to 10mL. Samples were further diluted 1/10 prior to ICP analysis. Figure [35], shows the inorganic composition profiles of materials accumulated on both aluminum and mild steel electrodes, and the composition profiles of the formed sludge.

Comparison between the composition profiles of sludge and the accumulated layers indicate similarity when aluminum electrodes are used. However, when mild steel electrodes are used significant increases of iron species were appeared on the electrode surfaces which is attributed to the higher affinity of the complex coagulate to attract to the anode surface.

Table [3]: The concentration of various elements in real boiler blowdown water prior and following EC process using design 2 cell and stationary electrode.

	Original water	Mild steel electrode following charge loading of 5000C/L	Aluminum electrode following charge loading of 5000C/L
Al	0.53 ± 0.2	0.53 ± 0.2	315.4 ± 15.7
Mn	0.012	0. 012	0.09
Fe	0.89 ± 0.2	63.13 ± 3.1	0.90 ± 0.04
Mg	0.32 ± 0.1	0.13 ± 0.01	2.16 ± 0.1
Si	**133.3 ± 22.8**	**66.23 ± 3.31**	**4.35 ± 0.21**
B	226.7± 3.2	223.1 ± 11.18	216.9 ± 10.8
K	385.1 ± 6.5	374.3 ± 18.7	376.4 ± 18.8
Na	14315 ± 255	13963 ± 698	14092 ± 704
Ca	17.4 ± 0.6	6.98 ± 0.3	4.79 ± 0.23
TOC	2051.8 ± 102	1890.2 ± 95	1599.4 ± 79

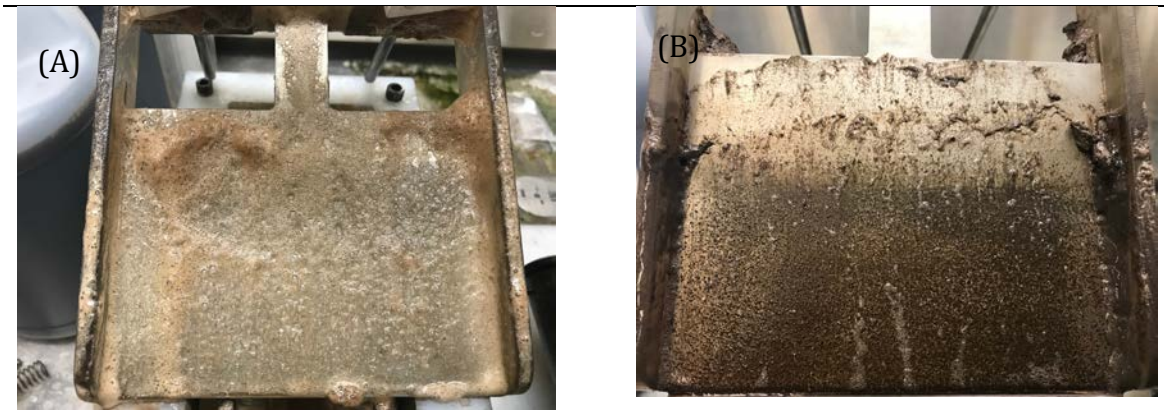

Figure [34]: A) the aluminium and B) mild steel electrodes following the EC treatment of the real blowdown water

In general, when applying a DC current to an EC reactor containing sacrificial electrodes, the anode generates coagulant species while cathode generates H_2 and hydroxide ions, respectively. However, depending on the surrounding pH conditions, the dissociated species of coagulant ions in the electrolyte medium will form an equilibrium with different species, contaminated pollutants, and hydroxide [5]. The neutrally charged accumulated species may precipitate in the bulk of the solution, whereas, still a possibility for the charged species to be attracted electrostatically to the electrode and neutralized there. These species may form an impermeable fouling layer that prevents the effective current and mass transports between the anode and cathode. Figure 35 and the corresponded Tables show the parentage and the actual amount of material found in sludges and on the electrodes following the application of the EC process using mild steel and aluminum electrodes.

After complete removal of silica from boiler blowdown, the amount of iron in both sludge and on electrodes are higher than those found when aluminum electrodes were used. This is consistent with the finding that a higher charge dose is required for silica removal with iron electrodes. A similar composition of sludge and accumulated materials on electrodes were found when aluminum electrodes are used. The concentration of silica was similar in both the sludge and in the fouling layer on the electrode for all experiments. However, when mild steel electrodes are used, the accumulated materials on electrode containing higher iron percentage. This result indicates that when a mild steel electrode is used, the formed coagulant/coagulate complexes obtain electrostatic charge that attracted toward the electrode surface. These species may enhance eventually the formation of fouling layers that reduce the efficiency of the EC process.

In this project, to prevent the formation of fouling layer we tried various approaches such as the application of polarity reversal (PR), electrode oscillation, application of magnetic field and compare the composition of sludges and the fouling layers.

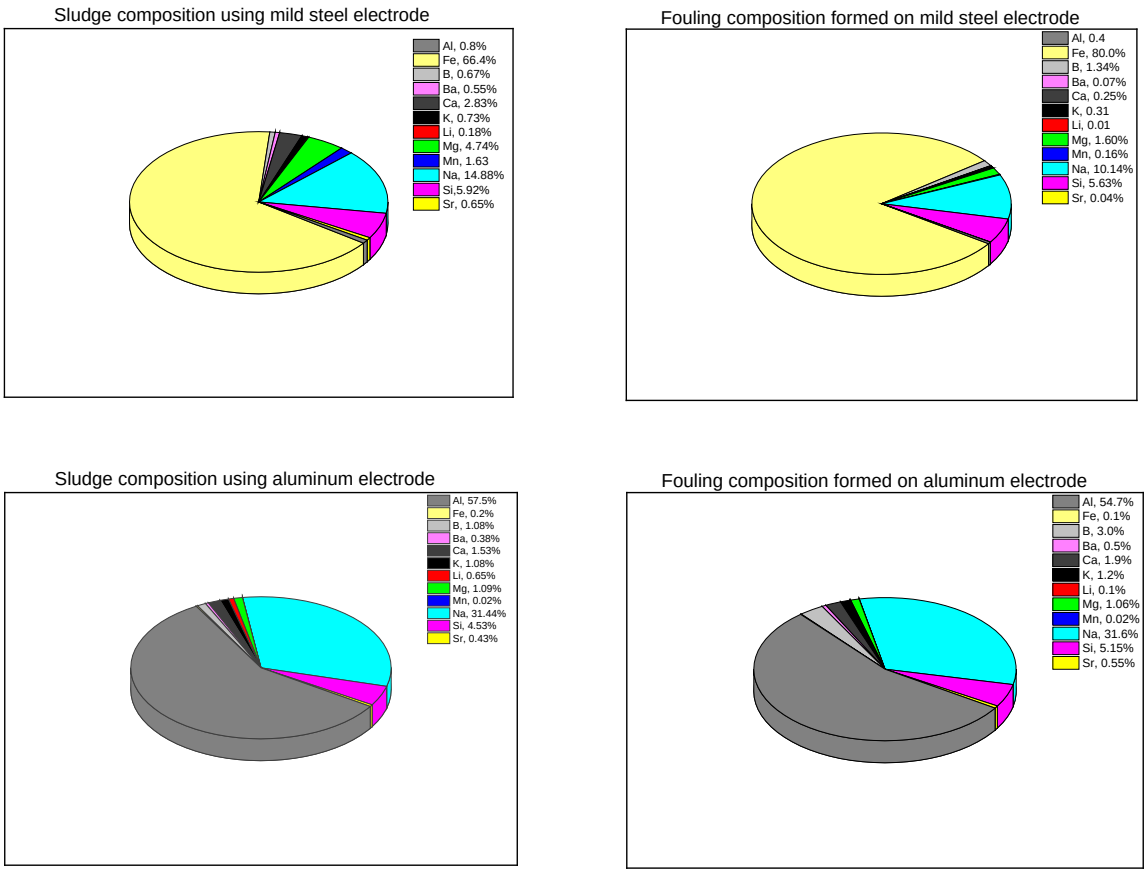

Figure [35]. The concentration of various elements in sludge and on electrode surfaces following the EC treatment of real boiler blowdown water. The charge loading was 5000 C/L using design 2 EC cell with stationary electrodes of mild steel or aluminum.

Electrode fouling analysis

	Al	Fe	B	Ba	Ca	K	Li	Mg	Mn	Na	Si	Sr
Fe (mg/l)	12.7	2367.8	39.6	1.97	7.3	9.2	0.3	47.3	4.7	299.9	166.5	1.2
Fe (%)	0.4	80.0	1.34	0.07	0.25	0.31	0.01	1.60	0.16	10.14	5.63	0.04
Al (mg/l)	1116.4	2.6	62.4	10.4	39.4	24.6	1.9	21.6	0.3	644.7	105.0	11.2
Al (%)	54.7	0.1	3.06	0.51	1.93	1.20	0.10	1.06	0.02	31.59	5.15	0.55

Sludge analysis

Electrode	Al	Fe	B	Ba	Ca	K	Li	Mg	Mn	Na	Si	Sr
Fe (mg/l)	21.9	1803.0	18.2	14.8	76.7	19.8	4.8	128.7	44.4	404.0	160.7	17.5
Fe (%)	0.8	66.4	0.67	0.55	2.83	0.73	0.18	4.74	1.63	14.88	5.92	0.65
Al (mg/l)	1318.0	5.5	24.7	8.6	35.0	24.8	14.8	25.0	0.4	720.1	103.7	10.0
Al (%)	57.5	0.2	1.08	0.38	1.53	1.08	0.65	1.09	0.02	31.44	4.53	0.43

In-situ Raman electrode fouling analysis

In-situ Raman spectra of fouling layer formed on the electrode during EC process was obtained using a specially designed 3-electrode EC cell (Figure [36]). The cell was designed and printed in the 3D printer using polycarbonate filament. The cell volume was 5 mL with either an aluminum or mild steel working electrode, Ag/AgCl (3 M KCl) reference electrode, and a platinum wire counter electrode. The uncovered contact surface area of the working electrodes is 20mm^2.

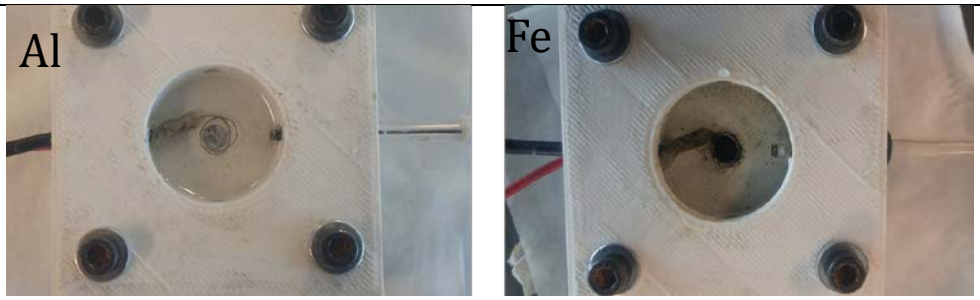

Figure [36]. Three-electrode EC cell used for in-situ Raman spectroscopy analysis.

In-situ Raman spectra collected during the electrolysis of synthetic produced water are presented in Figure [37]. Analysis of these spectra indicates the formation of polysulfur (S_8) and S_3^- on both type of electrodes (Al and Fe). However, a stability study of these peaks is under investigation on both type of electrodes. In addition, on mild steel electrode, the spectra indicate the formation of iron oxides (Fe_3O_4) and iron sulfide (FeS). Whereas, on aluminum electrode no evidence of Al_2S_3 which is chemically unstable compound in aqueous electrolyte, but a shoulder at 526nm appeared which is may be due to the formation of Al-O-Si bonding. The presence of sulfur groups on both aluminum and iron electrodes are in agreement with ex-situ investigation using SEM/EDS and ex-situ Raman results, and may due to the oxidation of sulfide species in

synthetic produced water to form stable complexes that cause electrode fouling. Further studies concerning the stability of the formed species on electrodes are ongoing.

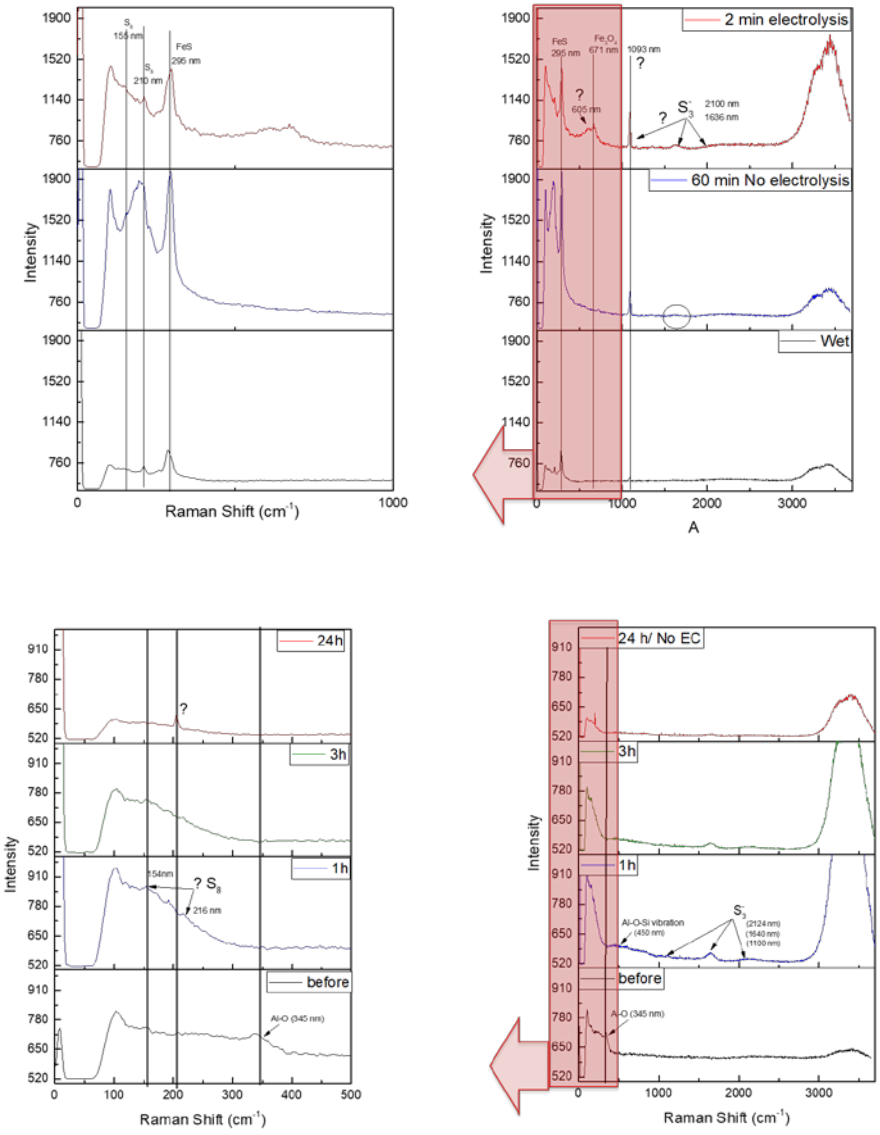

Figure [37]. Raman spectra collected from electrode surface in-situ during EC treatment of synthetic PW effluent.

The impact of polarity reversal on EC treatment of boiler blowdown water

The performance of EC with polarity reversal using both mild steel electrodes and aluminum electrodes were evaluated with real boiler blowdown samples and compared with those of direct current application. The silica removal rates and the total organic contents (TOC)

removal, as well as the inorganic/organic distributions in sludges, electrode surfaces and foams were monitored. Discussion on the silica removal as well as the inorganic distribution will be presented in this section, whereas, the organic analysis will be furnished in task C.

Figure [38] shows the percentage removal of both silica and TOC from the real blowdown samples applying a direct current and compared with a periodic polarity reversal current using mild steel and aluminum electrodes. A polarisation period of 20 seconds was chosen based on a a trade-off between the fouling and the filterability of the produced sludge. During treatment using aluminum electrodes, the removal rate of both Si and TOC in the polarity reversal experiment was slightly similar to those obtained using DC current but more efficient as compared with the mild steel electrodes. Moreover, with the mild steel electrodes, polarity reversal exhibits better performance for both Si and TOC removal as compared with the direct current. For example, applying 2500 C/L for the real boiler blowdown samples the percentages of silica removed were 98.4 and 98.5% when Al electrodes were used with both PR and DC, respectively, compared with 25.7 and 57.7% removal at the same charge loading using mild steel electrodes.

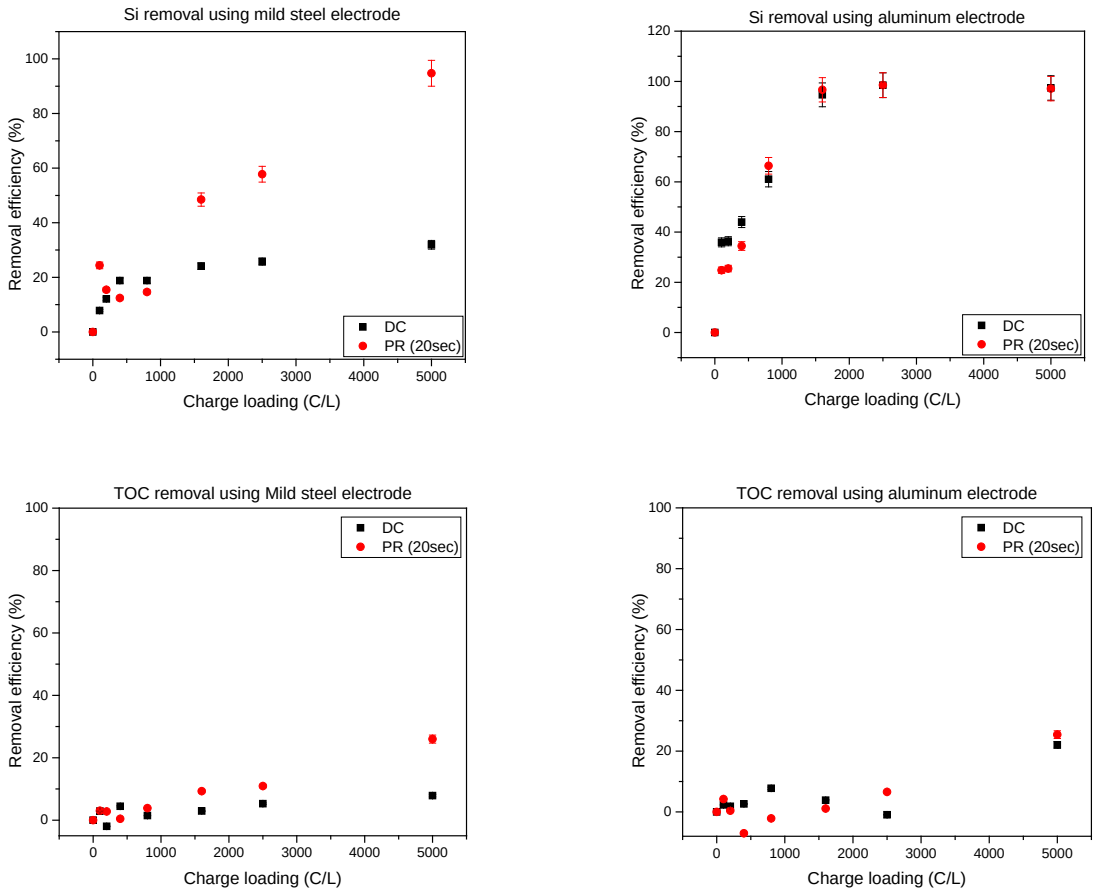

Figure [38]. Percentage of silica and TOC removals from real boiler blowdown water using; Mild steel and aluminum electrodes applying either polarity reversal or direct current. The initial silica concentration was 133.3 ± 22.8 ppm, initial TOC was 2051.8 ± 102 ppm, initial pH 8.2, solution flow rate 170 mL/min and the operating current density of 8 mA cm^{-2}.

It is worth at this point to monitor the composition of sludges as well as the accumulated materials on the electrode surface during treatment which may give insight about the chemistry of the EC processes when mild steel or aluminum electrodes were used in the EC process. Tables 4 and 5 represents the percentage of inorganic composition of sludges that are formed in the reactors and the solid accumulated on anodes following EC process. Studying the sludge composition (Table 4), indicate that when a mild steel electrode was used the amount of iron species nearly constant (about 66.4% of the total sludge composition) after treatment applying both DC and PR. However, monitoring the composition of the accumulated species on the electrode surfaces (Table 5) show that the percentage of iron species dramatically reduced when PR system is used (66.5%)

as compared with DC (80.0%). Moreover, considering the silica content on electrode surfaces, the data show nearly double the amount on the electrode when the DC system is used (5.6%) as compared with PR system (2.7%). These results indicate that the application of DC may lead to a more rapid build-up of silica containing a fouling on the electrodes. These layers may compose of iron complexed with silica and other species present in blowdown water which will reduce the EC efficiency.

Table [4]: Sludge composition

		Al	Fe	B	Ba	Ca	K	Li	Mg	Mn	Na	Si	Sr	Total
Direct current	Fe	0.8	66.4	0.6	0.5	2.8	0.7	0.2	4.7	1.6	14.8	5.9	0.6	100.0
	Al	57.5	0.2	1.1	0.4	1.5	1.1	0.6	1.1	0.02	31.4	4.5	0.4	100.0
Polarity reversal	Fe	0.5	66.9	1.0	0.6	2.5	0.9	0.2	0.3	1.8	22.3	2.2	0.7	100.0
	Al	48.3	2.0	1.1	0.5	1.6	1.5	0.7	1.2	0.07	36.7	5.7	0.5	100.0

Table [5]: Fouling layers formation

		Al	Fe	B	Ba	Ca	K	Li	Mg	Mn	Na	Si	Sr	Total
Direct current	Fe	0.4	80.0	1.3	0.1	0.2	0.3	0.01	1.6	0.16	10.1	5.6	0.04	100.0
	Al	54.7	0.1	3.06	0.5	1.9	1.2	0.1	1.0	0.02	31.6	5.1	0.5	100.0
Polarity reversal	Fe	0.2	66.5	2.8	0.3	1.3	1.2	0.01	0.1	1.36	23.1	2.7	0.3	100.0
	Al	43.9	1.7	2.7	0.5	2.1	1.8	0.05	1.0	0.06	34.8	10.6	0.5	100.0

The impact of polarity reversal and oscillation on the treatment of boiler blowdown water

To enhance the mass transfer and reduce the fouling formation on electrode surface during the EC treatment of blowdown samples, we performed anode oscillation in addition to polarity reversal systems using both mild steel electrodes and aluminum electrodes. The obtained results then compared with those of direct current application. The silica removal rates and the total organic contents (TOC) removal, as well as the inorganic/organic distributions in sludges, electrode surfaces were monitored.

Figure [39] shows the percentage removal of silica from the real blowdown samples using oscillation system with both direct and periodic polarity reversal current using mild steel and

aluminum electrodes. A polarization period of 20 seconds was chosen for these studies to minimize fouling effects without compromising the ease of separation of the sludge. Irrespective of the system used of direct current, rapid polarity reversal, aluminum or mild steel electrodes, the silica removal increased when the anode was oscillated compared to the results obtained from a stationary anode.

Using aluminum electrodes, although the percentage of silica removal increased by oscillating the anode the removal rate without oscillation were already high as compared with mild steel electrodes. However, with an aluminum electrode, the oscillation accelerates the removal rate of silica only at the initial stages of the EC process. For example, using an oscillating aluminum anode the silica removal with DC current system was 87% after charge loading of 800 C/L and reached a maximum (> 95% removal) after charge loading of 1600 C/L, whereas with a stationary anode the silica removal was 61% at 800C/L and reached a maximum after charge loading of 2500 C/L.

Considering, however, the mild steel electrodes, the maximum removal of 60.3% was reached with oscillating anode after direct current charge loading of 5000C/L, whereas, only 31.9% was removed after the same charge loading with a stationary anode. Applying polarity reversal, however, the maximum removal (>95%) was reached after charge loading of 1600C/L when the anode was oscillated as compared with the 5000C/L when the electrode was stationary. At this stage, we could well establish that in EC reactors, to achieve a high rate of electrochemical reaction and a high rate of mass transfer, a dynamic flow of reactants should be provided at the electrode-solution interface.

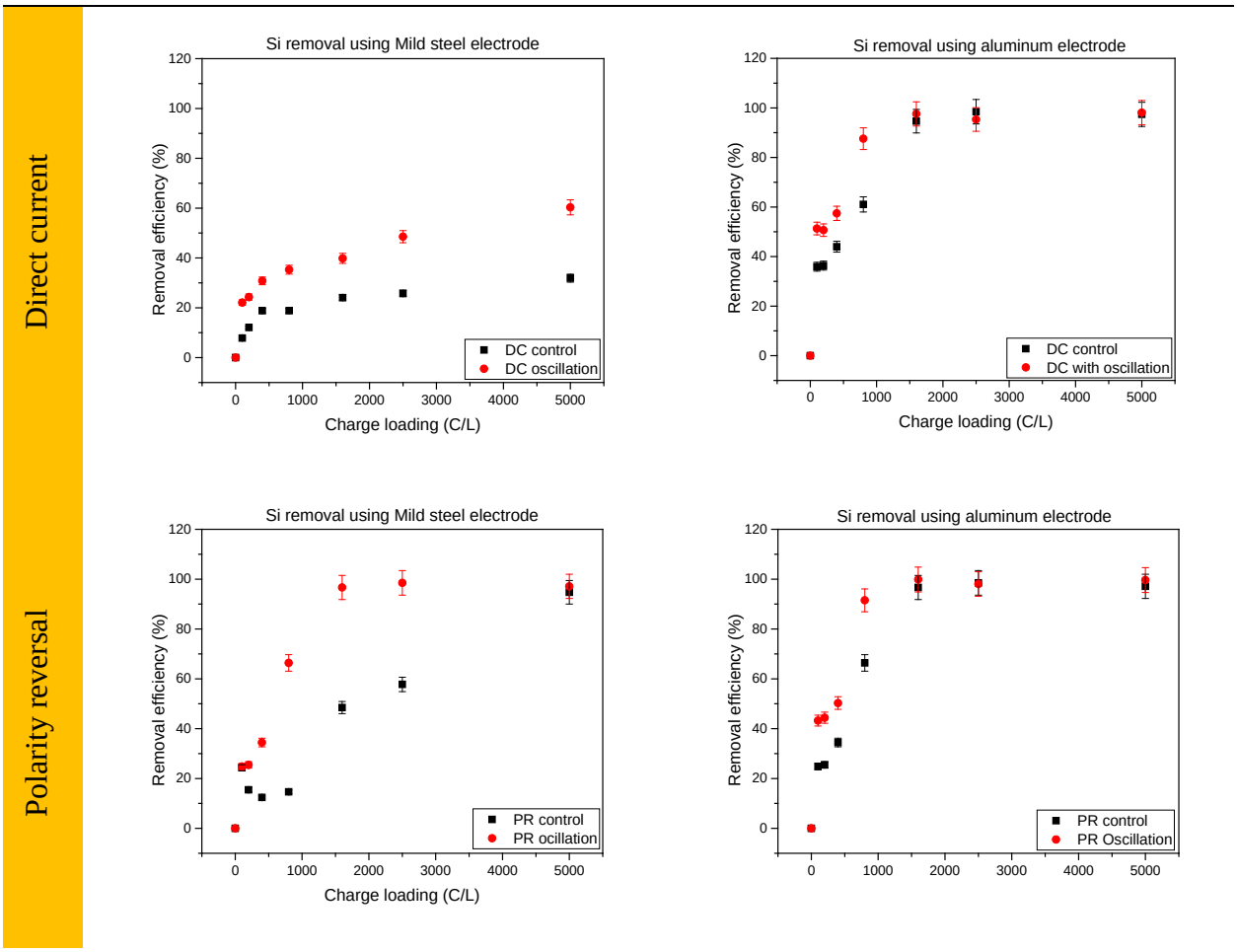

Figure [39]. Percentage of silica removals from real boiler blowdown water using; Mild steel and aluminum electrodes applying either direct current or polarity reversal. The initial silica concentration was 133.3 ± 22.8 ppm, initial pH 8.2, solution flow rate 170 mL/min and the operating current density of 8 mA cm^{-2}.

Monitor the composition of the accumulated materials on the electrode surface after treatment will give insight about the chemistry of the EC processes when either of mild steel or aluminum electrodes were used in the EC process. Tables 6 & 7 below represent the percentage of inorganic composition of the inorganic materials accumulated on anodes following EC process. During both, the direct current and reversed current applications, using mild steel electrodes the amount of iron species is slightly higher when the electrodes oscillated. At the same time, the percentage of silica reduced from 5.6% when the electrode was stationary with direct current to nearly constant values in the range 2.2-3.0% by oscillation. These results indicate that the oscillation of mild steel electrodes may help to increase the efficiency of silica removal but has no

impact on the fouling layer formation. Considering, on the other hand, the oscillation of an aluminum electrode, although there are no significant changes in the percentage of both aluminum and silica accumulated on the electrode when polarity reversal was used, there was a slight variation in the both elements when direct current is applied. These differences consider within the experimental error that show no indications for a significant improvement in treatment.

Table 6. Fouling layers composition, direct current

		Al	Fe	B	Ba	Ca	K	Li	Mg	Mn	Na	Si	Sr	Total
Stationary	Fe	0.4	80.0	1.3	0.1	0.2	0.3	0.01	1.6	0.16	10.1	5.6	0.04	100.0
	Al	54.7	0.1	3.06	0.5	1.9	1.2	0.1	1.0	0.02	31.6	5.1	0.5	100.0
Oscillation	Fe	0.1	88.3	0.53	0.1	0.05	0.04	0.0	0.1	0.04	8.2	2.5	0.01	100.0
	Al	50.3	0.2	2.93	0.6	2.1	1.4	0.1	1.6	0.01	35.6	4.5	0.5	100.0

Table 7. Fouling layers composition, polarity reversal

		Al	Fe	B	Ba	Ca	K	Li	Mg	Mn	Na	Si	Sr	Total
Stationary	Fe	0.5	66.9	1.0	0.6	2.5	0.9	0.2	0.3	1.8	22.3	2.2	0.7	100.0
	Al	48.3	2.0	1.1	0.5	1.6	1.5	0.7	1.2	0.1	36.7	5.7	0.5	100.0
Oscillation	Fe	0.1	70.0	0.9	0.4	2.0	0.7	0.1	0.7	1.7	19.6	3.0	0.6	100.0
	Al	48.6	0.5	1.1	0.4	1.6	1.4	0.7	1.2	0.02	38.4	5.5	0.5	100.0

The impact of polarity reversal and magnetic field on the treatment of boiler blowdown water

The application of magnetic field will exploit the principle of Lorentz force that in the presence of potential field between anode and cathode, the application of a magnetic field vertical to the electrical field will potentially create a driving force to move the dissolved cations in a direction that is vertical to both of magnetic and electrical fields (Lorentz force). This additional force will facilitate an extra motion that enhance the mass transfer of dissolved cation in an area close to the interface. Preliminary indicated that the enhancement of the EC process when a magnetic field was applied to treat produced water, especially with aluminum electrodes. Less fouling layers was formed on an aluminum electrode with increasing magnetic field strength. However, using a mild steel electrode, the implementation of a magnetic field enhanced fouling

formation. When a mild steel electrode was used along with an applied magnetic field, however, the magnetic field enhanced the magnetization process of both iron electrode surface as well as the precipitated iron species to result in enhancing the attraction of ferromagnetic particles to the electrode surface. Aluminum is a non-magnetic metal, so the magnetic field will not have any direct influence on the precipitated particles or the aluminum electrode. Hence the application of a magnetic field enhances the implementation of Lorentz force to accelerate the mass transfer of the freshly dissolved cations from electrode toward electrolyte.

As we discussed in the earlier section for produced water treatment, the implementation of a magnetic field may enhances the performance of the EC process and reduce the fouling of the aluminum electrode. Whereas, the application of magnetic field leads to increase fouling rates in the case of a mild steel electrode. Further investigation of the impact of a magnetic field on the remediation performance of blowdown water in the EC system was carried out. Electrochemical treatment was performed in batch experiments using the same EC system applying direct current and with polarity reversal, but with a magnet of 0.13 Tesla mounted on both sides of the EC reactor. The EC setup with a magnetic field is illustrated in previously in Figure [40]. The magnet was mounted in a position so that the magnetic field will be parallel to the electrodes in the EC cell. In this way, the magnetic field and the current flow between electrodes will be perpendicular.

During treatment of the real blowdown water using aluminum electrodes, the removal of silica increased slightly in an applied magnetic field compared to the results obtained from EC without magnetic field at either direct current or with polarity reversal (Figure [40]). The impact of oscillation in addition to the applied magnetic field was also investigated in this report. Thus, oscillating the electrode will provide extra mass transfer which is, in theory, will reduce fouling. Although oscillation provided a good tool to enhance the mass transfer and thus provide better efficiency (See Figure 40), the percentage of materials that are accumulated on the electrodes are also significantly impacted (see Tables 8 & 9 below). For example, during both, the direct current and polarity reversal treatment, using aluminum electrodes the amount of Al and Si species are less when the electrodes were exposed to magnetic field and oscillation. The percentage of silica reduced from 5.1% when the electrode was stationary with direct current to about 4.4% when a magnetic field was applied and to 2.55% when both MF and oscillation were used. A similar trend was also found for the direct current system. Thus, the increase in removal rate of silica in the presence of a magnetic field, and the reduction of fouling formation can be considered important

for reduced treatment time, and to extend the processing time thus reducing energy cost and operational issues.

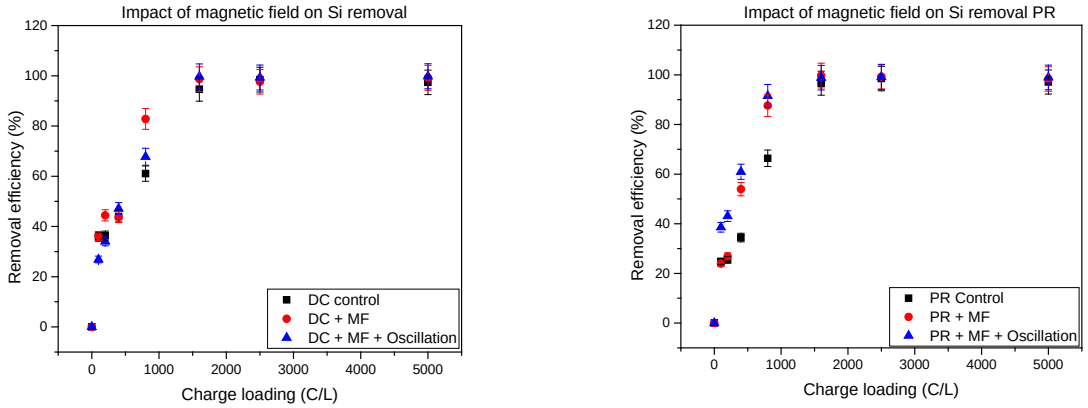

Figure [40]. The impact of magnetic field and oscillation on the percentage of silica removals from real boiler blowdown water using aluminum electrodes applying either direct current or polarity reversal. The initial silica concentration was 133.3 ± 22.8 ppm, initial pH 8.2, solution flow rate 170 mL/min and the operating current density of 8 mA cm^{-2}.

TABLE 8. FOULING LAYERS COMPOSITION, DIRECT CURRENT

	Al	Fe	B	Ba	Ca	K	Li	Mg	Mn	Na	Si	Sr	Total
Stationary	54.7	0.1	3.06	0.5	1.9	1.2	0.1	1.0	0.02	31.6	5.1	0.5	100.0
MF	53.3	0.2	2.50	0.4	1.4	1.3	0.04	2.6	0.02	33.4	4.4	0.3	100.0
MF + oscillation	17.8	0.1	1.78	0.20	1.1	1.1	0.05	0.28	0.01	74.78	2.55	0.2	100.0

TABLE 9. FOULING LAYERS COMPOSITION, POLARITY REVERSAL

	Al	Fe	B	Ba	Ca	K	Li	Mg	Mn	Na	Si	Sr	Total
Stationary	43.9	1.7	2.7	0.5	2.1	1.8	0.05	1.0	0.06	34.8	10.6	0.5	100.0
MF	64.5	0.3	2.9	0.3	1.4	0.8	0.06	1.3	0.03	23.1	4.6	0.4	100.0
MF + oscillation	22.8	0.1	1.9	0.3	1.3	1.6	0.04	0.6	0.01	65.7	5.2	0.3	100.0

Summary of progress on Task B

Bench-scale testing of EC treatment on synthetic produced water and real blowdown water indicated that aluminum electrodes removed silica more rapidly than mild steel. The application of our innovative systems of; 1) rapid polarity reversal, 2) oscillating electrode and 3) application of magnetic field, enhanced the removal rate as well as reduce the fouling formation. Monitoring the percentage of accumulated material on the electrode surface following the EC process indicates that aluminum electrodes outperformed mild steel electrodes in reducing the amount of fouling materials. Moreover, treatment with polarity reversal also showed better performance as compared with direct current. However, applying a magnetic field along with oscillation, significant reduction of both aluminum and silica percentage were observed on the electrode surface. These results indicate the possible implication of our aforementioned novel approaches to reduce fouling and at the same time enhance the EC remediation process. Further investigation is required to optimize the performance of the novel systems.

References

1. Schlichting, H. and K. Gersten, *Boundary-layer theory*. 2016: Springer.
2. Cañizares, P., et al., *Study of the Electrocoagulation Process Using Aluminum and Iron Electrodes.* Industrial & Engineering Chemistry Research, 2007. **46**(19): p. 6189-6195.
3. Yasri, N.G. and S. Gunasekaran, *Electrochemical technologies for environmental remediation*, in *Enhancing Cleanup of Environmental Pollutants*. 2017, Springer. p. 5-73.
4. Panikulam, P.J., N. Yasri, and E.P.L. Roberts, *Electrocoagulation using an oscillating anode for kaolin removal.* Journal of Environmental Chemical Engineering, 2018. **6**(2): p. 2785-2793.
5. Garcia-Segura, S., et al., *Electrocoagulation and advanced electrocoagulation processes: A general review about the fundamentals, emerging applications and its association with other technologies.* Journal of Electroanalytical Chemistry, 2017. **801**: p. 267-299.

2.3 Task C. Analysis and modelling of inorganic and organic contaminants in solution, in the flocculated solids and in the electrode fouling layer.

Milestone C.1: Data on inorganic and organic composition of the samples of produced water from CNRL's Peace River Complex and blowdown from an Alberta oil-sands SAGD production site.

Milestone C.2: Data on composition of treated water, sludge and fouling layers.
Milestone C.3 Report on geochemical modelling of solution speciation, and recommended operating conditions for improved removal and reduced fouling.

Objectives:

The objective of Task C is to identify the major and the minor trace inorganic, silica and selected trace elements, as well as a comprehensive analysis of the organics in the produced water and the treated products. In addition, analytical results from fluid, sludge and fouling analyses will be used for advanced geochemical computer modeling to investigate the solution chemistry and the environmental conditions that facilitate electrode fouling. The outcome will be an improved understanding of EC contaminant removal and fouling mechanisms for the produced water and blowdown applications.

Methods and Achievements for millstone C.1 and C.2
(For clarity these two milestones are considered together).

The analyzed produced water contains a complex mixture of organic/inorganic compounds. The analysis of inorganic compounds during and after treatment in sludge, on electrodes, foams, and in solution were monitored and presented in the aforementioned task B. on the other hand, the organic compounds have a wide range of properties, including interfacial/surface active properties which can interfere with process operations. In this task, we characterized the organic composition of the produced waters from Peace River Complex and boiler blowdown water sampled from CNRL using ultra-high resolution mass spectrometry with different ionization techniques. Samples were analyzed with a Bruker 12T SolariX ultra-high resolution Fourier Transform Ion Cyclotron Resonance Mass Spectrometer (FTICR-MS) using electrospray ionization in negative ion mode (ESI-N) and atmospheric pressure photoionization in positive ion mode (APPI-P) [see Appendix for terminology explanation].

The first task was to analyze the range of organic compounds present in the produced water. The produced water when analyzed in electrospray ionization in negative ion mode (ESI-N) comprises of 39 compound classes (Fig. 41a). Of the compound classes characterized, more than half (25) of the classes containing at least one sulfur atom per molecule which reflex the sulfur

richness of the heavy oil/bitumen. A predominance of compound classes with 2 and 4 oxygen atoms per molecule was observed for the compound class groups O_x, SO_x, and S_2O_x. In addition, low abundances of organic water constituents belonging to compound class groups NO_x and NSO_x were also detected.

Produced water when characterized in atmospheric pressure photoionization in positive ion mode (APPI-P) shows a different compound class distribution (Fig. 41b). APPI-P produces protonated (PRO) ions and radical (RAD) ions. 53 compound classes (including both protonated and radical ions) were identified with about half (28) of the species containing at least one sulfur atom per molecule which again reflex the sulfur richness of the heavy oil/bitumen. The overall most abundant compound class is the SO_2 (RAD) class.

The **boiler blowdown** water when analyzed in electrospray ionization in negative ion mode (ESI-N) comprises of 31 compound classes (Fig. 42a). The boiler blowdown water is enriched in multi-oxygenated species, where class group O_x (x=2-9) is the most abundant detected in the water. Similar trends of multi-oxygenated species were observed in APPI-P ion mode, with about 31 compound classes.

A comparison of the produced and boiler blowdown water shows that boiler blowdown is about four times as concentrated as the produced water sample, as observed by their measured extraction yields (Table 10, Fig. 43). The extraction yields of the produced water were measured to be 133 mg/L, in contrast to more concentrated boiler blowdown water with yield of 416 mg/L (Table 10). The ESI-N ion mode analyses of the consolidated double bond equivalent (DBE) (Fig. 44a) and carbon number (Fig. 44b) distribution reveals that the boiler blowdown water is enriched in higher DBE group species (7-24) and carbon number species (17-46), compared to the produced water. This trend indicates a higher concentration of more aromatic compounds and larger compounds in the boiler feedwater sample, compared to the produced water sample.

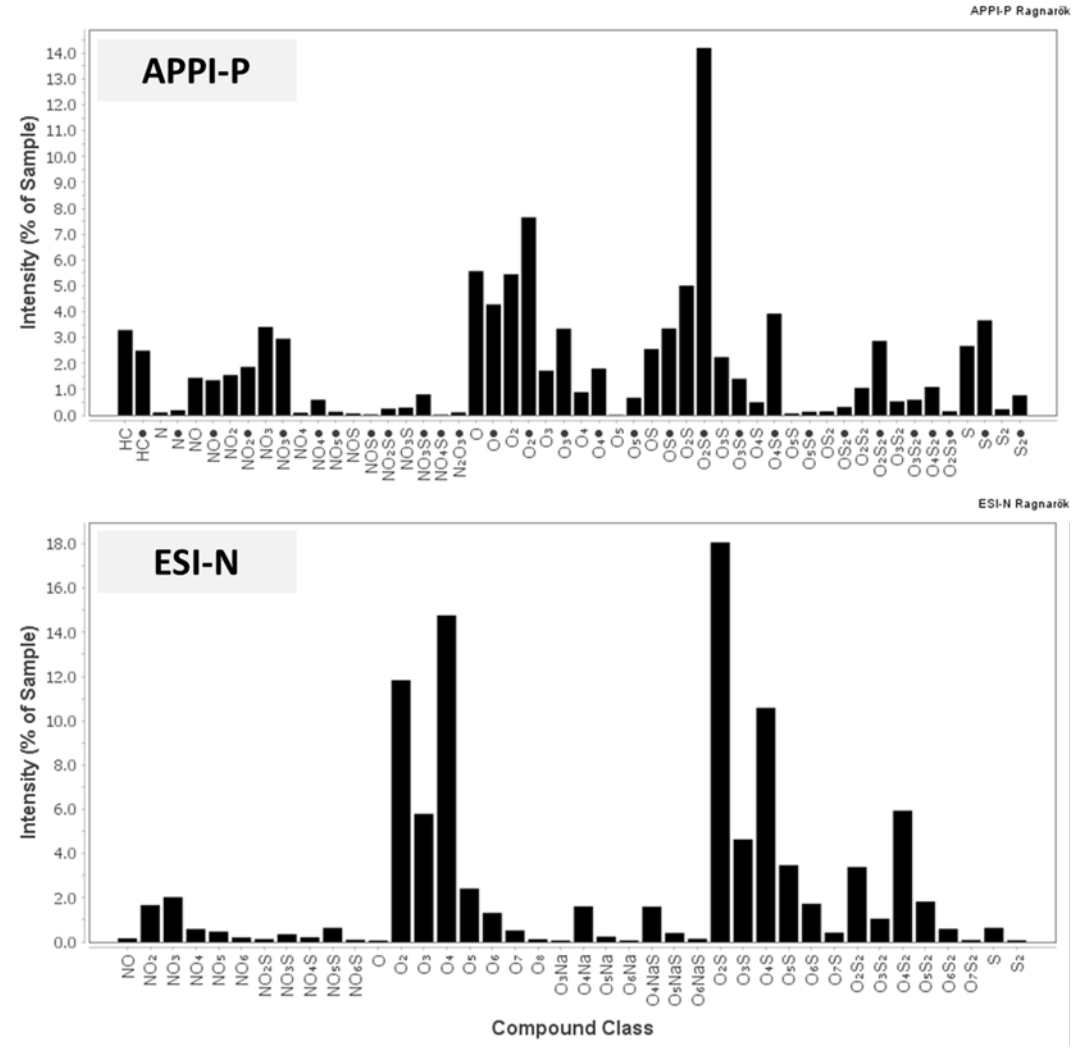

Figure [41]. Compound class distribution of the non-treated produced water sample measured in (a) APPI-P and (b) ESI-N ion modes. [In APPI-P ion mode the dot indicates radical heteroatom or hydrocarbon classes; the other classes are found as protonated species.]

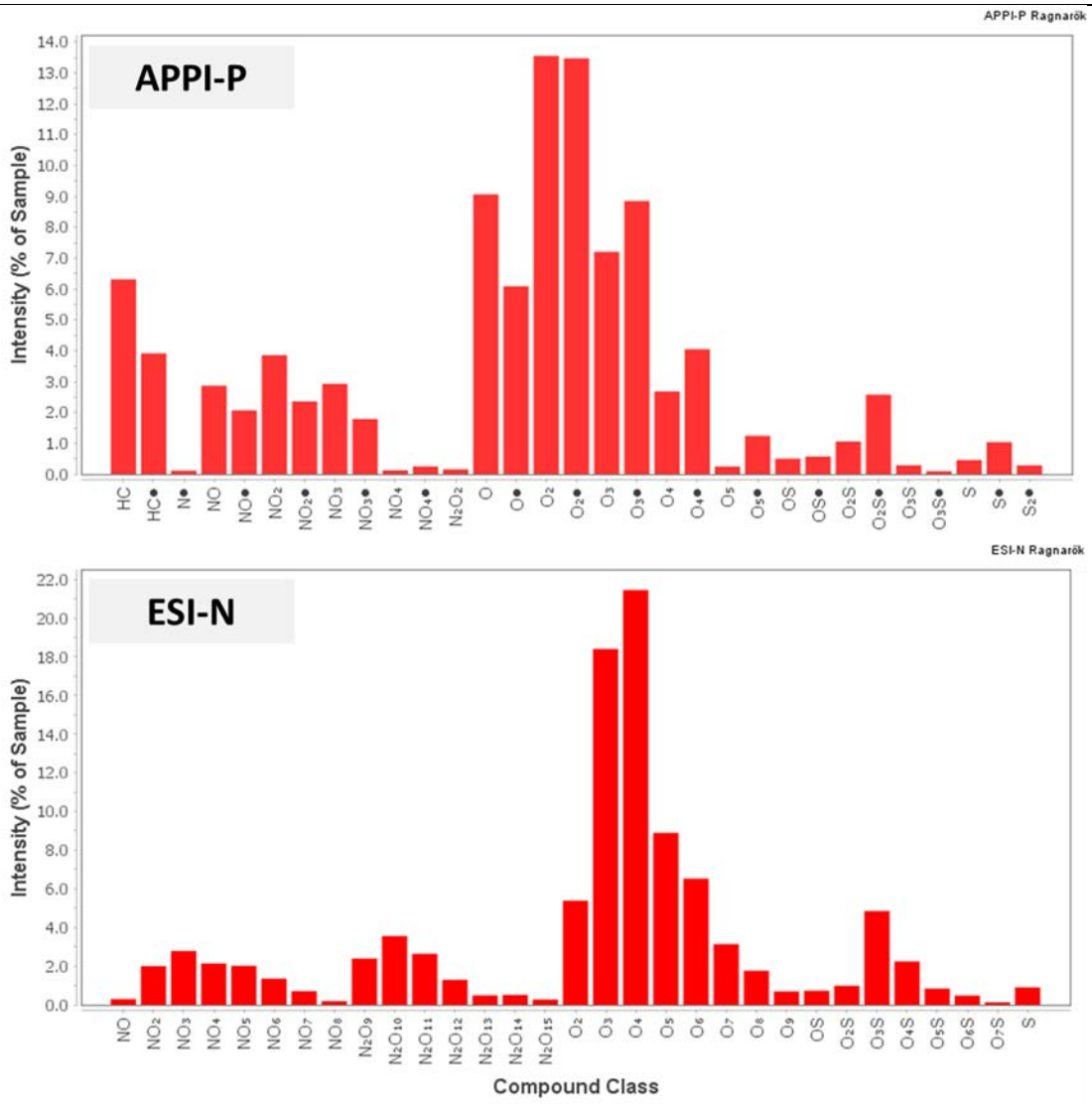

Figure [42]. Compound class distribution of the non-treated boiler blowdown water sample measured in (a) APPI-P and (b) ESI-N ion modes. [In APPI-P ion mode the dot indicates radical heteroatom or hydrocarbon classes; the other classes are found as protonated species.]

Table 10: Extraction yields of the produced water and boiler blowdown water

Sample type	Amount of sample used for extraction (mL)	Extraction yield (mg/L)

Produced water	20	133
Boiler blowdown water	20	416

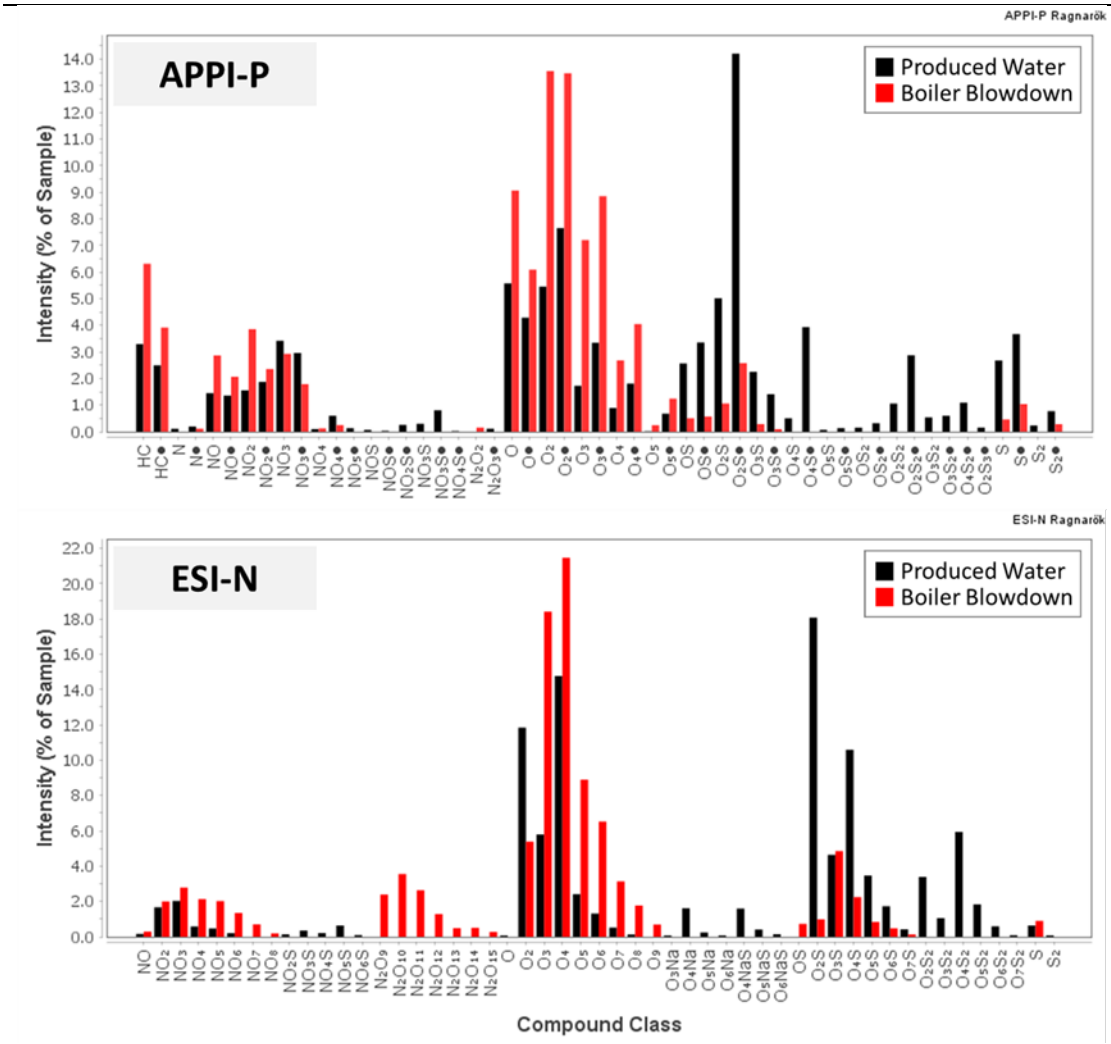

Figure [43]. Compound class distribution comparing the spectra of the non-treated produced water and boiler blowdown sample in (a) APPI-P and (b) ESI-N ion modes. [In APPI-P ion mode the dot indicates radical heteroatom or hydrocarbon classes; the other classes are found as protonated species.]

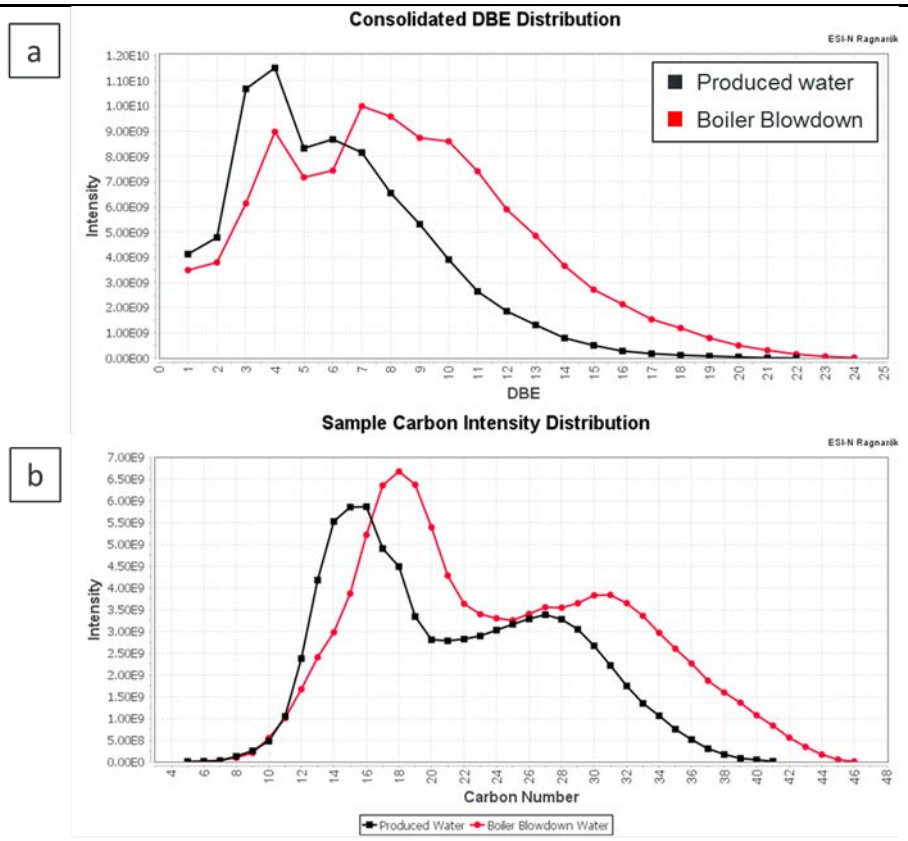

Figure [44]. (a) Consolidated DBE distribution of the non-treated produced water (black) and boiler blowdown water (red) sample measured in ESI-N ion mode; (b) overall carbon number distribution of the non-treated produced water (black) and boiler blowdown water (red) sample measured in ESI-N ion mode.

Data on organic composition of treated water, sludge and fouled electrodes from novel EC operating conditions

Method development:

During method development of organics extraction of the analyzed electro-coagulation treated produced waters, white precipitated particles were identified in the extracts (Fig. 45). Several different solvents such as water, dichloromethane, methanol, toluene, acetic acid, isopropanol alcohol and tetrahydrofuran were experimented with, in order to access the solubility of the precipitate. The precipitate however continued to remain insoluble.

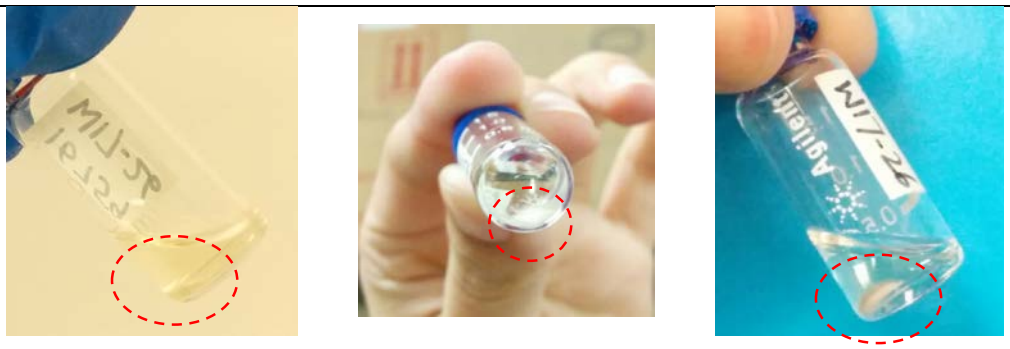

Figure [45]. Some contamination was detected after solvent extraction of the treated samples which is likely related to inorganic matter (e.g. sodium sulfate; investigation ongoing); these contaminations have impact on semi-quantitative assessment of the organic concentrations after treatment with different electrodes with and without magnetic field.

The precipitate was then analyzed via ion chromatography (IC) and inductively coupled plasma (ICP) to identify the anion and cation composition of the precipitate, respectively (Table 11). The solids comprised predominantly of sodium sulfate (Na_2SO_4) with smaller amounts of calcium and chloride present. Sodium sulfate is used during the extraction process to remove any additional water that might be present in the organic extract dissolved in dichloromethane. To prevent the addition of sodium sulfate salt to the organic extract, the experimental protocol was modified in terms of column preparation. Two frits were added to the column to capture the sodium sulfate and prevent it from eluting with the extract. The conducted test runs confirmed the efficacy of the new experimental protocol.

Table 11: The de-ionized water-soluble anion/cation (at 25°C, 30min) characterization of the precipitated particles

PRG Sample#	Anions		Cations			Salt	
	Cl	SO_4	B	Na	Ca	$Na:SO_4$	$Na:SO_4$
	(mg/L)	(mg/L)	(mg/L)	(mg/L)	(mg/L)	Measured	Expected
16759	3.4	1255.2	4.33	673.6	7.3	0.54	0.48
16690	1.1	949.3	3.99	500.8	1.5	0.53	0.48
16691	0.2	338.1	4.08	186.3	0.3	0.55	0.48
16692	0.1	390.2	6.09	201.1	0.4	0.52	0.48

Characterization of organics following EC for Produced water

The produced water treated with electrocoagulation were characterized using FTICR-MS along with the sludge and fouling layers that were developed. The original produced water and the produced water treated with iron and aluminium electrodes were analyzed for the organics using FTICR-MS.

Treated water using iron electrodes

The use of the iron electrodes for electrocoagulation of the produced water shows a strong reduction especially of compound classes containing sulfur in both ESI-N and APPI-P ion mode. In addition, in the ESI-N ion mode the decrease was also significant for the O_2, O_3, and NO_2 and NO_3 species, suggesting a potential removal during electrocoagulation treatment (Fig. 46). A closer inspection of the compound classes of the treated produced water shows a decrease in the abundance of all DBE groups in the O_2 and SO_2 classes and within each DBE group, there was a decrease observed in each of the broad carbon number ranges of the organics (Fig. 47).

The ESI-N analysis revealed that the carbon number distribution also shows a strong decrease in the overall abundances of the organics after treatment compared to the original produced water. The decrease observed around C15 and for higher carbon number organics (C# 24-38; Fig. 48).

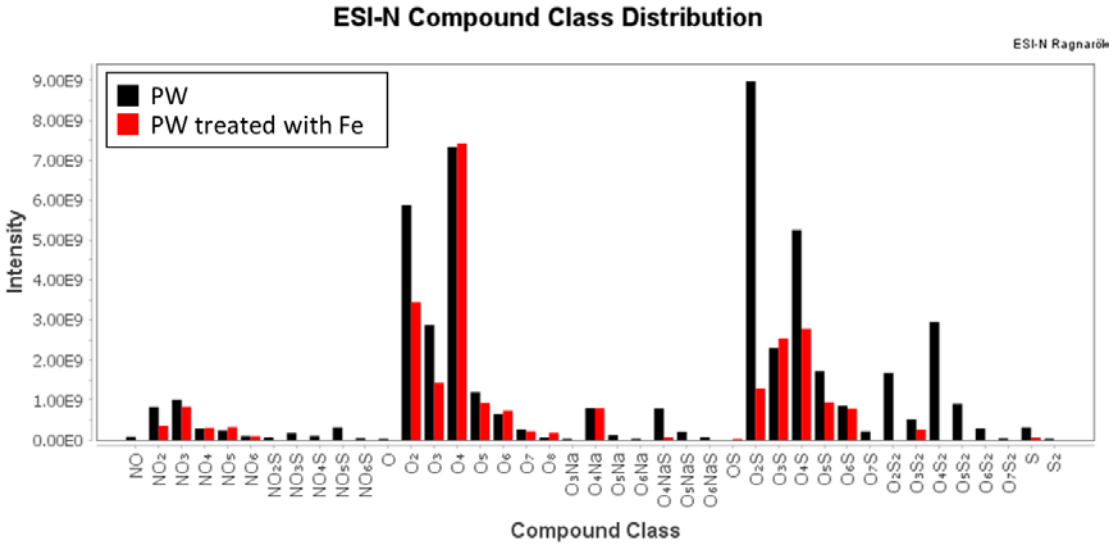

Figure [46]. ESI-N compound class distribution of the non-treated produced water sample and produced water sample treated with iron electrodes. The electrocoagulation treatment with iron showed a decrease in several compound classes, especially ones containing sulfur heteroatoms in the produced water.

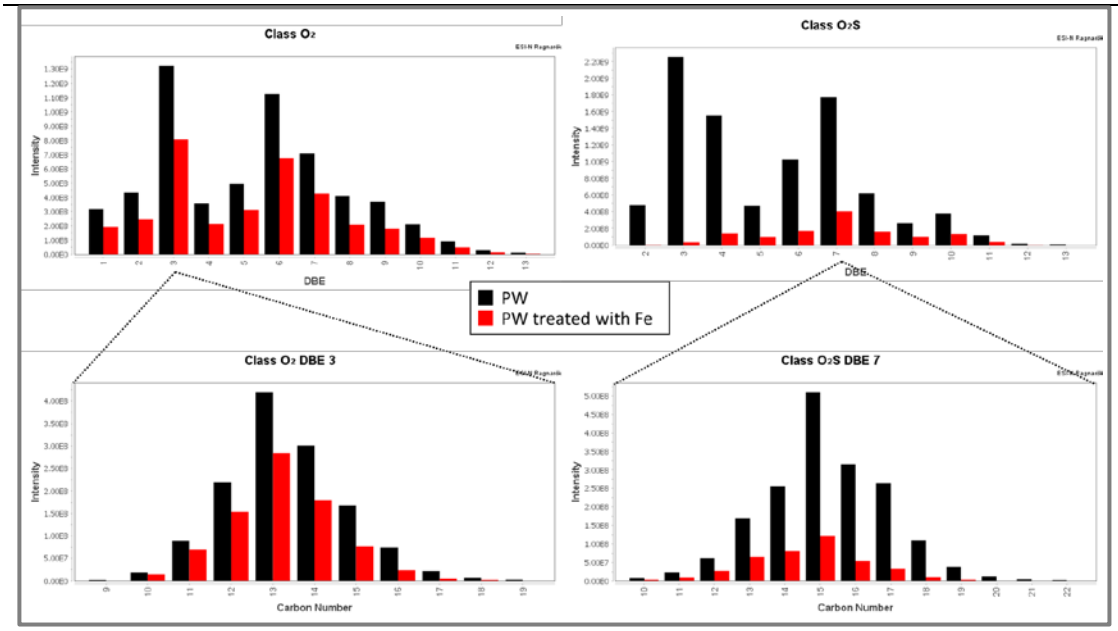

Figure [47]. ESI-N sample compound class distribution for Class O_2 and O_2S of the non-treated produced water sample and produced water sample treated with iron electrodes. The electrocoagulation treatment with iron showed a decrease in the intensity of the organics present from the produced water.

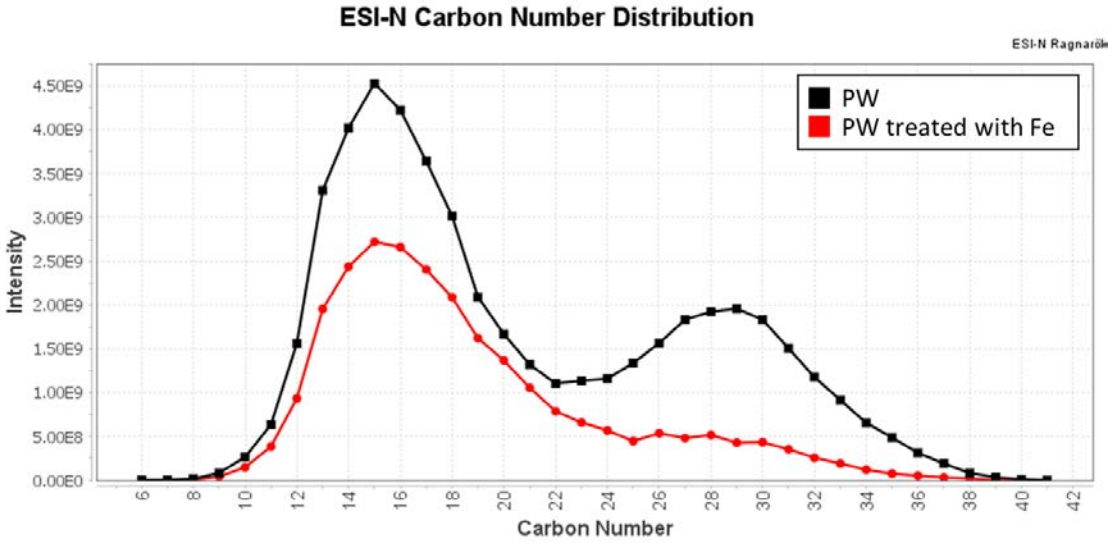

Figure [48]. ESI-N carbon number distribution of the non-treated produced water sample and produced water sample treated with iron electrodes. The electrocoagulation treatment with iron showed a decrease in the relative intensity of the organics in the produced water, especially in the higher carbon number range.

Treated water using aluminum electrodes

The use of the aluminum electrodes for electrocoagulation of the original produced water shows a decrease in only a few compound classes in both ESI-N and APPI-P ion mode. In ESI-N ion mode a significant decrease was only observed for the O_2 and O_2S species, suggesting a lower organics removal potential compared to the iron electrocoagulation treatment (Fig. 49). The ESI-N carbon number distribution also shows only a minor decrease in the relative intensity of the organics after treatment of the original produced water sample (Fig. 50).

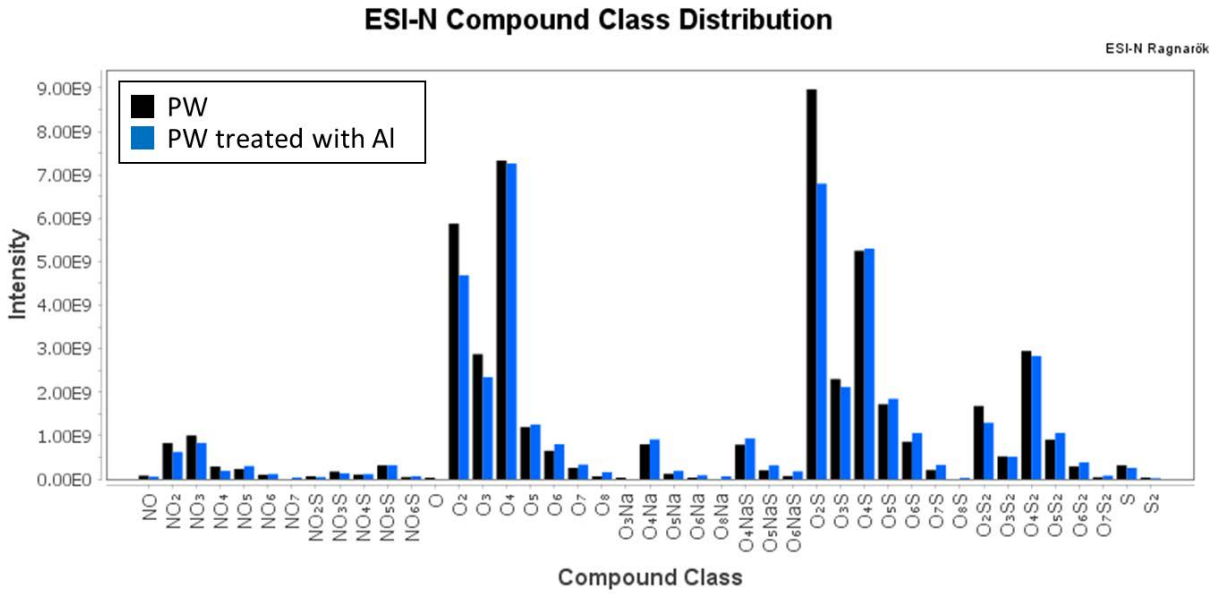

Figure [49]. ESI-N compound class distribution of the original produced water sample and the water treated with aluminum electrodes. The electrocoagulation treatment with aluminum showed only a minor decrease in a few compound classes.

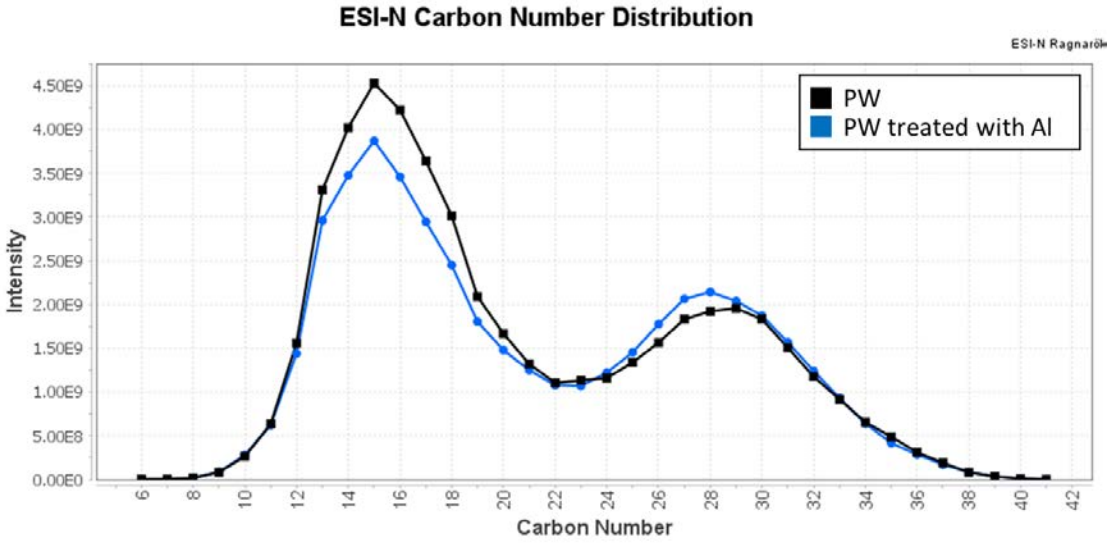

Figure [50]. ESI-N carbon number distribution of the original produced water sample and the water treated with aluminum electrodes.

Sludge

During the electrocoagulation experiments sludge was observed to form at the bottom of the electrodes. The sludge was analyzed using FTICR-MS in ESI-N and APPI-P ion mode. The sludge was observed to be made of a large part of oily components present in the produced water sample, especially hydrocarbon and sulfur containing compound classes without oxygen when analyzed in APPI-P ion mode (Fig. 51 & 52).

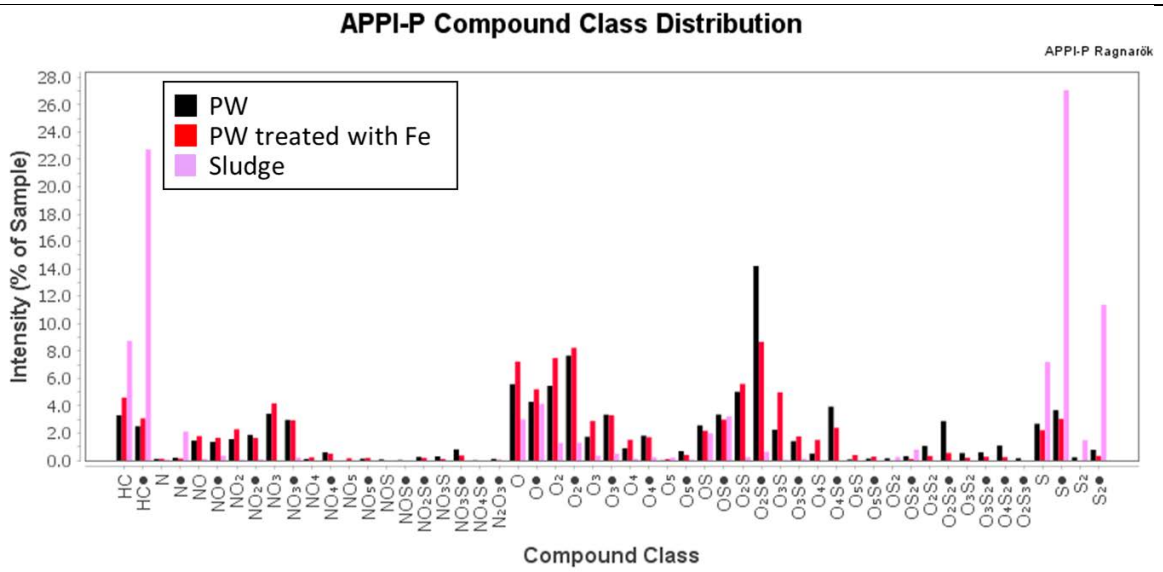

Figure [51]. APPI-P compound class distribution of the non-treated produced water sample, produced water sample treated with iron electrodes and sludge formed during electrocoagulation treatment with iron electrodes.

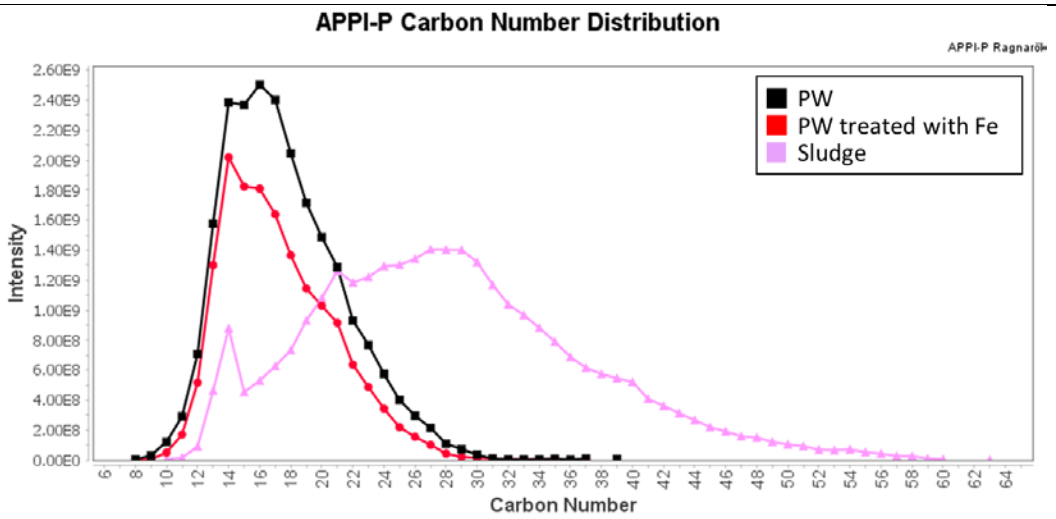

Figure [52]. APPI-P carbon number distribution of the non-treated produced water sample, produced water sample treated with iron electrodes and sludge formed during electrocoagulation treatment with iron electrodes.

The sludge showed compounds with higher carbon number (C# 10-60) relative to both original and treated produced water (C# 8-39) (Fig. 53) which attributes to the oil-like organics present in it. Since the produced water was filtered during extraction, the oil-like organics emulsified in the sample would have separated from the water before extraction. However, since the solid sludge was washed/extracted with organic solvents without any filtering possible, the oil-like organics adsorbed to the sludge were extracted. This trend was less obvious when analyzed in ESI-N ion mode for both iron and aluminum electrode treatments (Figs. 53 and 54).

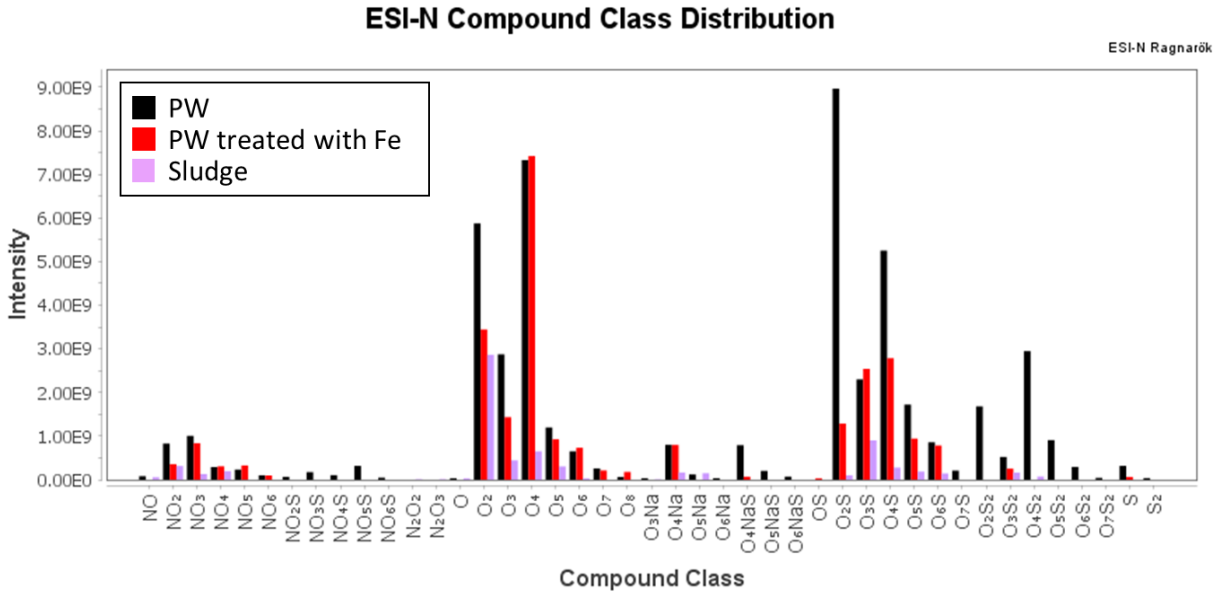

Figure [53]. ESI-N compound class distribution of the non-treated produced water sample, produced water sample treated with iron electrodes and sludge formed during electrocoagulation treatment with iron electrodes.

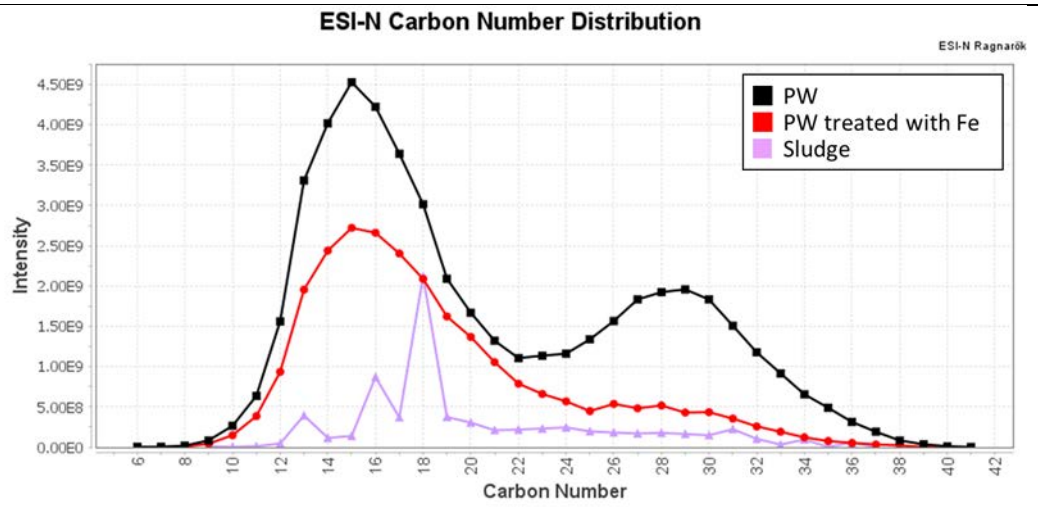

Figure [54]. ESI-N carbon number distribution of the non-treated produced water sample, produced water sample treated with iron electrodes and sludge formed during electrocoagulation treatment with iron electrodes.

The solvent extract of the sludge produced from the water treatment with aluminum electrodes contains the same compound classes when analyzed in APPI-P ion mode; however the intensities of the oil constituents are lower compared to the sludge from the iron electrodes (Figs. 55 and 56).

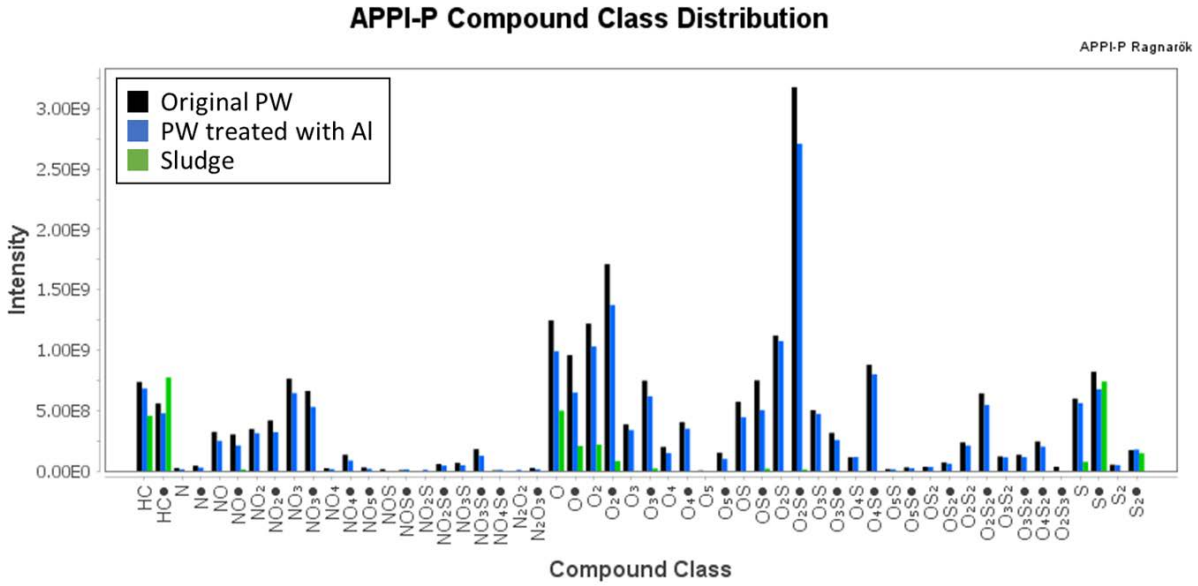

Figure [55]. APPI-P compound class distribution of the non-treated produced water sample, produced water sample treated with aluminum electrodes and sludge formed during electrocoagulation treatment with aluminum electrodes.

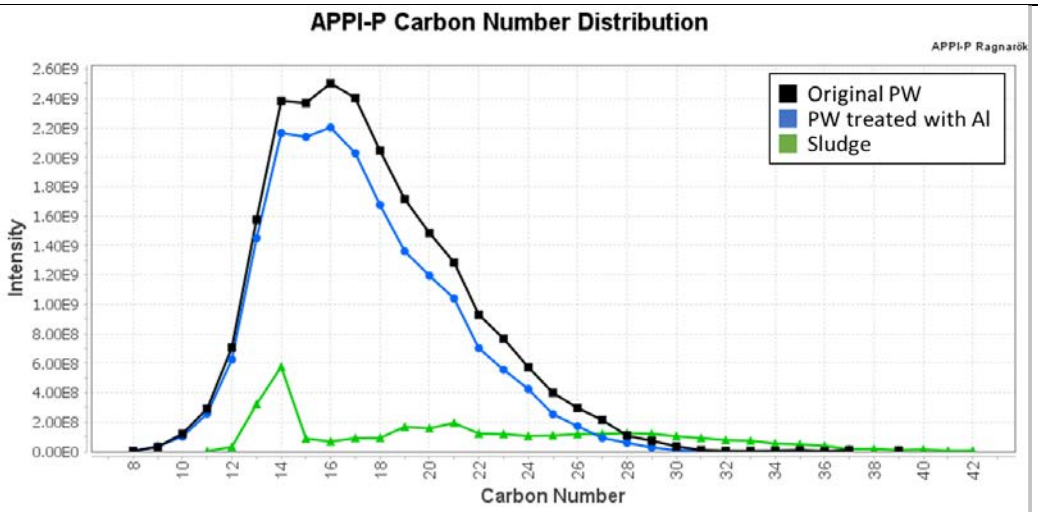

Figure [56]. APPI-P carbon number distribution of the non-treated produced water sample, produced water sample treated with aluminum electrodes and sludge formed during electrocoagulation treatment with aluminum electrodes.

Characterization of organics following novel EC operating conditions for Produced water

The produced water was treated using the following novel electrocoagulation methods in addition to iron and aluminum electrodes:

- Magnetic field
- Oscillating electrodes
- Oscillating electrodes with magnetic field
- Alternating current (AC)
- Oscillating electrodes and alternating current (AC)
- Oscillating electrodes and alternating current (AC) with magnetic field

Magnetic field

A comparison of the produced water treated with aluminum electrodes versus produced water treated with aluminum electrodes and magnetic field shows the greatest change of all treatment methods. A strong decrease in the intensities of all organic compound classes is observed with the use of electrodes in combination with magnetic field with the effect being highest for larger molecules with higher carbon numbers (Fig. 57). A removing behavior of organics is expected since the application of a magnetic field enhances the mass transfer of the dissolved cations towards the electrolyte, thereby increasing the extent of the electrochemical reaction. Lab issues of experiments with iron electrodes didn't allow reliable DOM data analysis.

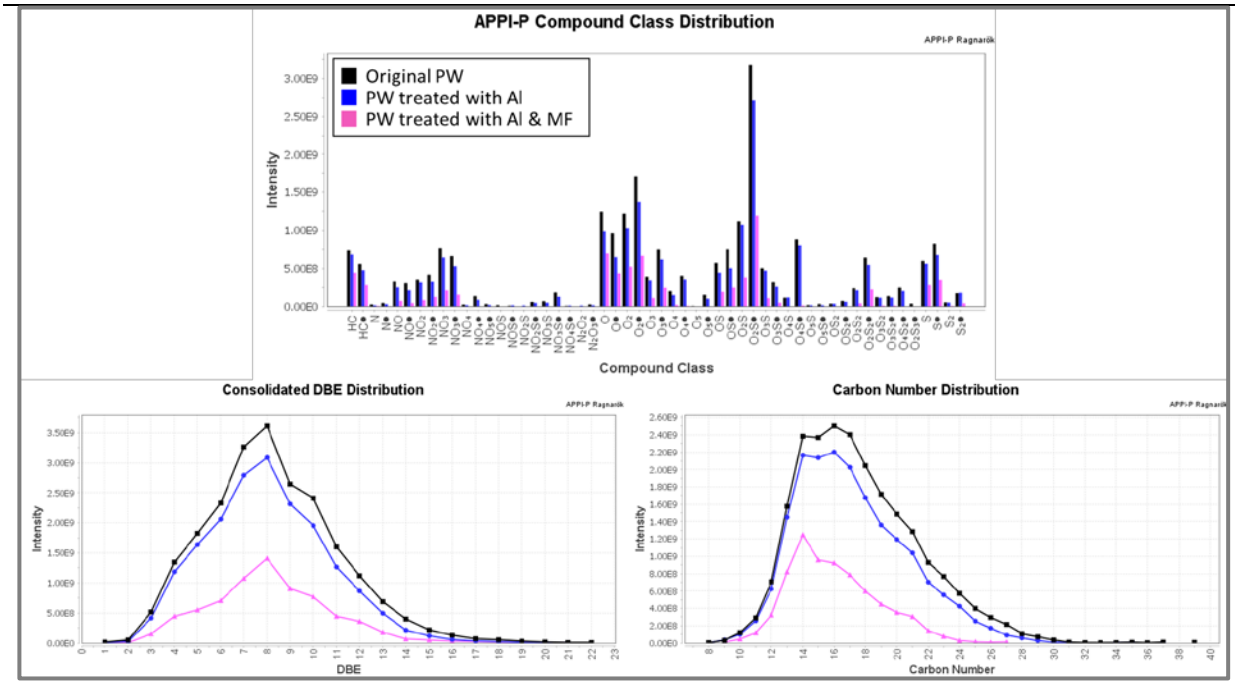

Figure [57]. APPI-P compound class, DBE and carbon number distribution of the original produced water, produced water sample treated with aluminum electrodes, and produced water sample treated with aluminum electrodes (Al) and magnetic field (MF).

Oscillating electrodes

A comparison of the produced water treated with iron/aluminum electrodes versus produced water treated with oscillating iron/aluminum electrodes shows mixed results. Whereas the experiments with aluminum electrodes show a decrease in organics abundances and the aromatic species measured in APPI-P ion mode by using iron electrodes appear to have only minor impact, the acidic species measured in ESI-N indicate that the decrease in the intensity of organics following electrocoagulation is greater with the use of iron/aluminum electrodes without oscillations (Fig. 58); i.e. oscillation has no additional positive effect on DOM removal for iron electrodes.

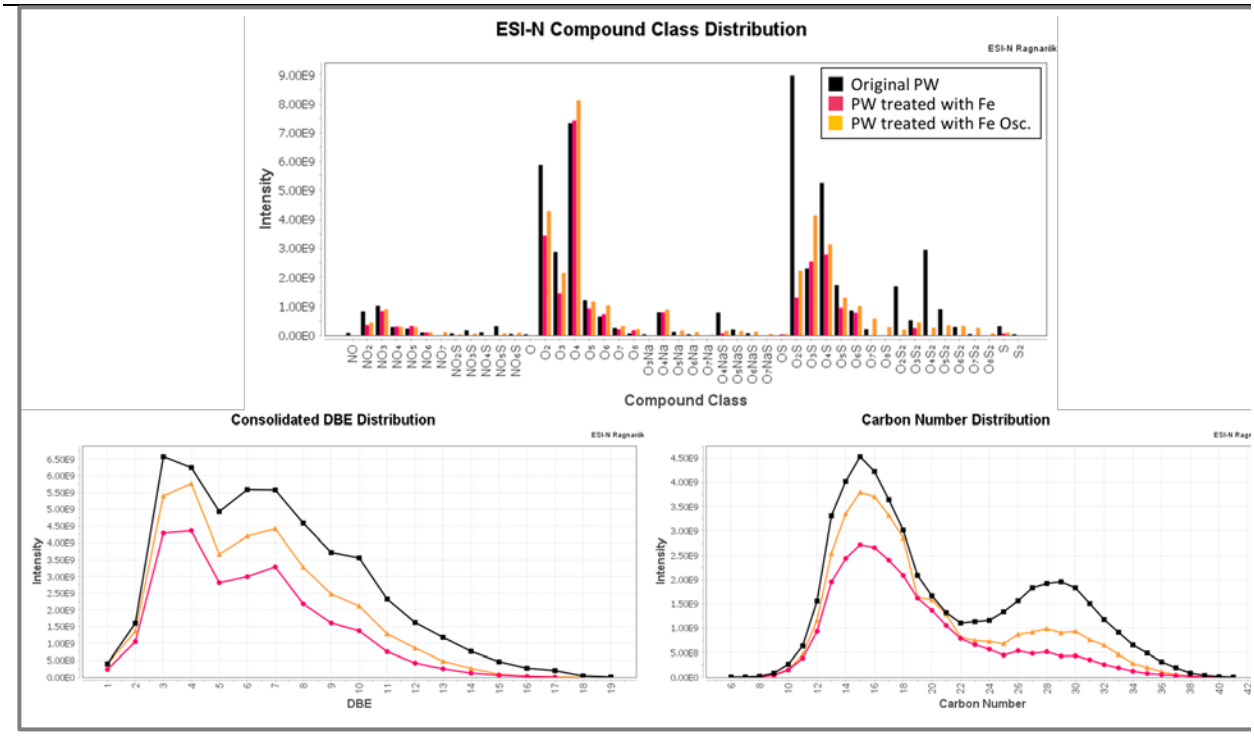

Figure [58]. ESI-N compound class, DBE and carbon number distribution of the original produced water, produced water sample treated with iron electrodes, and produced water sample treated with oscillating iron electrodes.

Oscillating electrodes with magnetic field

A comparison of the produced water treated with aluminum electrodes versus produced water treated with oscillating aluminum electrodes with magnetic field shows that the decrease in the intensity of organics following electrocoagulation is similar in the two cases (Fig. 59). The application of magnetic field increases the effect of organics reduction with electrocoagulation, by enhancing the mass transfer of the dissolved cations towards the electrolyte as shown in Figure 59. This positive effect on DOM removal is reversed when using the magnetic field with oscillating electrodes. In summary, oscillation has no additional positive effect on DOM removal in the electrocoagulation process of SAGD production water; in fact ion some cases it is reversing positive effects of other treatment processes. Lab issues of experiments with iron electrodes didn't allow reliable DOM data analysis.

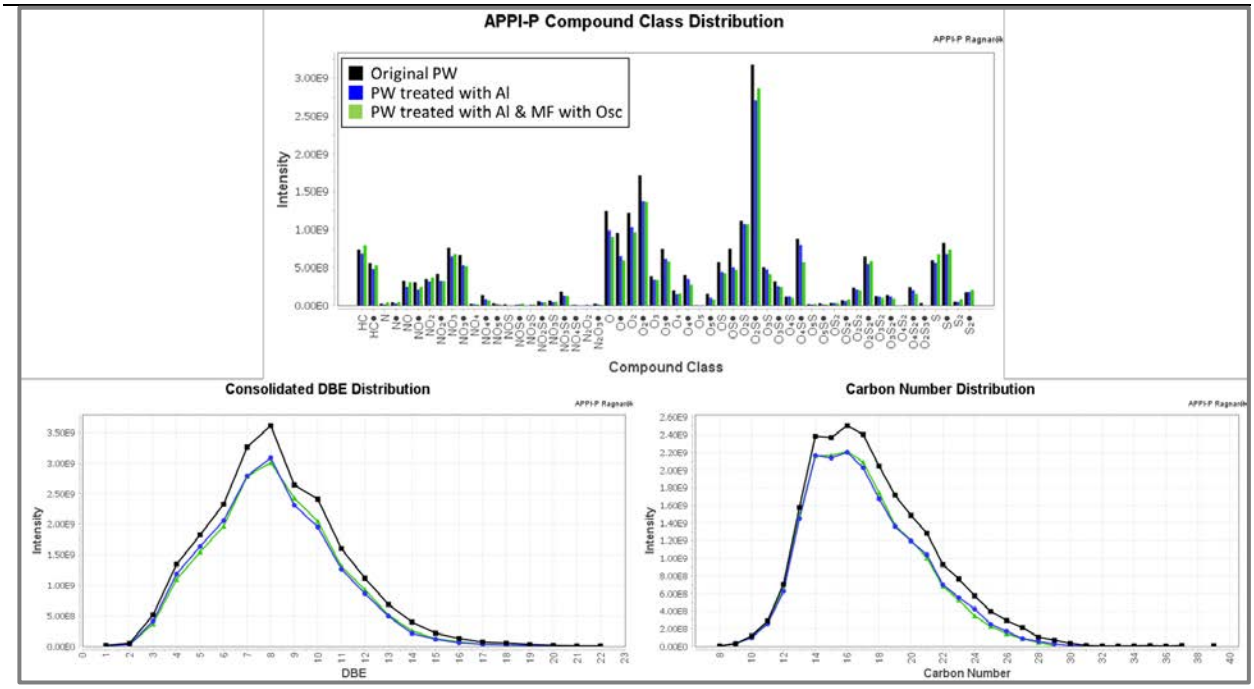

Figure [59]. APPI-P compound class, DBE and carbon number distribution of the original produced water, produced water sample treated with aluminum electrodes, and produced water sample treated with aluminum electrodes and magnetic field.

Alternating current

A comparison of the produced water treated with aluminum electrodes using common direct current (DC) versus produced water treated with alternating current (AC) shows that the decrease in the intensity of organics following electrocoagulation is greater with the use of alternating current and especially for larger molecules with higher carbon numbers (Fig. 60). This behavior is expected since the use of alternating current increases the efficiency of electrocoagulation by reducing electrodes fouling. Note: all experiments were carried out using direct current (DC) if not specified/labeled as AC (alternating current). Lab issues of experiments with iron electrodes didn't allow reliable DOM data analysis.

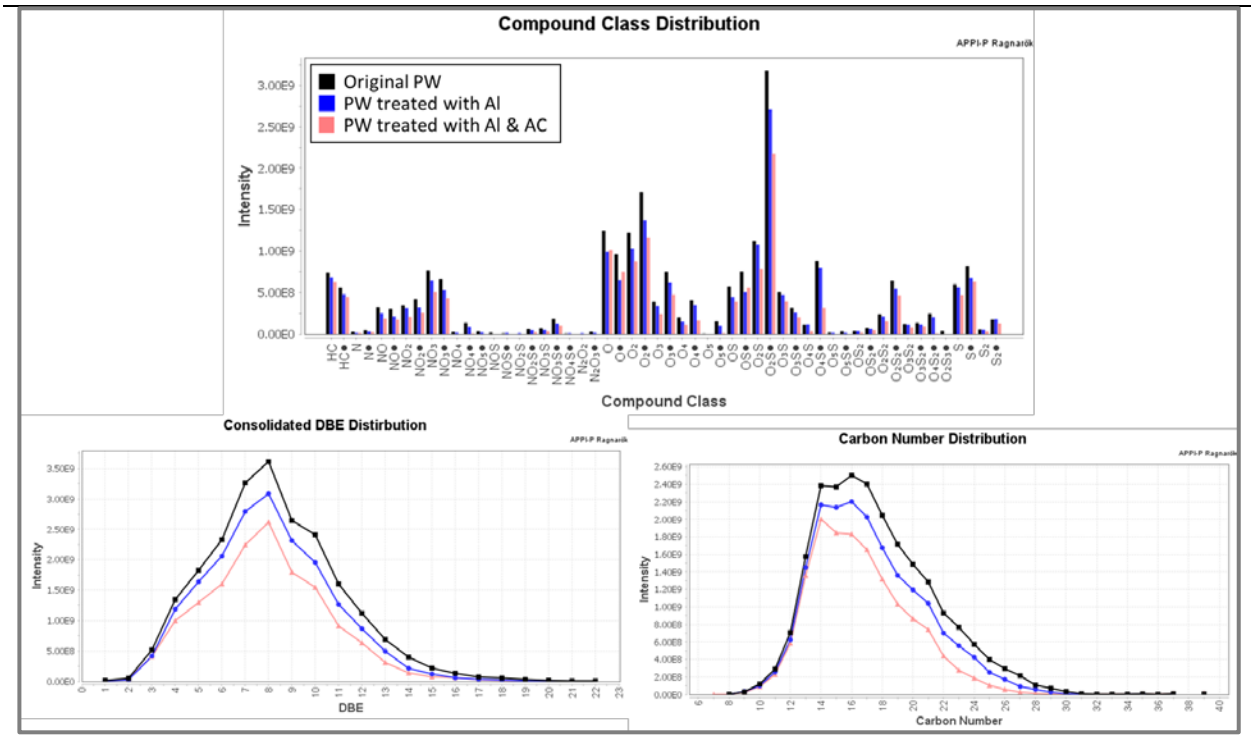

Figure [60]. APPI-P compound class, DBE and carbon number distribution of the original produced water, produced water sample treated with aluminum electrodes using direct current (DC), and produced water sample treated with aluminum electrodes using alternating current (AC). Note: all experiments were carried out using direct current (DC) if not specified/labeled as AC (alternating current).

Oscillating and alternating current

A comparison of the produced water treated with alternating current iron/aluminum electrodes versus produced water treated with oscillating and alternating current iron/aluminum electrodes shows that oscillating the electrodes does not have an additional impact of removing organics following electrocoagulation when using aluminum electrodes and alternating current (Fig. 61) and oscillating the electrodes even reduces the positive organics removing effect of alternating current when using iron electrodes (Fig. 62).

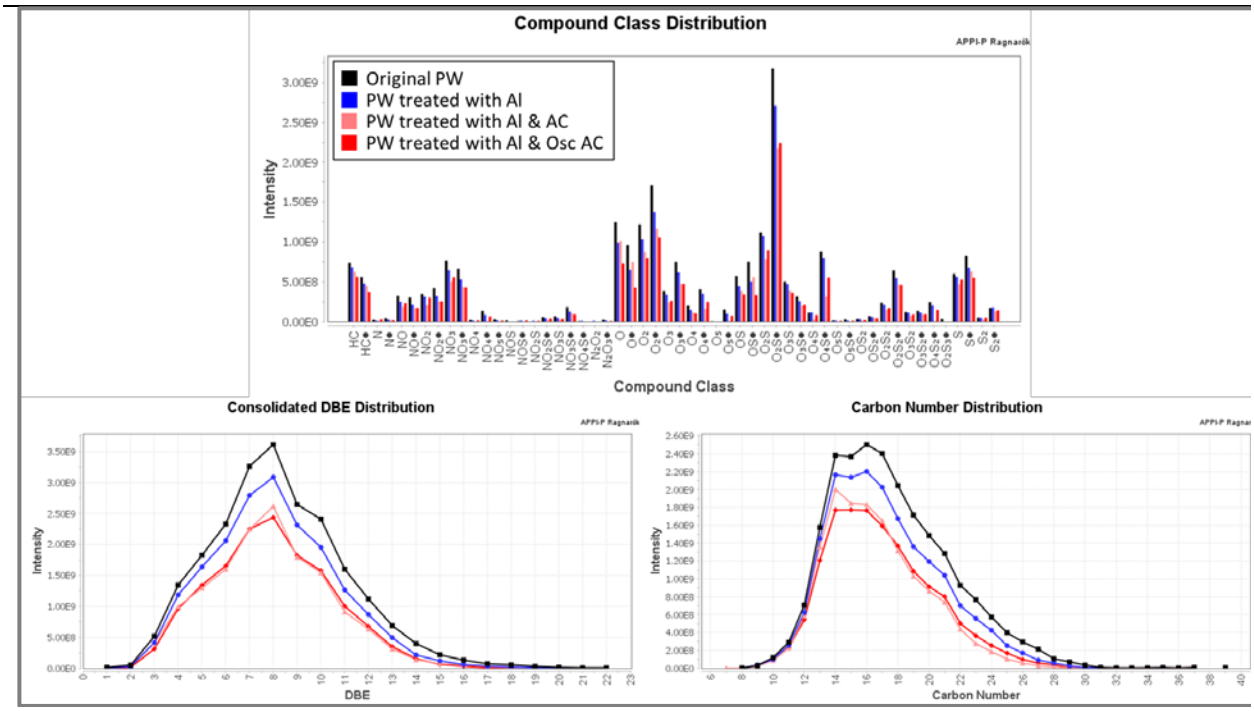

Figure [61]. APPI-P compound class, DBE and carbon number distribution of the original produced water, produced water sample treated with aluminum electrodes, and produced water sample treated with aluminum electrodes and alternating current.

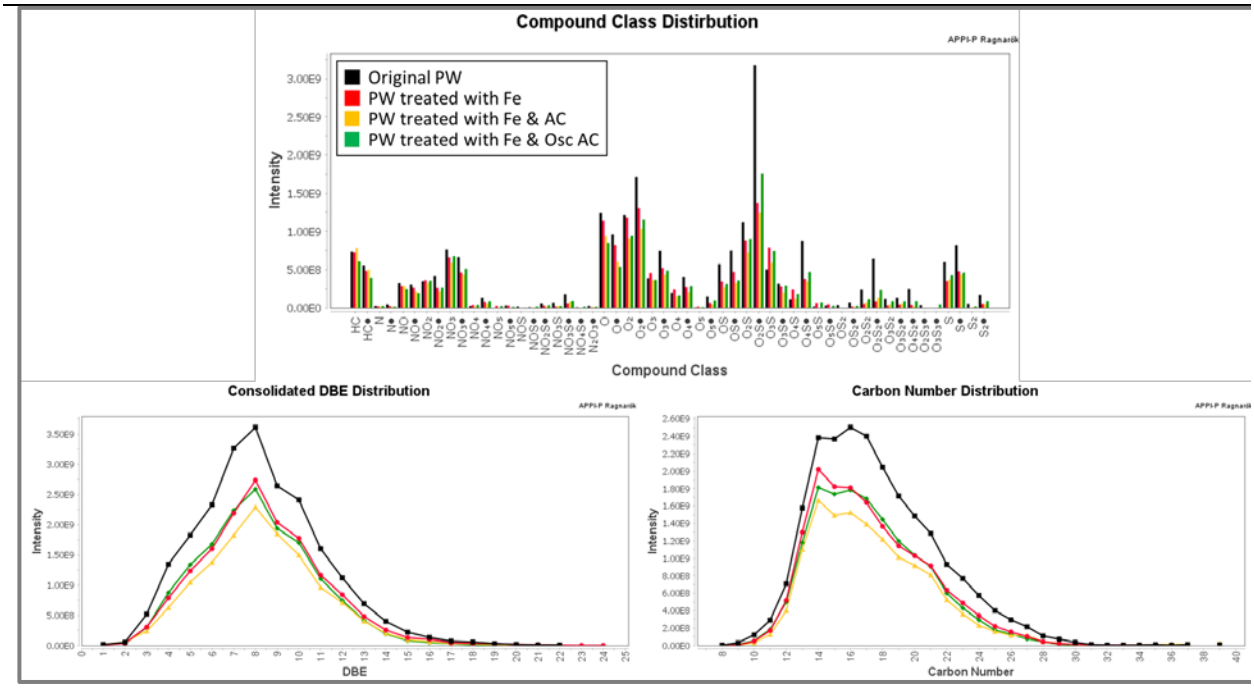

Figure [62]. APPI-P compound class, DBE and carbon number distribution of the original produced water, produced water sample treated with iron electrodes, and produced water sample treated with iron electrodes and alternating current.

Oscillating and alternating current with magnetic field

The decrease in the organics with electrocoagulation is observed to be slightly higher for treated with oscillating and alternating current with aluminum electrodes and magnetic field, than without the magnetic field (Fig. 63). As observed earlier the magnetic field itself has a strong positive impact on organics removal and is expected since the application of magnetic field enhances the mass transfer of the dissolved cations toward the electrolyte, thereby increasing the extent of the electrochemical reaction. However, the effects of oscillation, alternating current and magnetic field do not linear add up for organics removal. Lab issues of experiments with iron electrodes didn't allow reliable DOM data analysis.

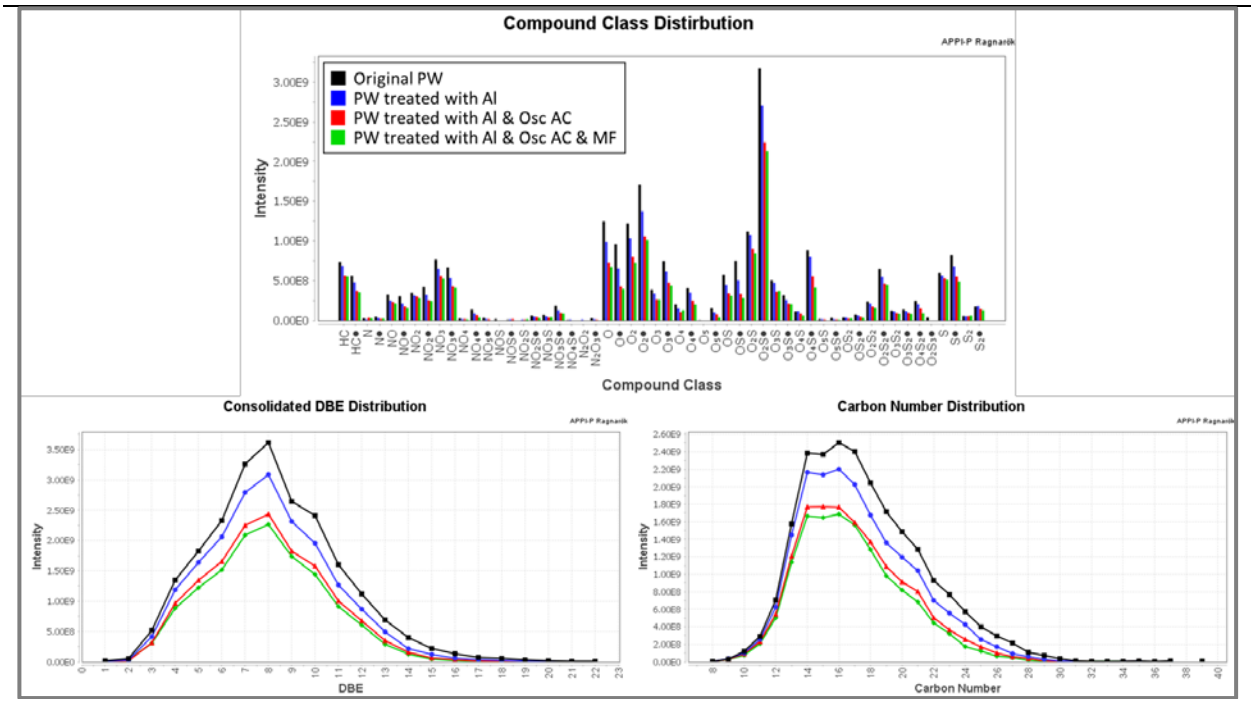

Figure [63]. APPI-P compound class, DBE and carbon number distribution of the original produced water, produced water sample treated with aluminum electrodes, produced water sample treated with aluminum electrodes and oscillating alternating current, and produced water sample treated with oscillating alternating current aluminum electrodes with magnetic field.

Sludge

During electrocoagulation experiments sludge was observed to form at the bottom of the electrodes and represents a small fraction of the original produced water composition. The analyzes of the sludge using FTICR-MS in ESI-N and APPI-P ion mode revealed that it is made of a large part of oily components (likely oil droplets) present in the produced water sample, evident especially due to high concentrations of hydrocarbon and sulfur containing compound classes (Figs. 64, 65). The sludge composition of all experiments are similar and group together and represent similar carbon number and DBE distributions, suggesting that the process of the sludge formation forms a similar methodology in each of the electrocoagulation experiments conducted.

The sludge showed compounds with higher carbon number (C# 10-58) relative to both original and treated produced water (C# 8-39) (Fig. 66) which attributes to the oil-like organics present in it. Since the produced water was filtered during extraction, the oil-like organics emulsified in the sample would have separated from the water before extraction. However, since the solid sludge was washed/extracted with organic solvents without any filtering possible beforehand, the oil-like organics adsorbed to the sludge were extracted. This trend was less obvious when analyzed in ESI-N ion mode for both iron and aluminum electrode treatments.

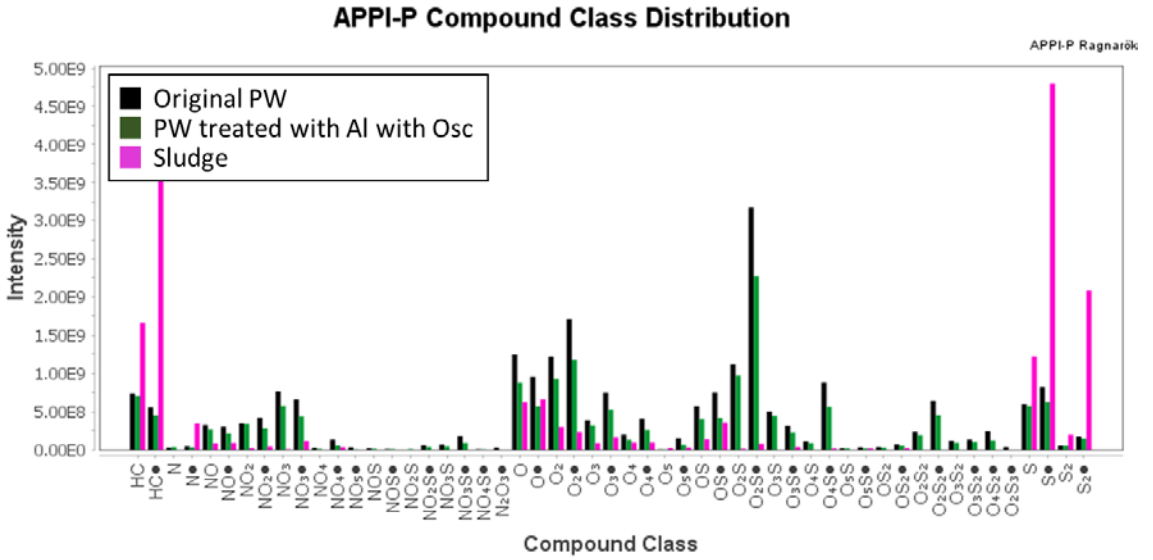

Figure [64]. APPI-P compound class distribution of the original produced water, produced water sample treated with aluminum electrodes with magnetic field and sludge formed during the electrocoagulation treatment with aluminum electrodes with oscillating current.

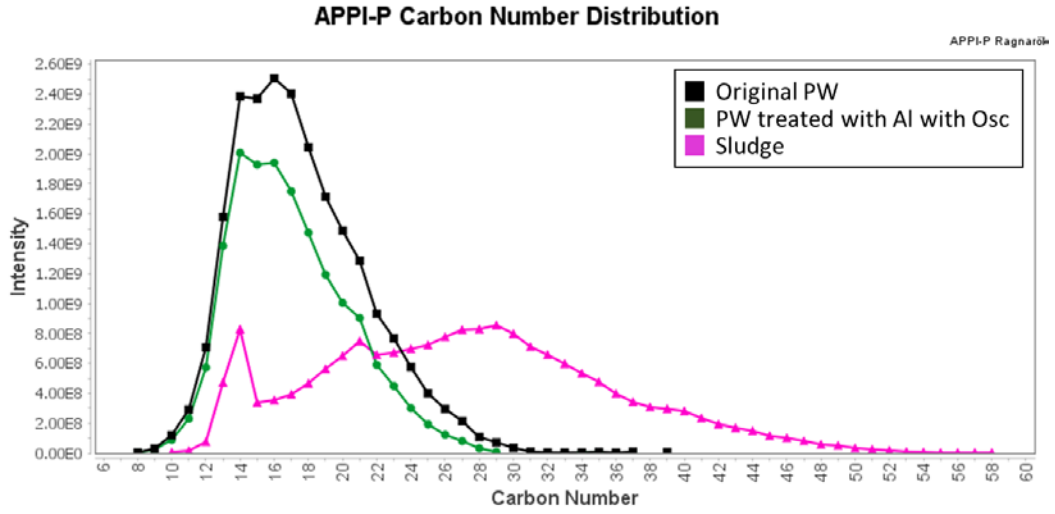

Figure [65]. APPPI-P carbon number distribution of the original produced water, produced water sample treated with aluminum electrodes with magnetic field and sludge formed during the electrocoagulation treatment with aluminum electrodes with oscillating current.

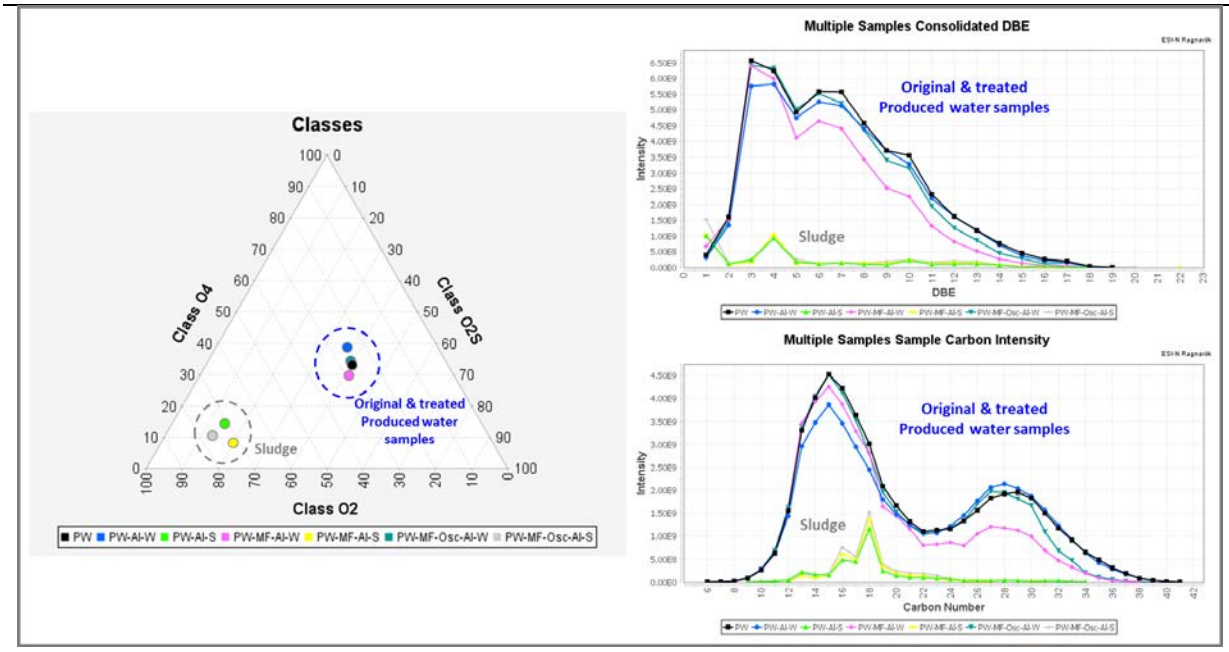

Figure [66]. ESI-N DBE and carbon number distribution of the original produced water, produced water sample treated with aluminum electrodes using various novel electrocoagulation treatment methods and sludge (-S) formed during the respective novel electrocoagulation process. The treated produced water samples show a similar distribution, while the sludge samples group together.

Foam

The electrocoagulation treatment of produced water with aluminum electrodes was found to produce foam on top of the produced water surface but was found to collapse after a few hours without disturbance. The composition of the foam analyzed using FTICR-MS in APPI-P and ESI-N ion modes revealed that is was fairly similar to the treated produced water, with similar compound classes observed in its composition, indicating that the foam is more a result of the experimental conditions (Figs. 67, 68). Due to the differences in concentration the comparison of the samples is restricted to qualitative analysis only here.

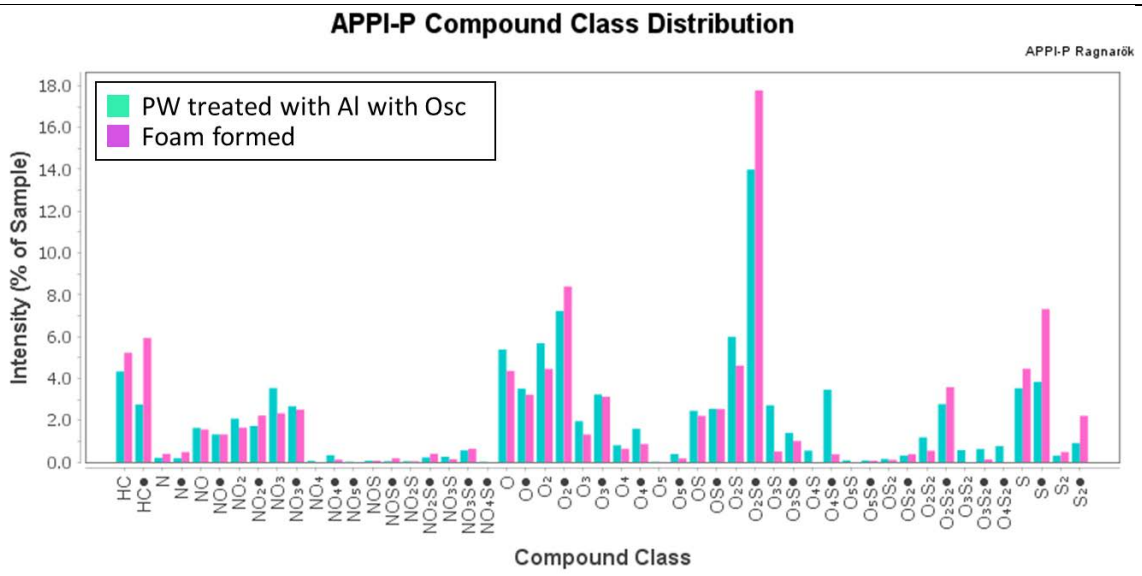

Figure [67]. APPI-P compound class distribution of produced water sample treated with aluminum electrodes with oscillation and foam formed during the electrocoagulation treatment, shows a very similar distribution.

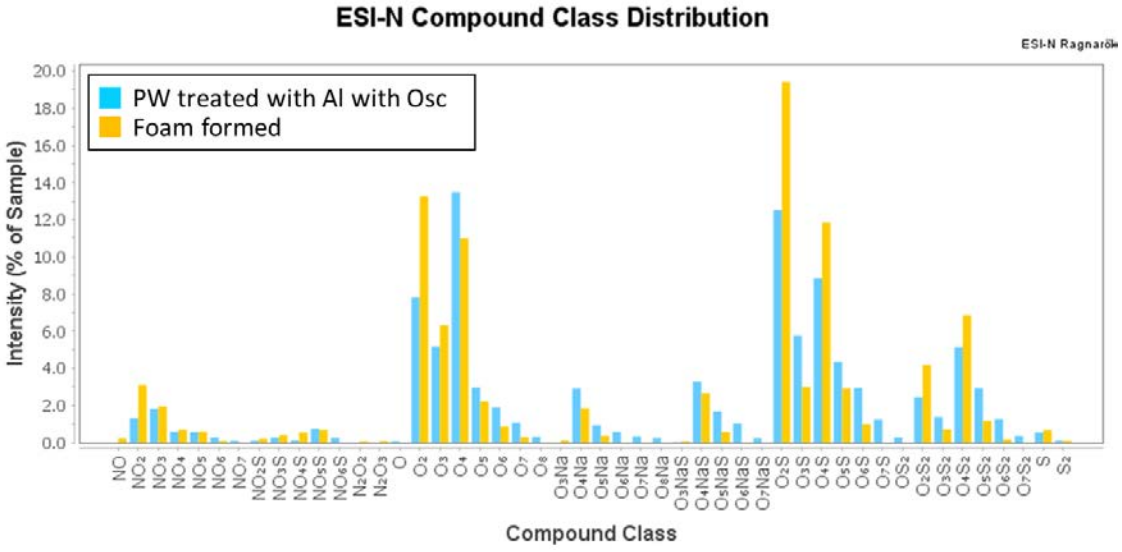

Figure [68]. ESI-N compound class distribution of produced water sample treated with aluminum electrodes with oscillation and foam formed during the electrocoagulation treatment, shows a very similar distribution.

Characterization of organics following EC for Boiler Blowdown Water

The CNRL boiler blowdown sample was treated with iron and aluminum electrodes with DC and AC current. The analysis of these samples was very challenging due to the high concentration of inorganic ions in the water. Even after several attempts to minimize the impact by e.g. running the extracts through sodium sulfate the inorganic ions continued to have strong ion depression and clustering effects. Therefore the results of the FTICR-MS analysis in both ESI-N and APPI-P ion mode of these experiments can only be considered as qualitative and overall compositional changes. Figure 69 shows that the major compound classes were detected in all samples.

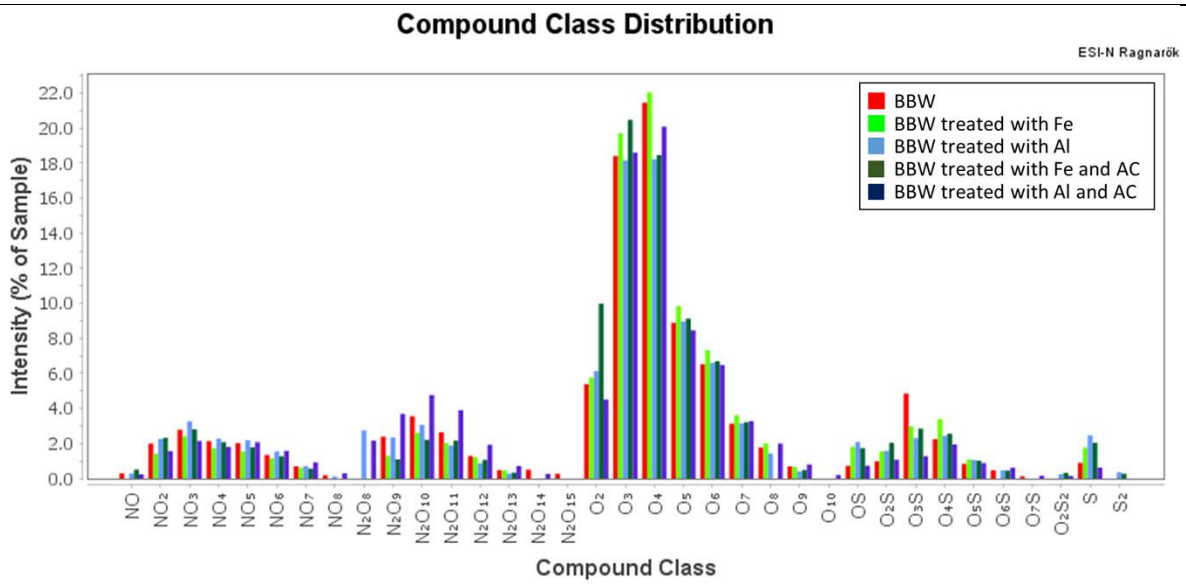

Figure [69]. ESI-N compound class distribution of the original boiler blowdown sample and boiler blowdown sample treated with iron and aluminum electrodes with DC and AC current.

A closer inspection of the compositional changes between the compound classes shows some differences between iron and aluminum electrodes and direct versus alternating current use for electrocoagulation. Figure 70 illustrates triangular plots comparing different compound classes measured in ESI-N ion mode. For instance, the aluminum electrodes with DC and AC have a strong reduction in the relative abundance O2 class naphthenic acids when compared to O2 containing the nitrogen and sulfur species. The effect is stronger with DC compared to AC (Fig. 70a). Surface active interfacial material like alkyl benzene sulfonates (SO3 class) are strongly reduced when compared to the less oxygenated species (Fig. 70b).

Similar effects were observed when the samples were analyzed in APPI-P ion mode. Direct current had a stronger relative reduction in abundances of O2 and O3 species when compared to their corresponding nitrogen and sulfur species in comparison to alternating current use for the electrocoagulation treatment (Fig. 71).

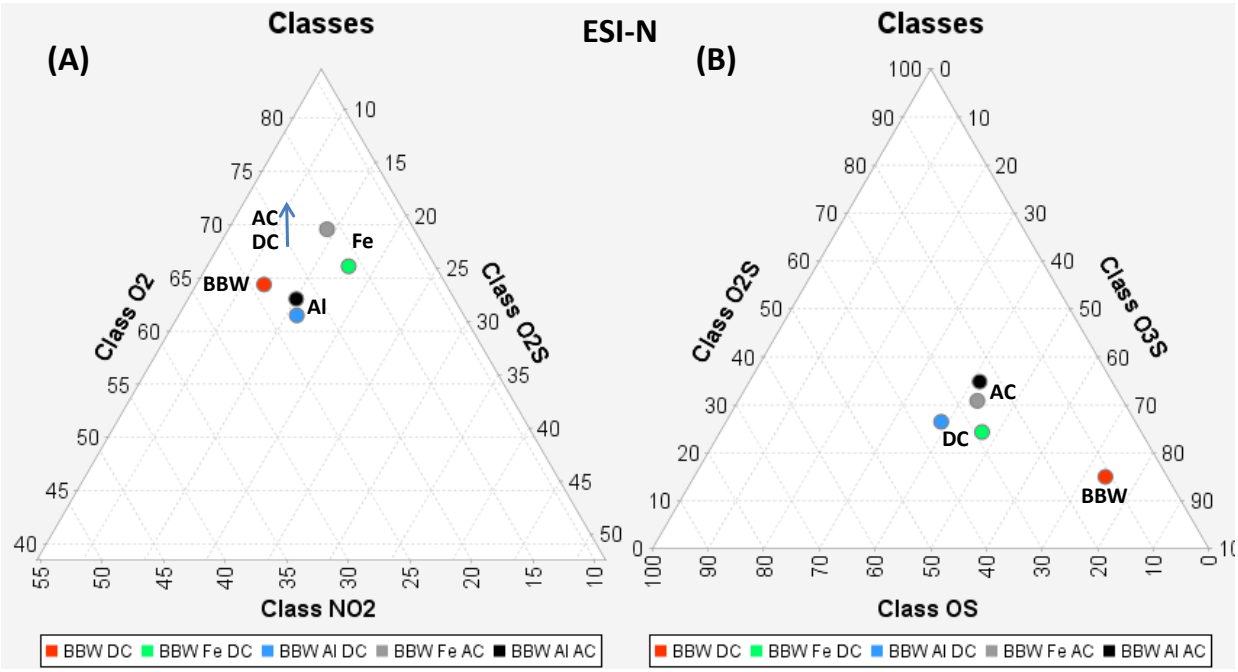

Figure [70]. ESI-N ternary plot of compound classes O_2, O_2S and NO_2 (A) and OS, O_2S and O_3S (B) of original boiler blowdown water and boiler blowdown sample treated with iron electrodes with DC and AC current.

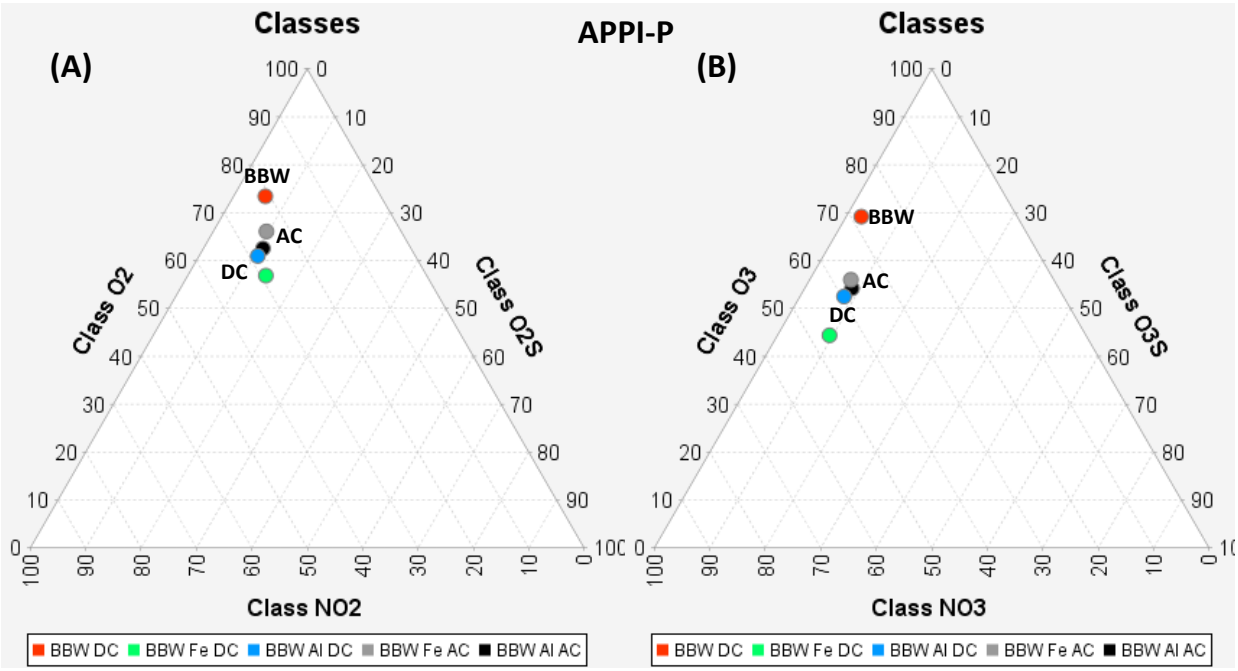

Figure [71]. APPI-P ternary plot of compound classes O_2, O_2S and NO_2 (left) and O_3, O_3S and NO_3 (right) of original boiler blowdown water and boiler blowdown sample treated with iron electrodes with DC and AC current.

Summary of results from Task C1 and C2

The produced water sample is strongly enriched by sulfur containing organic species (more than half of all detected compound classes contain at least one sulfur atom per molecule measured either in ESI-N or APPI-P ion mode. The boiler blowdown water is enriched in multi-oxygenated species and is about four times as concentrated than the produced water sample. The boiler blowdown water comprises of higher concentration of higher DBE and higher carbon number containing compounds relative to the produced water sample.

The precipitated particles at the bottom of the organic extracts of the electro-coagulation treated produced waters were analyzed for their cationic and anionic composition. The analysis showed that they comprised primarily of sodium sulfate salt, which was getting introduced in the sample due to an experimental step (Figure 72). The experimental protocol was then modified to remove the addition of the salt to the extract. The ion chromatography (IC) and inductively coupled plasma (ICP) of the precipitated particles also showed a high percentage of boron species. Further work is needed to understand this precipitation.

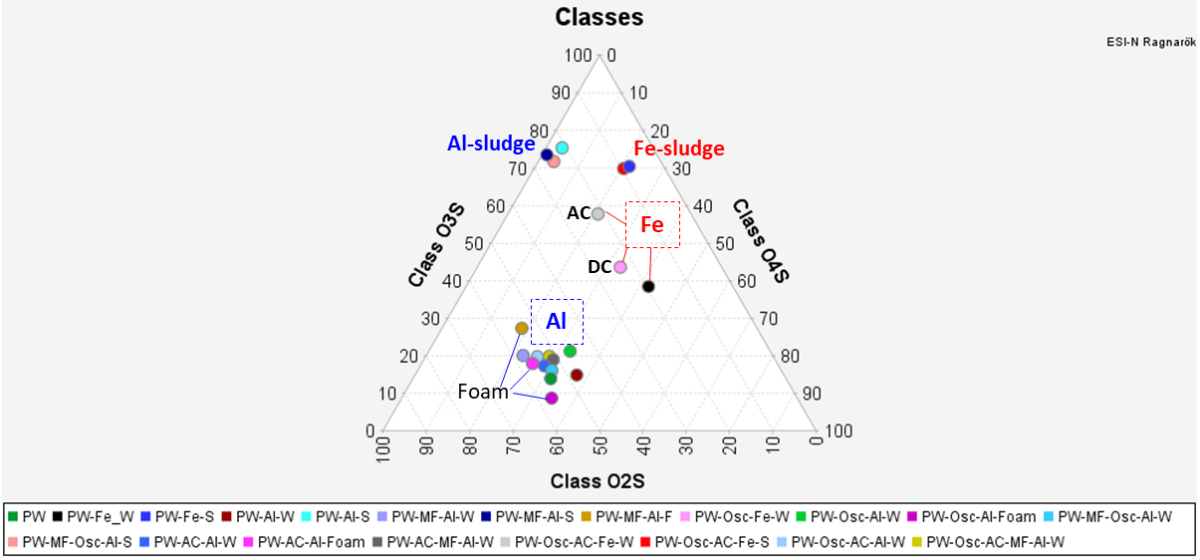

Figure [72]. ESI-N ternary plot distribution of O_2S, O_3S and O_4S compound classes for the analyzed original and electrocoagulation treated produced water samples, along with the respective sludges and foam formed during the treatment process.

Overall, the electrocoagulation with iron electrodes showed a higher percentage removal of organics from the produced water relative to the aluminum electrode when compared without any of the novel treatment methods.

Within the use of novel techniques for electrocoagulation treatment, the application of magnetic field was shown to increase the removal of few of the organic compound class groups present in the produced water. The use of oscillating electrodes showed no, minor or even hindering effects when used in addition to other novel EC techniques for the removal of organics from produced water. The use of AC current was found to increase the removal of few of the organic compound class groups present in the produced water compared to the DC current, likely caused due to the improved treatment efficiency by reducing fouling.

Over the course of the electrocoagulation, sludge was deposited at the bottom of the electrodes. The sludge was observed to be composed of oil-like organics with high concentration of hydrocarbons and sulfur containing compounds. The sludge comprised of higher carbon number containing organics relative to the produced water. This trend was observed in the grouping of the sludge and produced water samples (Fig. 69).

In addition to the sludge, foam was observed to be formed following treatment with aluminum electrodes. The composition of the organics present in the foam was found to be similar

to that in the treated produced water with the aluminum electrodes indicating that there is no significant separation of organic compounds between the foam and the treated water.

The analysis of boiler blowdown water treated with electrocoagulation was very challenging due to high inorganic ions in the water interfering with the organic when analyzed in different ion modes using FTICR-MS technology due to ion suppression and clustering effects. However, some overall compositional changes on compound class level were observed to differentiate between iron and aluminum electrodes as well as direct versus alternating current use.

The process or possible reaction systems behind the removal of organics during water treatment with electrocoagulation are not well understood. It could be a side effect of silica removal due to sorption effects of the organics on the silica or the organics themselves are reacting at the electrodes.

APPENDIX

The typical heteroatom classes detectable with the different ionization techniques:

- The ESI-N (negative ion mode), technique allows the optimal detection and monitoring of acidic compounds, i.e. compounds which are able to deprotonate, such as compounds, including carboxylic acids, alcohols, pyrroles (Qian et al., 2001a).
- The ESI-P (positive ion mode), technique allows the detection of basic compounds, i.e. compounds which can be readily protonated- for example compounds with pyridinic nitrogen groups (Qian et al., 2001b).
- The APPI-P technique allows the detection of analyte components as protonated and/or radical ion species. What ions are formed depends on the proton and electron affinities of the dopant relative to the analyte. With a toluene dopant, if the proton affinity of the analyte is higher than the proton affinity of the benzyl radical, a protonated molecule can form. If the electron affinity of the toluene radical cation is higher than the electron affinity of the analyte (lower or equal ionization energy than toluene) a radical molecular ion can form (Purcell et al., 2006).

Methods and Achievements for Task C.3

Report on geochemical modeling of solution speciation and recommended operating conditions for improved removal and reduced fouling. Computer modeling of Electrocoagulation.

Objective

The objective of this milestone is to investigate the potential of using computer modeling of synthetic waters in electrocoagulation. The saturation indicies (SI) of various calcium, magnesium and silicate minerals are monitored as a function of distance between the two electrodes. SI is an indication of the potential for mineral formation and the computer models will indicate where minerals are likely to form in solution.

Methodology

The main stages in electrochemically assisted coagulation are shown in Figure [73]. An electrochemical cell oxidizes the aluminum electrode providing the aluminum ion, Al^{3+}, to the system. Al^{3+} is a coagulant reagent and reacts to destabilize the colloidal pollutant or break the emulsion. Turbulence is also generated by oxygen and hydrogen evolution which further helps to destabilize the colloids resulting in their flocculation. The last step involves the removal of the pollutant from the waste by sedimentation, filtration or floatation. The bubbles from hydrogen formation can help in the efficiency of the flotation process, electro-flotation.

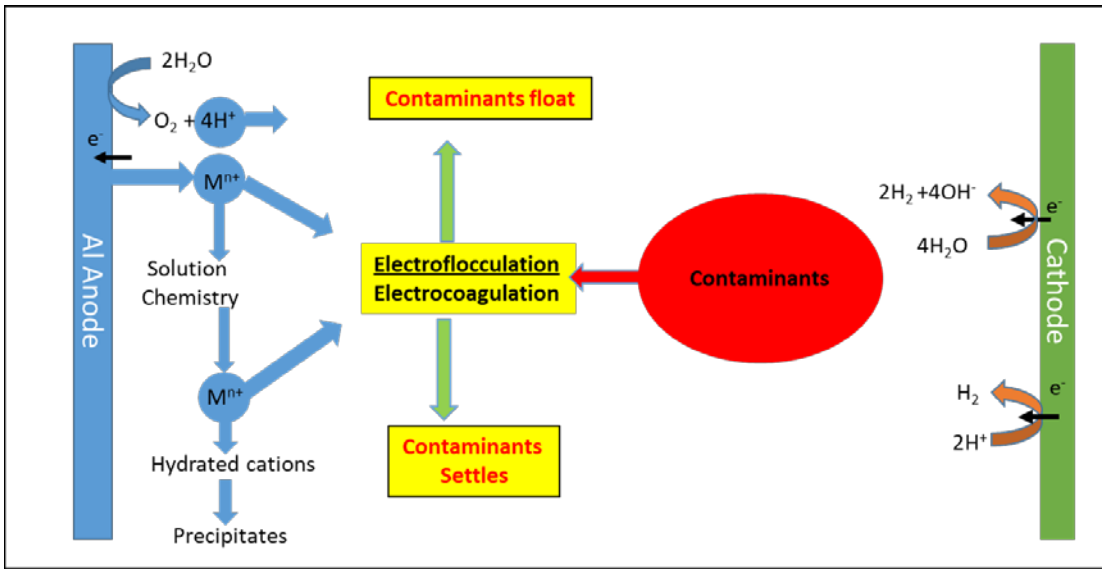

Figure [73]. Electrocoagulation main stages.

The proposed method for computer modeling was to link two programs, Comsol® and Phreeqc using an interface program iCP, (interface Comsol® Phreeqc). However, implementation of the iCP program proved unsuccessful, so an alternate strategy is designed.

To link Comsol® and Phreeqc, the concentrations of each species from Comsol® is written to an output file, resulting in 496 files. These output files were then read into a fortran program and Phreeqc input files were created and these input files are run. The Phreeqc output files are then reassembled into a single output file which allowed for contour plots for the different mineral saturation indices to be constructed. The process listed is controlled by Unix scripting and the process is repeated for each desired timestep.

Comsol® is a cross-platform finite element analysis, solver and multiphysics simulation software. It provides an integrated development environment for electrical and chemical applications. Comsol® is used to model the two dimensional electrocoagulation cell, i.e. the two electrodes with a constant current and an effluent of constant composition flowing through the cell. Comsol® computes the concentrations of the different electrochemical and chemical species, the latter which has undergone electro-migration. The concentrations of the given species at each node on the 2D grid were written to an output file which is processed by the Unix scripts to create the Phreeqc input files.

Current Electrocoagulation Model

The current electrocoagulation system model is composed of two parallel aluminum plates, which are the electrodes, one positive and the other negative, with fluid flowing them. The length of the electrodes is 2 cm and the distance between the electrode pair is 5 mm.

The primary reaction at the positive electrode is the production of Al^{3+} ions via the following reaction:

$$Al^{3+} + 3e^{-} \rightleftharpoons Al \qquad (1)$$

with an electrode potential (Rumble et al., 2018):

$$E_{Al^{3+}} = -1.676 - \frac{RT}{nF} ln \left[\frac{1}{a_{Al^{3+}}}\right] \qquad \text{(ii)}$$

$$= -1.676 + \frac{0.02569}{n} ln[a_{Al^{3+}}]$$

Unfortunately, according to the literature, this is not the product in a in an alkaline solution. The generally accepted reaction listed in the electrochemistry literature is: (MacDonald et al., 1988a):

$$Al(OH)_4^- + 4e^- \rightleftharpoons Al + 4OH^- \qquad (2)$$

with an electrode potential (Rumble et al., 2018):

$$E_{Al(OH)_4^-} = -2.310 - \frac{RT}{nF} \ln \left[\frac{a_{OH}^4}{a_{Al(OH)_4^-}}\right] \text{(i)}$$

$$= -2.310 - \frac{0.02569}{n} \ln \left[\frac{a_{OH}^4}{a_{Al(OH)_4^-}}\right]$$

In reality, the mechanistic reaction of Al with OH^- proceeds through four individual steps, as shown below (MacDonald et al., 1988):

$$Al + OH^- \overset{k_1}{\rightarrow} Al(OH)_{ads} + e^- \qquad (3)$$

$$Al(OH)_{ads} + OH^- \overset{k_2}{\rightarrow} Al(OH)_{2,ads} + e^- \qquad (4)$$

$$Al(OH)_{2,ads} + OH^- \overset{k_3}{\rightarrow} Al(OH)_{3,ads} + e^- \qquad (5)$$

$$Al(OH)_{3,ads}OH^- \overset{k_4}{\rightarrow} Al(OH)_4^- \qquad (6)$$

However, in the electrocoagulation literature Al^{3+} is considered to be chemical species formed at the electrode surface by reaction sequence (Rxn 1), and this reaction is used in the model. (e.g. Lu et al., 2017).

A secondary reaction is also considered at the positive electrode, the production of hydrogen gas via the following reaction:

$$2H^+ + 2e^- \rightarrow H_2 \qquad (7)$$

with an electrode potential (Rumble et al., 2018):

$$E_{H_2} = 0.00 - \frac{RT}{nF}\ln\left[\frac{a_{H_2}}{a_{H^+}^2}\right] \qquad (ii)$$
$$= 0.00 + \frac{RT}{nF}\ln\left[a_{H^+}^2\right]$$

This reaction is introduced after the primary reaction sequence, Rxn 1, is considered in detail.

The complimentary half reaction to the dissolution of aluminum to Al^{3+} at the positive electrode is the reduction of water at the negative electrode:

$$2H_2O + 2e^- \rightarrow H_{2(gas)} + 2OH^- \qquad (8)$$

with an electrode potential (Rumble et al., 2018):

$$E_{OH^-} = -0.828 - \frac{RT}{nF}\ln[a_{OH^-}^2] \qquad (iiI)$$

This reaction occurs in a two-step process (MacDonald, 1988):

$$Al + H_2O + e^- \overset{k_5}{\rightarrow} Al(H)_{ads} + OH^- \qquad (9)$$

$$Al(OH)_{ads} + H_2O + e^- \overset{k_6}{\rightarrow} Al + H_2 + OH^- \qquad (10)$$

For these two reactions, reaction 9 is the rate determining step. Again, the electrocoagulation literature considers the simpler direct reaction, Rxn 8, at the negative electrode.

Iron electrodes are also used in electrocoagulation with the following reaction being considered the most important and is used in the modelling:

$$Fe^{2+} + 2e^- \rightleftharpoons Fe \qquad (11)$$

with an electrode potential (Rumble et al., 2018):

$$E_{Fe} = -0.447 - \frac{RT}{nF} \ln\left[\frac{1}{a_{Fe^{2+}}}\right] \qquad (iv)$$

The electrode reaction forming Fe^{3+} has been shown to be negligible in the electrochemical literature and is not considered (Hakizimana et al, 2017).

The rate of the reaction is expressed as current density and is also affected by the potential difference between the positive electrode and negative electrode. The rate of an electrochemical reaction can be expressed by the Butler-Volmer equation:

$$i = i_0\left[e^{-\alpha_a nF\eta/RT} - e^{-\alpha_c nF\eta/RT}\right] \qquad (v)$$

where i = *electrode current density*

i_0 = *exchange current density*

α = *charge transfer coefficient (anodic or cathodic) = 0.5*

η = *activation overpotential*

n = *number of electrons in the reaction*

The charge transfer coefficient for the reactions at the aluminum electrodes are set to 0.5 for both the anodic and cathodic reactions which is a default condition when the actual parameters are unknown. Exchange current densities vary depending on the metal used, from 10^{-3} A/cm^2 for palladium and platinum to 10^{-12} A/cm^2 for lead and mercury (Sawyer et al., 1995). Unfortunately, the exchange current density for aluminum is also unknown so this is set by trial and error.

Comsol® Model

A Comsol® model is constructed using a non-uniform grid of 496 points (Figure 74a). The inlet is located at the bottom of the diagram and the outlet at the top. The right side of the cell is the positive electrode and the left side is the negative electrode. At the boundary of the two electrodes a non-uniform grid is used and is also used at the inlet. Fluid flowed from the bottom to the top and observed a no-slip boundary conditions (see Figure 74b), with the inlet fluid velocity of 5 X 10^{-4} m/s.

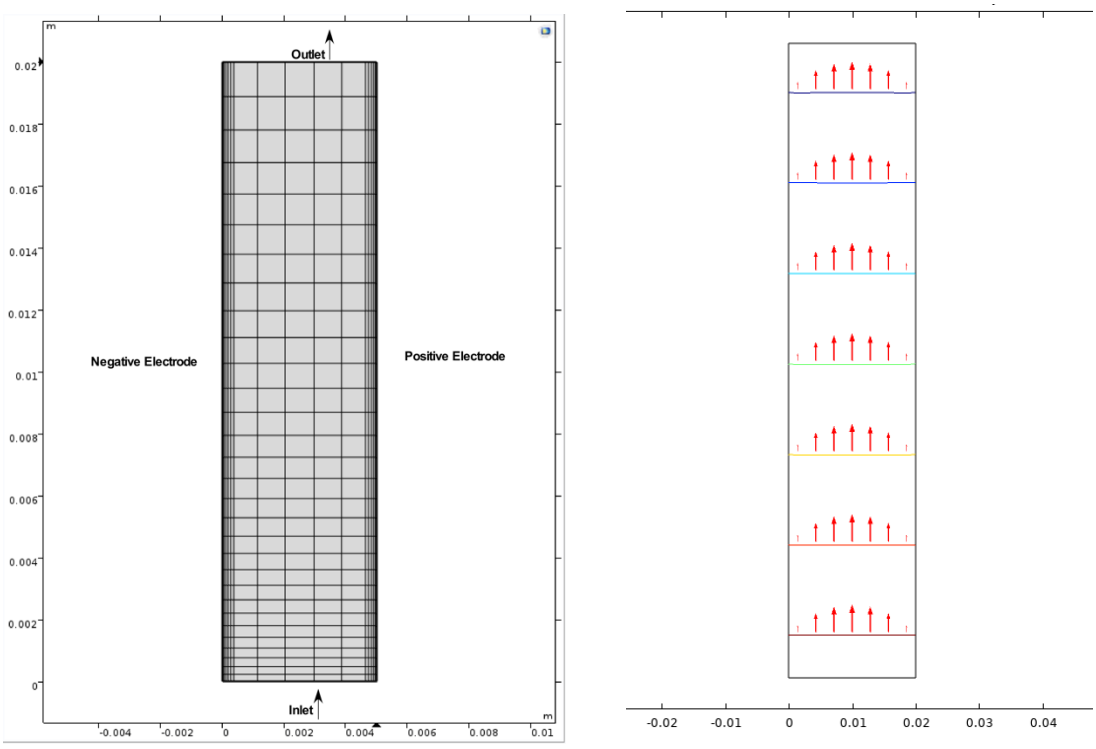

Figure [74]. a) Grid used in Comsol® model.
b) Velocity profile inside cell using no-slip boundary conditions.

The chemical parameters for the model are listed in Table 12. The composition of the synthetic and produced waters is taken from the electrocoagulation report dated April 30, 2017 with a small amount of aluminum or iron added to the system. For the produced waters, only cations and sulphate concentrations are listed so a charge balance with chloride is done to ensure that the produced effluent is charge balanced. The diffusion coefficients are taken from the CRC Handbook (Rumble et al., 2018).

Table 12: Concentration of Species in Effluent and Diffusion Coefficient Used in the Comsol® Model

Species	Synthetic produced water Concentration (mM)	Produced water Concentration (mM)	Diffusion Coefficient (10^{-5} cm^2/s)
Na^+	82.6	82.6	1.334
Cl^-	54.9	108.6	2.032
HCO_3^-	27.9	-	1.185
Mg^{2+}	0.8	0.82	0.706
Ca^{2+}	1.6	1.62	0.792
Si^{2+}	2.0	0.42	1.170
Al^{3+} (for Al electrode)	1 X 10^{-3}		0.541
Fe2+ (for Fe electrode)			
$H_{2(g)}$	4X10^{-7}		5.11
$O_{2(g)}$	0.27		2.42
pH	8.0	8.0	
Conductivity	8.86 mS/cm		

Phreeqc Model

Phreeqc (Parkhurst and Apello, 2013) is used to determine the saturation index for a number of minerals thought to be important in scale buildup in OTSG's (Nightingale et al, 2017). The database used for the Phreeqc modeling is the Thermoddem database (Blanc et al., 2012). The Thermoddem database is used for all of the modeling calculations as it has a more complete mineral data base than either the phreeq.dat or pitzer.dat databases included with Phreeqc.

Results

$Al(OH)_4^-$ Model in Synthetic produced water

The results for the $Al(OH)_4^-$ are shown in Figure 75, at times 2.5, 10, 50, 100 and 500s. Shown in the figure is a section at the top of the cell near the outlet. This region is examined as it

has the largest variation in concentration, as shown in Figure 75a. At 2.5 sec there is a very narrow band of $Al(OH)_4^-$ adjacent to the electrode surface. The region of $Al(OH)_4^-$ increases until at 40 sec the region of increased $Al(OH)_4^-$ reaches a steady state, the region of $Al(OH)_4^-$ does not increase at 100 or 500s. The reactions modelled are for Rxn 2, the net reaction, not the individual steps, Rxns 3-6.

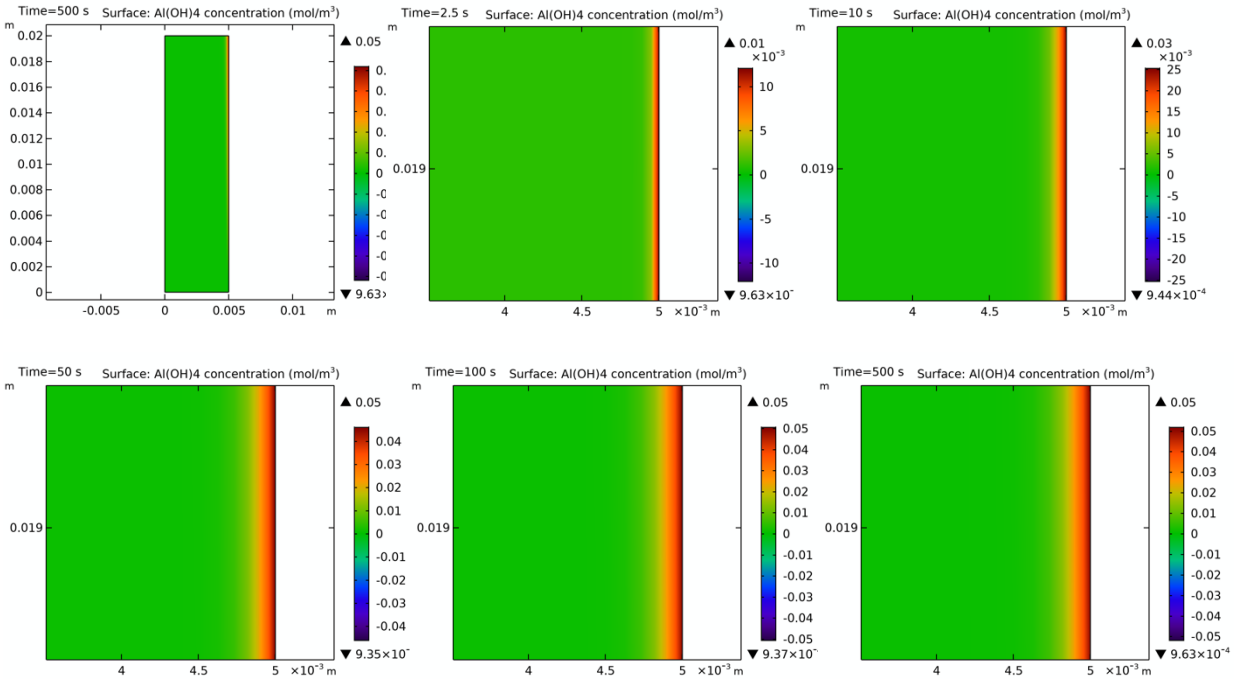

Figure [75]. Concentration of $Al(OH)_4^-$ at positive electrode at times 500, 2.5, 10, 50, 100, 500s.

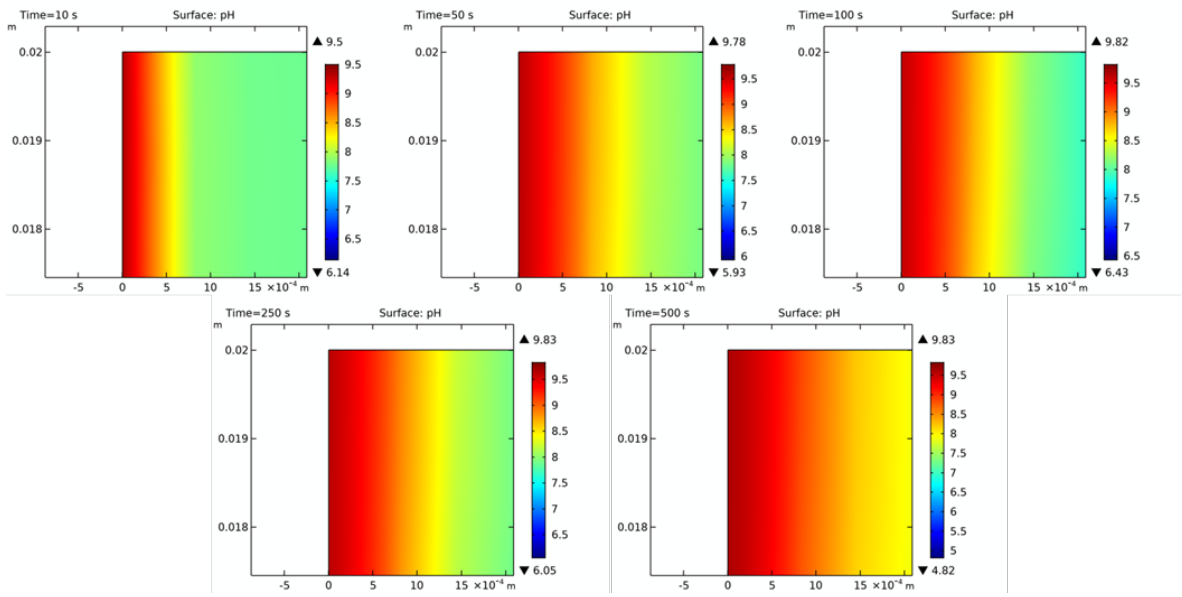

Figure [76]. pH of effluent at the negative electrode at times 10, 50, 100, 250 and 500 sec.

Figure 76 shows the changes in pH with applied current in the effluent at the negative electrode. Initially, at t=0 sec the pH is uniform, at 8.0. After current has been applied for 10 s there is an increase in the pH to 9.5 near the boundary of the negative electrode. The pH decreased from 9.5 adjacent to the surface of the electrode to 8.0 as the distance from the electrode increased. After 50 s the region of increased pH had widened with a maximum pH had increased 9.78 on the boundary of the negative electrode. This region of higher pH continues in all subsequent time slices, as can be seen in Figure 76. The increase in the pH on negative electrode is due to the reduction of water, as given by Rxn 8 resulting in two OH^- ions and $H_{2(gas)}$ being produced at the surface of the electrode.

Al^{3+} Electrode Model in Synthetic produced water

To model the aluminum electrode, current densities have been be determined. For the positive electrode reaction, Rxn 1, the current density is set at 10^{-6} A/m^2 and the negative electrode reaction, Rxn 8, the current density is set at 10^{-4} A/m^2. These values produced a successful model. Both values fall within the range listed by Sawyer et al. (1995) for palladium (10^{-3} A/cm^2) and lead (10^{-12} A/cm^2), which is reasonable given that aluminum is not a noble metal and a better conductor than lead.

The results for the oxidation of the electrode to produce Al^{3+} are shown in Figure 77 at 2.5, 10, 40 and 80 s. Figure 77 shows the concentration of Al^{3+} at 2.5s. At the inlet there is a small length with a parabolic increase in concentration which becomes uniform in thickness over the length of the electrode. Examination of the outlet region, as shown in Figure 77b, shows the concentration of $Al^{3+}$is greatest near the surface of the electrode. Figure 78 shows a decrease in concentration as the distance from the surface increases. At 2.5s there is a very narrow band of Al^{3+} ranging in concentration from a maximum of 0.014 mol/m^3 at the surface of the electrode and decreasing rapidly as distance from the electrode surface increases. The region of Al^{3+} increases, as can be seen in Figures 77 from 2.5s to 80 s. The region of increased Al^{3+} reaches at a steady state at 40s as seen in Figure 77. Figure 78 shows the region of increased Al^{3+} is 0.00011 m thick with a maximum concentration of 0.014 mol/m^3 at 2.5s and 0.001 m thich with a maximum concentration 0.026 mol/m^3 after 80s.

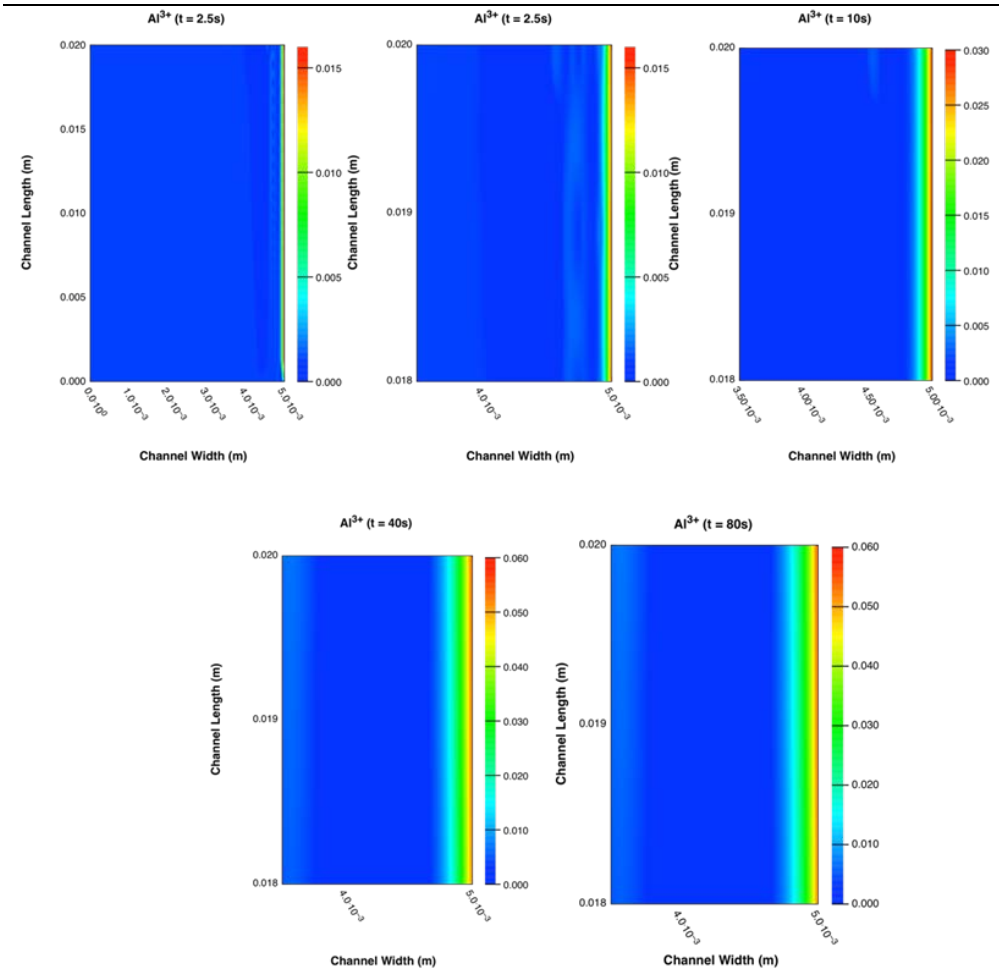

Figure [77]. Al^{3+}concentration at the positive electrode at times 2.5, 2.5, 10, 40 and 80 s.

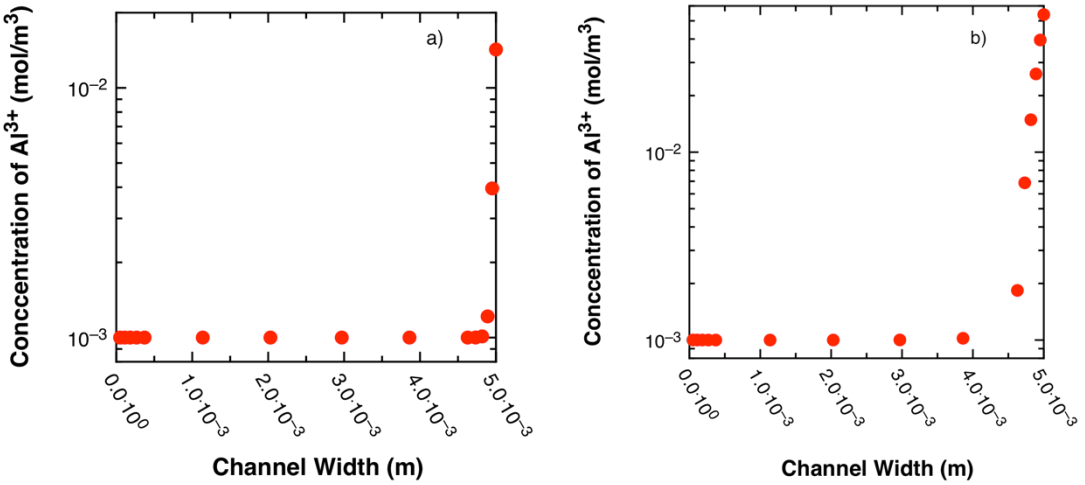

Figure [78]. Concentration of Al^{3+} at outlet for a) 2.5 s b) 80 s.

Figure 79 shows the pH at the negative electrode at different times. Near the inlet there is a small parabolic distance where the pH increases followed by a thin region of uniform thickness where the pH increases along the channel length. After 2.5s the pH in the region adjacent to the electrode surface is more alkaline, increasing from the solution pH of 8 to ~9 then to ~9.5 at 10s. As time progresses the surface pH at the surface electrode increases until a constant value of ~9.7 occurs at 40s. The region of increased alkalinity growths in thickness, as shown at 10s and 40s where it reaches a steady state. At 80s the region of increased alkalinity has not grown in thickness, as seen in Figure 79.

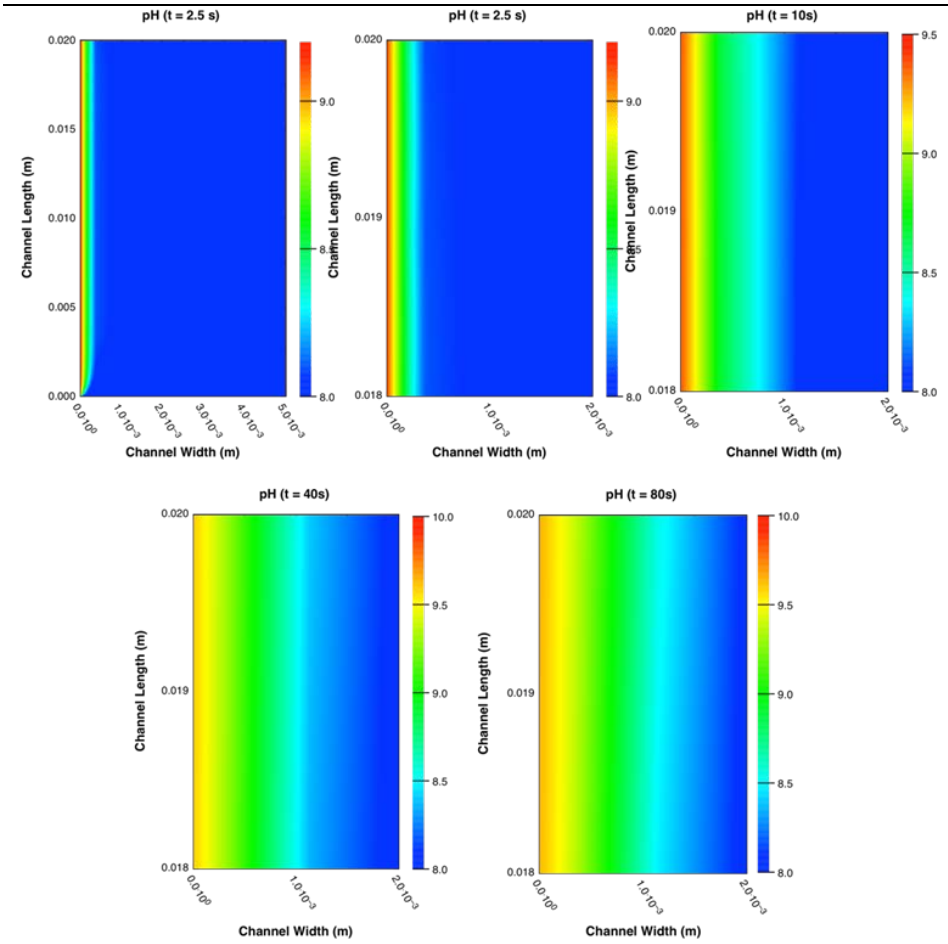

Figure [79]. pH of the effluent at the negative electrode at times 2.5, 2.5, 10, 40 and 80 s

In addition to OH- production at the negative electrode, $H_{2(gas)}$ is also produced. Figure 80 shows the change in concentration of $H_{2(gas)}$ with time. Near the inlet there is a region of parabolic flow . As for the OH^-, there is a very thin region adjacent to the surface of the negative electrode where the gas concentration is high, 6 X 10^{-3} mol/m^3. After 10s, the surface concentration increases to 0.012 mol/m^3 and reaches a steady state value of 0.03 mol/m^3 after 40s. The system is in steady state around the negative electrode for $H_{2(gas)}$ after 40s, given that the steady state region does not increase from 40 to 100s.

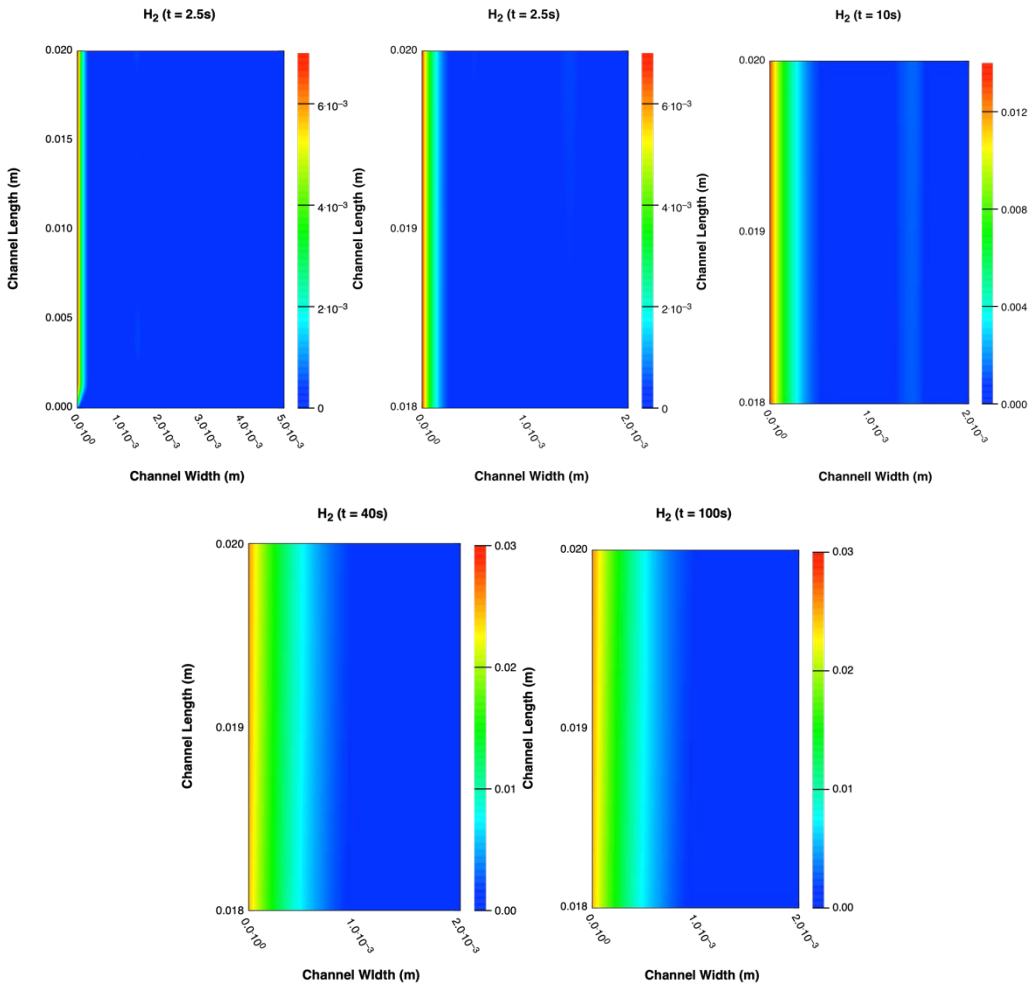

Figure [80]. $H_{2(gas)}$ concentration in the effluent at the negative electrode at times 2.5, 2.5, 10, 40 and 100 s.

Phreeqc modelling uses the concentrations at each node in the electrocoagulation cell to calculate the saturation index (SI) for a given mineral at the node. The SI is an indication of the potential for the mineral to form. A rule of thumb is SI>0.3 indicates that the mineral is oversaturated and has a slight probability to form and SI>1 the solution is supersaturated and has a high probability of forming. The formation of the mineral also depends on kinetics, and this is not considered for this model.

The Thermoddem database contains hundreds of minerals with close to a hundred identified in a Phreeqc output for each node, so it is impractical to consider all of them. A subset of minerals is selected, based on the report of Nightingale et al (2017) where 19 minerals are identified as important to OTSG operation. From these 19 minerals, a subset of 6 minerals is

selected to monitor. Table 13 shows the minerals chosen and their chemical formula. The minerals are an aluminum hydroxide, gibbsite ($Al(OH)_3$), an iron hydroxide ($Fe(OH)_2$), a carbonate (magnesite), chalcedony, a pure silicate (SiO_2), and three aluminosilicate minerals or ferrisilicate minerals. These minerals give an indication of the potential to form aluminosilicate and ferrisilicate minerals which are important to prevent OTSG scaling.

Table 13: Minerals considered in Phreeqc Models

Mineral (Aluminum Electrode)	**Chemical Composition**	**Mineral (Iron Electrode)**	**Chemical Composition**
Gibbsite	$Al(OH)_3$	Fe(OH)2	Fe(OH)2
Magnesite	$MgCO_3$	Chalcedony	SiO_2
Chalcedony	SiO_2	Chrysotile	$Mg_3(Si_2O_5)(OH)_4$
Chrysotile	$Mg_3(Si_2O_5)(OH)_4$	Greenalite	$Fe_3(Si_2O_5)(OH)_4$
Clinochlore	$Mg_5Al(AlSi_3)O_{10}(OH)_8$	Fayalite	Fe_2SiO_4
Laumontite	$Ca(Al_2Si_4)O_{12}:4H_2O$	Forsterite	Mg_2SiO_4

Figure 81 shows the SI for gibbsite with a background SI ~ 1.0. At 2.5s, there is a very thin strip parallel to the positive electrode with a SI for gibbsite of ~2.0. At the negative electrode there is also a thin strip but with the SI <0. This trend continues as time progresses. After 40s the SI for gibbsite is ~3.0 near the positive electrode and near the negative electrode the SI ~-1. The regions of altered SI from the background forms a round ‘v’shape.

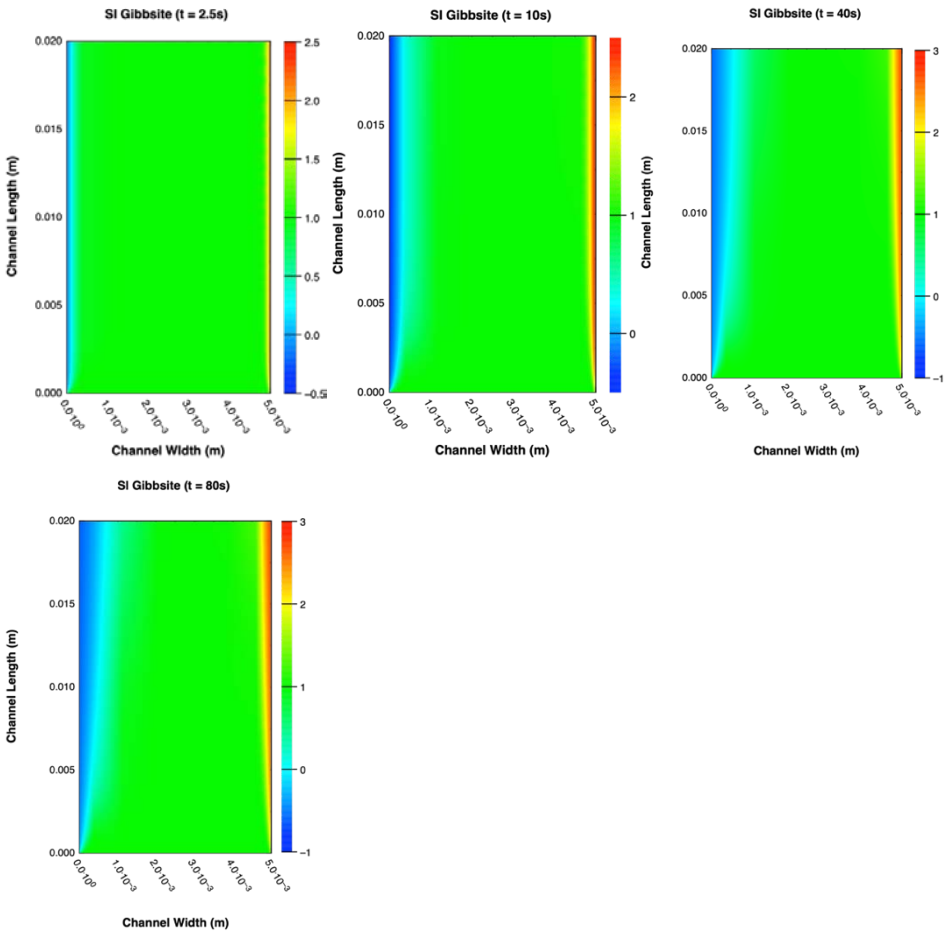

Figure [81]. Saturation Index for gibbsite in the effluent at time 2.5, 10, 40 and 80 s.

Figure 82 shows the SI for magnesite with the background SI ~1.35. At 2.5s a thin band of increased SI forms near the negative electrode with SI~2.2 and decreases as distance from the negative electrode surface increases. As time progresses the region of increased SI for magnesite increases but only in the negative electrode region. The SI in the region adjacent to the negative electrode remains fairly constant at ~2.3. At the positive electrode, there is no change in the SI, i.e. it maintains the background SI ~1.35.

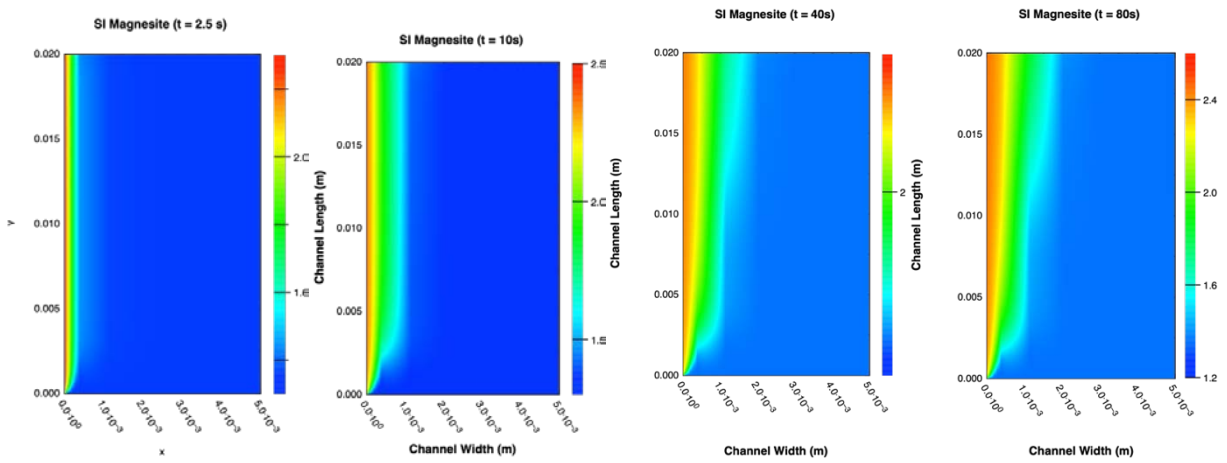

Figure [82]. Saturation Index for magnesite in the effluent at time 2.5, 10, 40 and 80 s.

Figure 83 shows the SI for chalcedony. Initially, the background has a SI ~0.07. After 2.5s there is a region near the negative electrode with a decreased SI, ~0.0. The SI continues to decrease slightly over time while the region of depleted SI increases with time. After 80s the region adjacent to the negative electrode has a SI ~ -0.02. The region of depleted SI has increased and forms a rounded 'v" shape but the maximum area covered reaches its maximum after 10s. After this time the SI in the region slowly decreases over time.

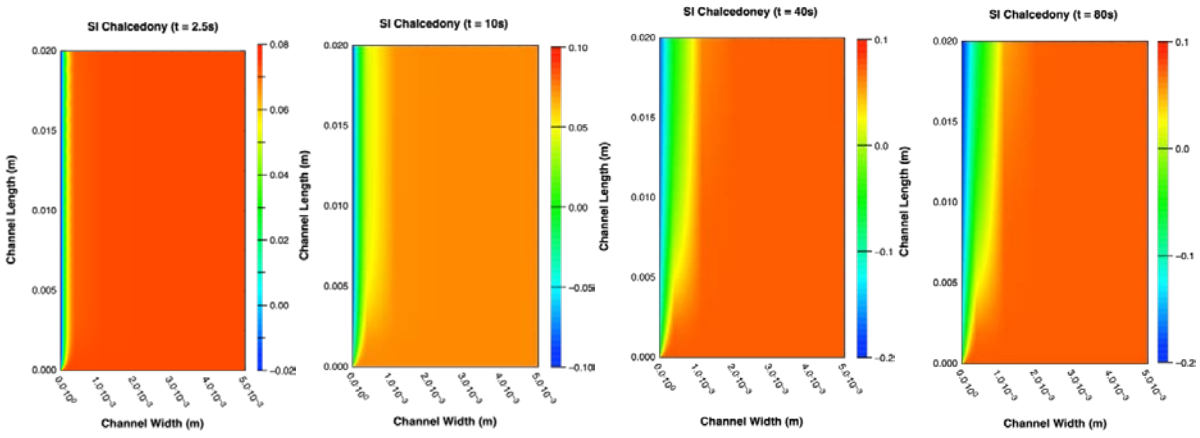

Figure [83]. Saturation Index for chalcedony in the effluent at time 2.5, 10, 40 and 80 s.

The SI for chrysotile is shown in Figure 84 and has a background SI ~-2.5. After 2.5s in the region immediately adjacent to the negative electrode has the SI increase to ~3.3. There is a narrow band of increased SI bordering the negative electrode. As time progressed the SI adjacent to the negative electrode increased to ~4.5 after 10 s and ~5.7 after 40s where it remained constant.

The region of increased SI also increased in area with time becoming stable after 40s. The regions adjacent to the positive electrode saw no changes in the SI, i.e. it remained at background values of SI ~-2.5.

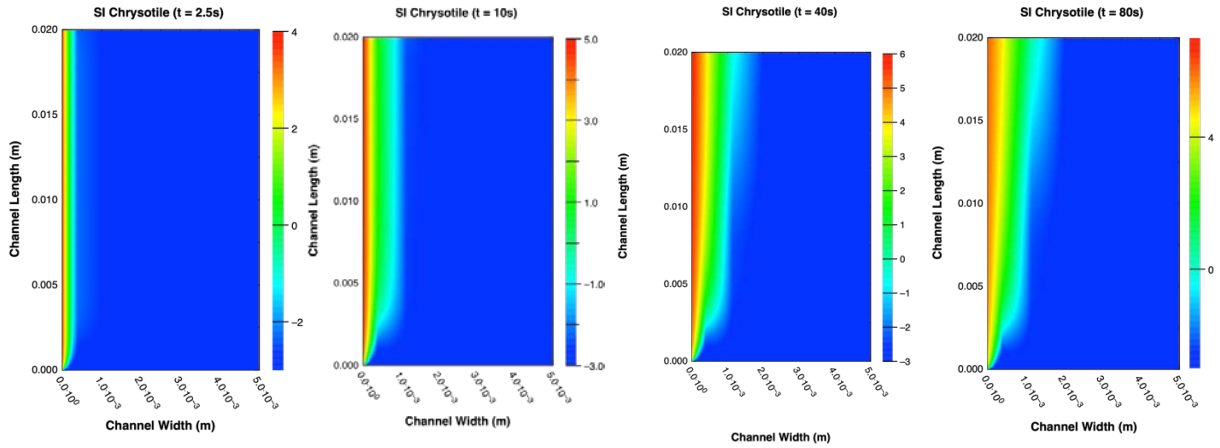

Figure [84]. Saturation Index for chrysotile in the effluent at time 2.5, 10, 40 and 80 s.

The SI for clinochlore is shown in Figure 85 with a background SI ~8.0. After 2.5s immediately adjacent to the negative electrode has a SI ~ 16. A region of decreasing SI is observed as distance from the negative electrode increased, as is observed for chrysotile. After 10s the SI bordering the negative electrode increased to ~18 and to ~19 after 40s and then remained constant. The region of increased SI also increased in size, as can be seen in Figure 81 as time increased from 2.5s to 40s. The region around the positive electrode also had the SI increase with time. After 2.5s the SI increased to ~10 adjacent to the positive electrode. As with the negative electrode, there is a region of increased SI. After 40s the SI adjacent to the positive electrode increased to ~11.3 and remained constant.

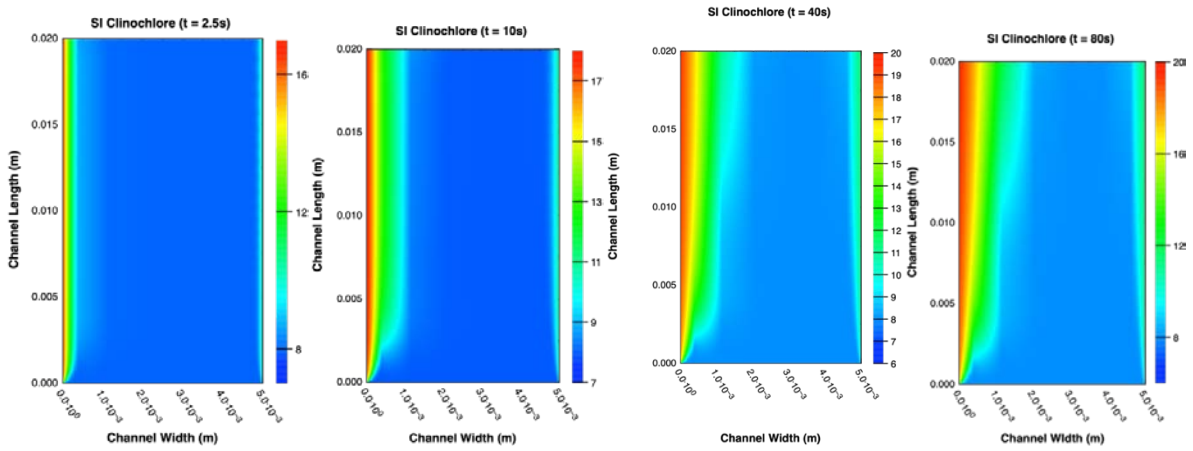

Figure [85]. Saturation Index for clinochlore in the effluent at time 2.5, 10, 40 and 80 s.

SI for laumontite is shown in Figure 86 having a background SI ~5.0. After 2.5s the SI in the region adjacent to both the positive and negative electrodes has changes, increased to a SI ~7.3 for the positive electrode and decreased at the negative electrode to SI ~4.5. As time progressed there is a further small increase in the SI to ~8 adjacent to the positive electrode and ~4.2 neighboring the negative electrode. After 40s a steady state for SI is achieved with SI ~8.4 adjacent to the positive electrode and ~3.9 bordering to the negative electrode.

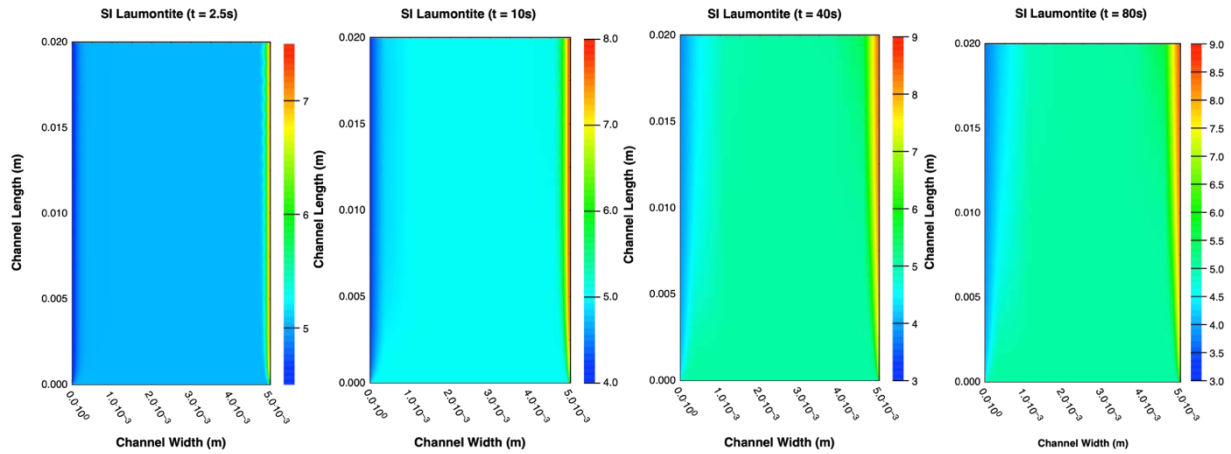

Figure [86]. Saturation Index for laumontite in the effluent at time 2.5, 10, 40 and 80 s.

Near the inlet a parabolic region is observed as the channel length distance increased. This parabolic region is consistent with the no-slip boundary conditions imposed on the system, no flow

at the electrode surface and increasing in a parabolic fashion as distance from the electrode surface increased.

The change in the concentration OH^- (and thus pH) and the $H_{2(gas)}$ produced at the negative electrode are linked since they are the result of the reduction of water. While the $H_{2(gas)}$ has been considered to be inert in the system, OH^- is reactive. The concentration of these products can be changed by adjusting the exchange current density at the negative electrode. This is set at 10^{-4} A/m^2, a value that is obtained by an understanding of exchange current density for different metals and trial and error. The value needs to be lower than platinum, which has an exchange current density of 10^{-3} A/m^2 but larger than lead, 10^{-12} A/m^2. Also it is linked to the exchange current density of the positive electrode, which is set at 10^{-7} A/m^2. Through trial and error, the values that worked the best in the simulation, i.e. did not cause it to crash are the values listed.

The main observation is that for each of the species examined, there is a region where concentration decreases as distance from the electrode surface increases. This region increases with time until a steady state is reached, ranging from 40s for Al^{3+} and $H_{2(gas)}$ and 80s for production of OH^-. In all cases there is a thin region adjacent to the electrode surface with the highest SI, except for the chalcedony where it is the lowest SI. This is a region where diffusion dominated the transport of the produced species given that for a no-slip boundary condition the effluent does not flow. As the species diffuses out a region where fluid flow begins to occur is reached. The produced species is carried down range but continues to diffuse. The combination of fluid flow and diffusion results in the concentration of the produced species increasing until a steady state is achieved. The no slip boundary conditions for fluid flow also creates the rounded 'v' region that was observed for the region of increased SI.

In all the cases examined the many of the potential reactions occur at the negative electrode. This is not unexpected since many of the silicates examined have OH present in their structure. Further, the system will undergo migration due to an electric to a small extent, as can be seen in Figure 87 for Mg^{2+}. Initially, the system had a uniform distribution of Mg^{2+} but under the electric field there is a slight increase in Mg^{2+} at the negative electrode, 8.21 X 10^{-3} mol/m^3. A similar pattern is observed for the other species present, Ca^{2+}, HCO_3^-, Si^{2+} and Na^+. This slight increase along with the increase in OH^- ions, due to reduction of water, results in the higher potential for the silicate products to form, as shown by the more positive SI's. i.e. SI>1 . The one exception is for chalcedony, which has a SI in the equilibrium range, i.e. -0.3<SI<0.3.

In the case of gibbsite, $Al(OH)_3$, the highest potential is at the positive electrode, where Al^{3+} production is occurring, as indicated by the positive SI. At the negative electrode, the SI is negative, indicating that this reaction is not likely to occur. While there is an excess of OH^- present at the negative electrode, the background concentration of Al^{3+} is 10^{-3} mmol/l so the potential of formation is low.

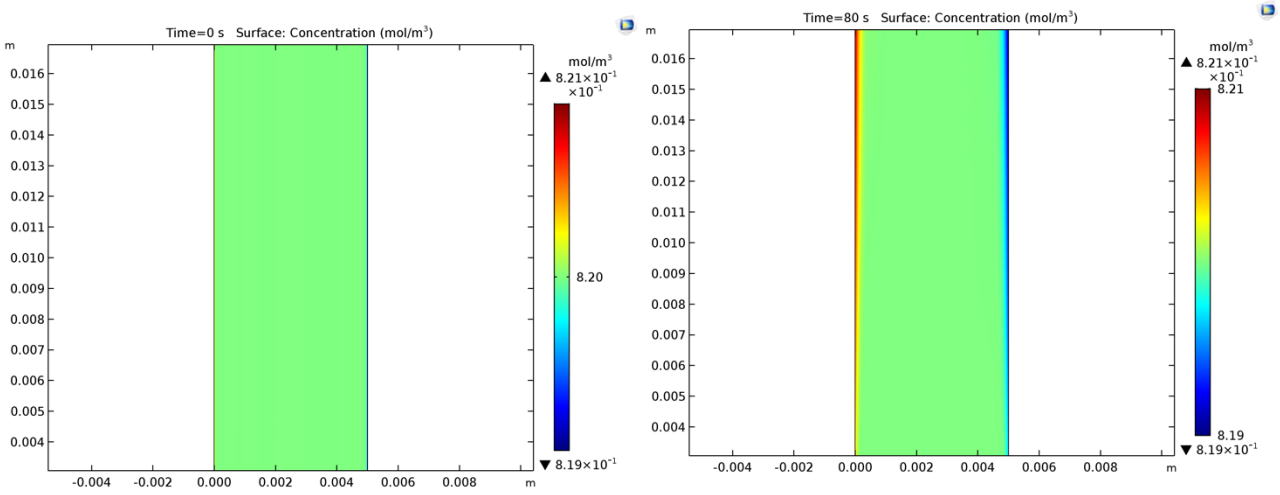

Figure [87]. Concentration of Mg^{2+} at 0 and 100s.

Fe^{2+} Electrode Model in Synthetic produced water

The modeling for the iron electrodes occurred using the same synthetic produced water and similar modeling conditions as for the aluminum electrodes. Figure 88 shows the concentration of Fe^{2+} in the effluent over time. As with the aluminum electrode, there is an increase in the concentration of Fe^{2+} over time at the surface of the positive electrode and the concentration decreases as the distance from the electrode increases. After 2.5s the Fe^{2+} concentration at the surface of the positive electrode is ~0.0165 mol/m^3 and decreases to the background concentration of 10^{-6} mol/m^3. After 10s the concentration at the surface increases to ~0.032 mol/m^3 and ~0.055 mol/m^3 after 40s. The thickness of the region of increasing Fe^{2+} concentration reaches a steady state after 40s, as seen in Figure 88.

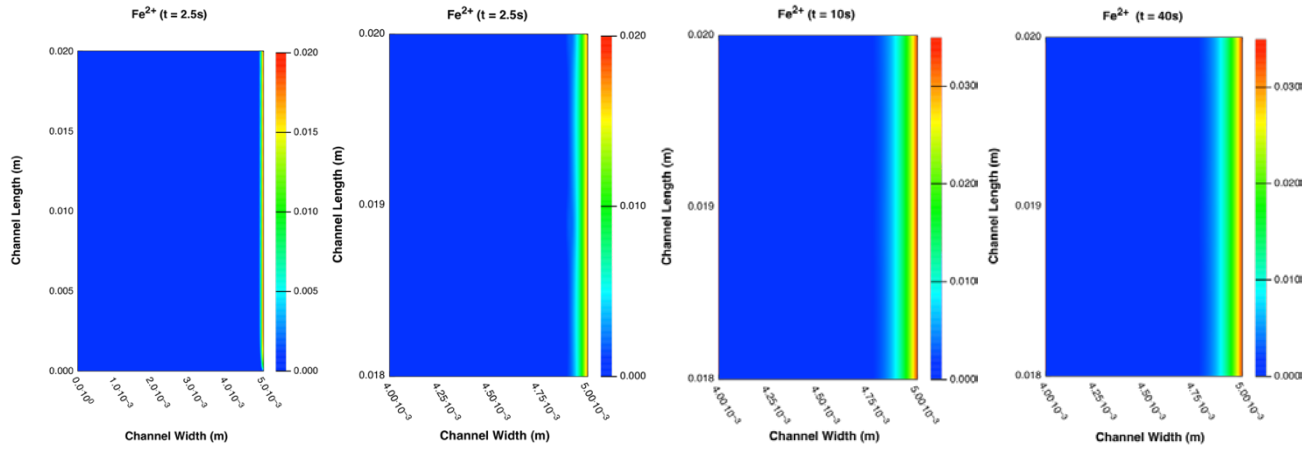

Figure [88]. Fe^{2+}concentration in the effluent at times 2.5, 5, 10 and 40s.

The pH of the effluent is shown in Figure 89. The pH in the bulk solution is 8.0 initially but as current is applied and time passes, the concentration of OH- at the surface of negative electrode increases, as seen by the increase in the pH in Figure 89. The region of increased pH increases with time, going from a very thin region bordering the negative electrode at 2.5s to a very wide, ~1.75 X 10^{-3}m in thickness, at 40s. This region does not increase in thickness after 40s.

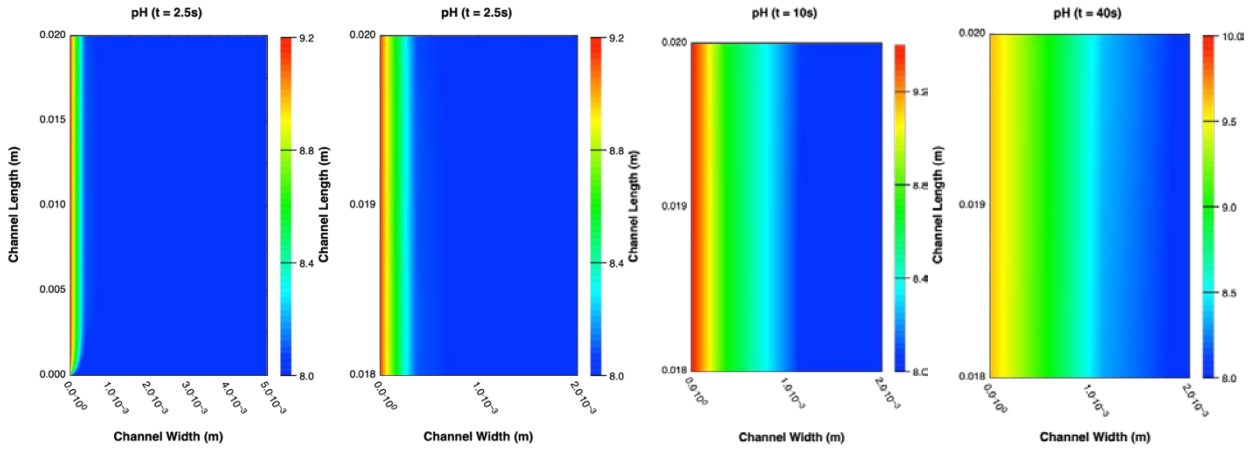

Figure [89]. pH of the effluent at the negative electrode at time 2.5, 2.5, 10 and 40 s.

Figure 90 shows the evolution of $H_{2(gas)}$ at the negative electrode with time. The evolution is very similar to that observed for the aluminum electrode, i.e. initially gas evolution occurs at the surface of the negative electrode with a very narrow region of increased gas concentration. Initially

the background concentration is ~4 X 10^{-7} mol/m^3 and after 2.5s the gas concentration immediately adjacent to the electrode surface is 6 X 10^{-3} mol/m^3. This increases to ~0.016 mol/m^3 after 40 s. The region of increased gas concentration also increases with time.

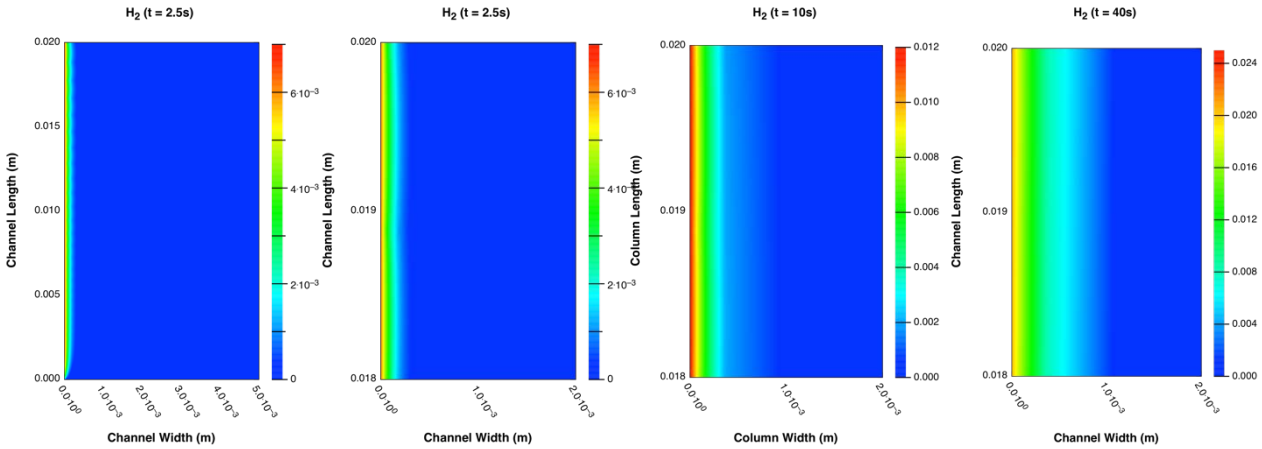

Figure [90]. H_2 concentration at the negative electrode at time 2.5, 2.5, 10 and 40 s.

Figure 91 shows the SI for $Fe(OH)_2$ over time having a background SI for $Fe(OH)_2$ ~-7.5. After 2.5s the SI in region adjacent to the positive electrode increased to ~-4.0. As time progresses, the SI continues to increase to ~-3.1 after 10s and to ~-2.8 after 40s. At the negative electrode there is a similar, but less intense increase in the SI. After 2.5s the SI adjacent to the negative electrode is ~-6.0 and remains constant near that value after 10 and 40s.

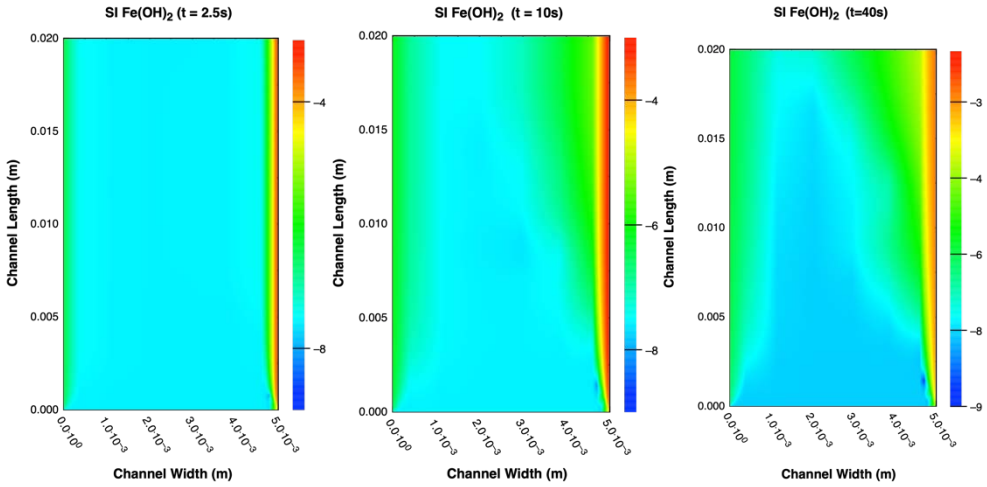

Figure [91]. Saturation Index for $Fe(OH)_2$ in the effluent at time 2.5, 10, 40 and 80 s.

The SI for chalcedony is shown in Figure 92. Initially, the background SI is ~0.07 that slightly decreases to ~-0.02 adjacent to the negative electrode. After 10s the SI is -0.09 bordering the negative electrode and further decreases to ~0.19 after 40s. The region of decreased SI increases in area as time progresses as seen in Figure 93.

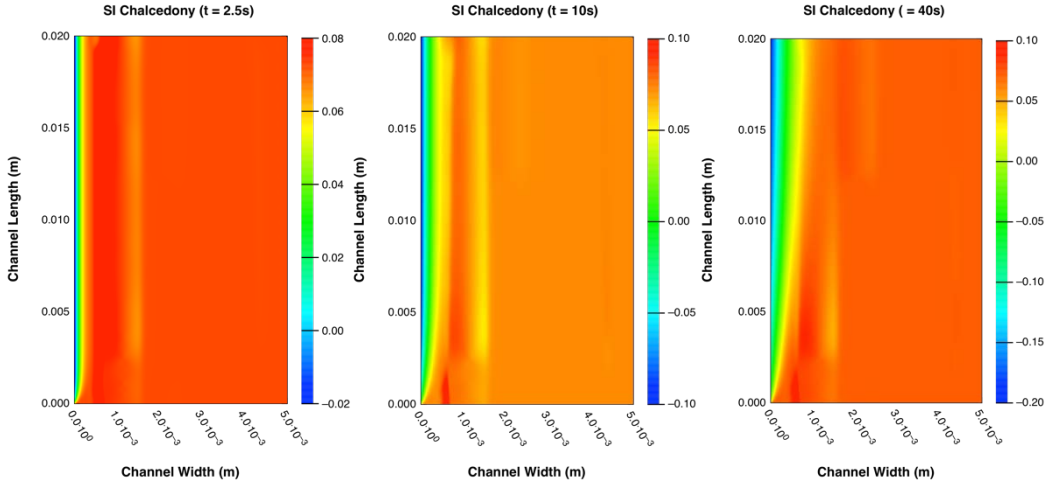

Figure [92]. Saturation Index for chalcedony in the effluent at time 2.5, 10 and 40 s.

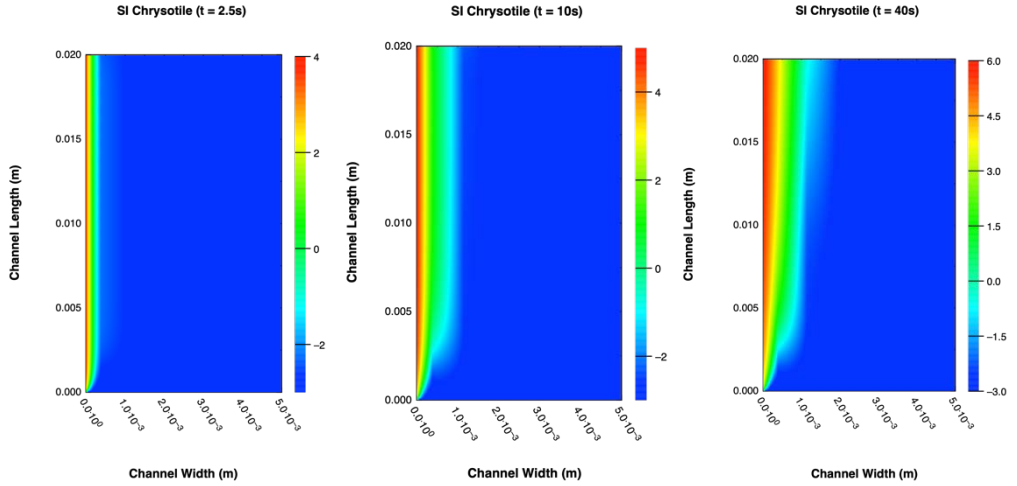

Figure [93]. Saturation Index for chrysotile in the effluent at time 2.5, 10 and 40 s.

Changes in the SI of chrysotile are shown in Figure 93 with a background SI ~-2.8. After 2.5s the SI bordering the negative electrode increases to ~3.3 and ~4.7 and ~5.4 after 10 and 40s respectively. As the distance from the negative electrode increases, the area of the region of increased SI also increases over time, as seen in Figure 93.

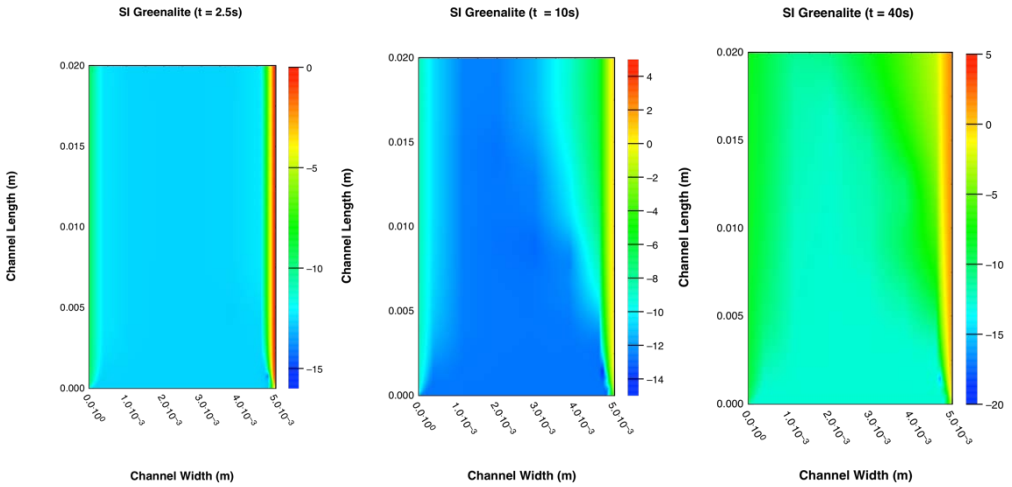

Figure [94]. Saturation Index for greenalite in the effluent at time 2.5, 10 and 40 s.

The background SI of greenalite is ~-12.7 and after 2.5s the SI adjacent to the positive electrode is ~-0.05 and ~-9.4 bordering the negative electrode, as seen in Figure 94. After 10s the SI bordering the negative electrode is ~-8.7 and ~0.84 adjacent to the positive electrode. The SI in the area surrounding the two electrodes also has increased from the initial value. After 40s the SI is ~-8.4 around the negative electrode and adjacent to the positive electrode the SI is ~1.58.

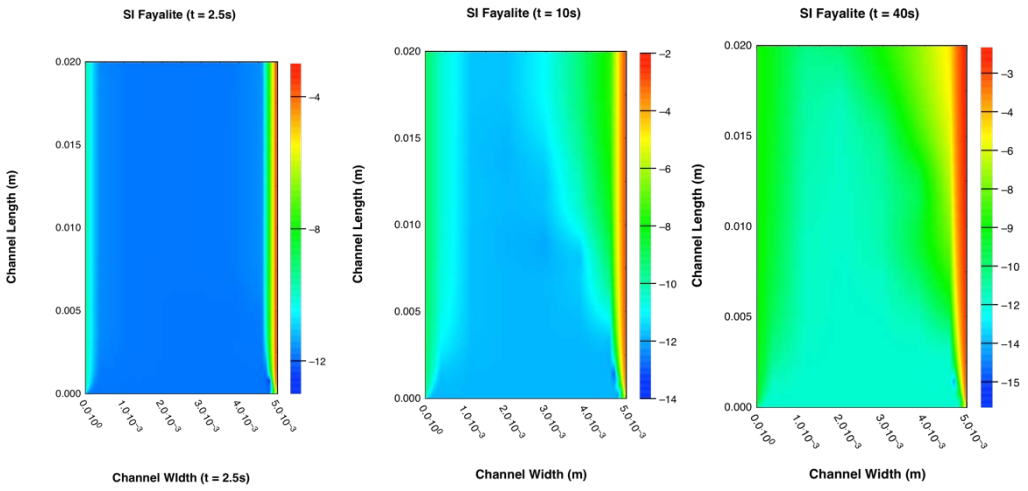

Figure [95]. Saturation Index for fayalite in the effluent at time 2.5, 10 and 40 s.

The changes in SI over time for fayalite are show in Figure 95. Initially, the SI is ~-11.8 and after 2.5s changes in the SI are observed at the positive electrode and to a lesser extent at the

negative electrode. The SI adjacent to the positive electrode is ~-3.4 and ~-9.6 at the negative electrode after 10s and these values remain constant for the remaining times. The area of decreasing SI bordering the positive electrode increase with time while that for the negative electrode appears to reach a maximum after 10s.

Changes in the SI of forsterite with time are shown in Figure 96. Initially, the background SI for forsterite is ~-7.0. After 2.5s the SI adjacent to the negative electrode's surface is ~-3.2, ~-1.7 after 10s and ~-0.8 after 40s. The area of decreasing SI increases with time, as shown in Figure 92.

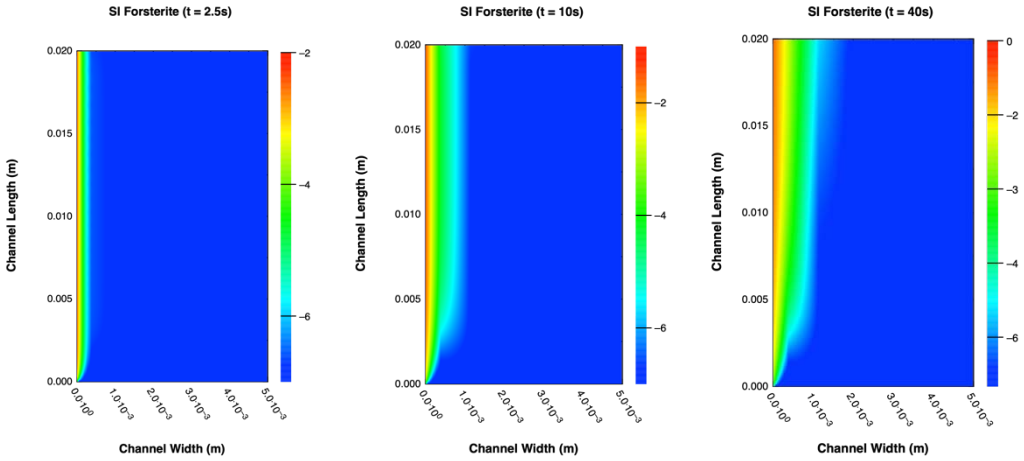

Figure [96]. Saturation Index for forsterite in the effluent at times 2.5, 10 and 40s.

The amount of Fe^{2+} produced mirrored that of the aluminum electrode, i.e. it is produced in a fairly narrow band and did not diffuse much laterally when compared to OH^- or $H_{2(gas)}$. In the case of the iron electrode this has an impact on the potential reactions that can occur. The first species that is impacted is $Fe(OH)_2$, which did not have a positive SI anywhere in the cell. Thus, despite having an alkaline pH, the potential for $Fe(OH)_2$ is very low.

The potential for formation of similar species, e.g. chrysotile ($Mg_3(Si_2O_5)(OH)_4$ and greenalite ($Fe_3(Si_2O_5)(OH)_4$) is more positive. Chrysotile has a positive SI in the region of the negative electrode (SI ~5.4 after 10s). For greenalite, the positive SI occurred around the positive electrode (SI ~0.84 after 10s). The region of formation for greenalite is restricted due to the constrained region where significant iron is present in solution. For chrysotile, Mg^{2+} is present in

large quantity through the solution, with a limiting species being OH^-, which is produced in abundance around the negative electrode. This limitation can be seen in the formation of other silicate species, e.g. diopside ($MgCaSi_2O_6$) and hedenbergite ($FeCaSi_2O_6$). Diopside has the potential to form around the negative electrode with SI ~ 2.0 after 40s. Hedenbergite, which requires iron to form, has negative SI around the positive electrode for all times modelled. Another pair of minerals with similar structure is forsterite (Mg_2SiO_4) and fayalite (Fe_2SiO_4). The SI for fayalite is ~-3.4 after 40s and ~-0.8 for forsterite In this case both silicate species were undersaturated and thus do not have a potential to form despite an excess of the three species.

Al^{3+} Model in Produced water

Models for the produced water have also been conducted for th aluminum electrodes. The model shows that the aluminum and pH are nearly identical to the synthetic produced waters. This is not unexpected since the synthetic produced water is modelled after the produced effluent. Figure 97 shows the Al^{3+} concentration in the cell over time. The evolution of the pattern is similar to that of the synthetic produced water, i.e. initially there is a narrow band adjacent to the positive electrode with a high concentration of Al^{3+}. The thickness of the band grows with time as the effluent flows. The evolution of pH over time is shown in Figure 98. As with the synthetic produced water, the pH, initially at 8.0, increases at the surface of the negative electrode due to the reduction of water to $H_{2(gas)}$ and OH^-. As the reduction continues, the OH^- concentration increases, increasing the pH of the effluent, and migrates laterally due to a combination of diffusion and advection. This continues until a steady state is reached after 40s.

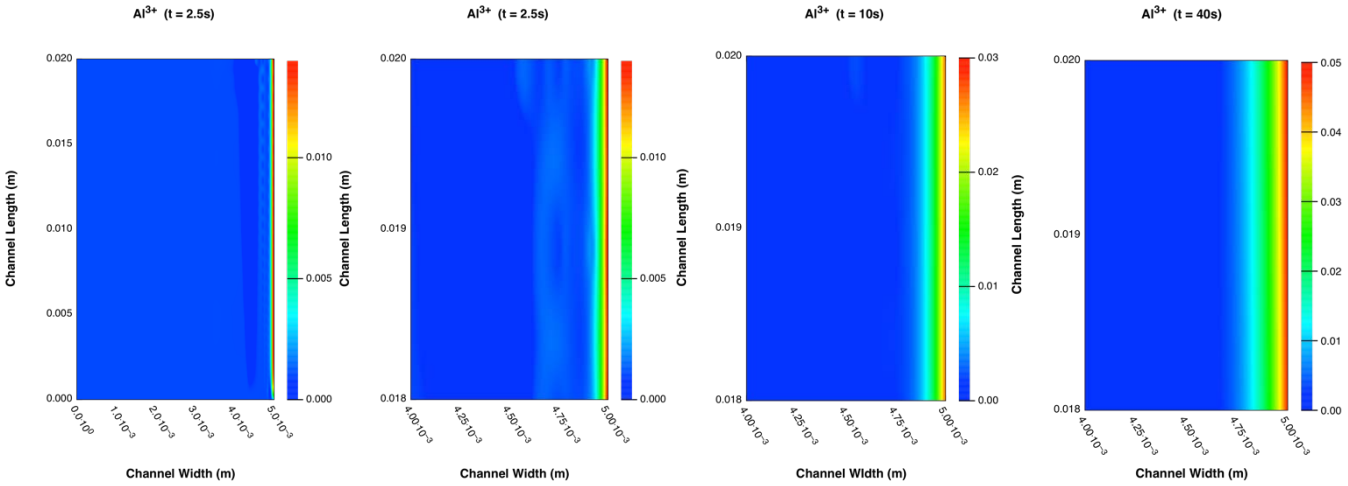

Figure [97]. Al^{3+} concentration in the effluent at the positive electrode times 2.5, 2.5, 10 and 40s

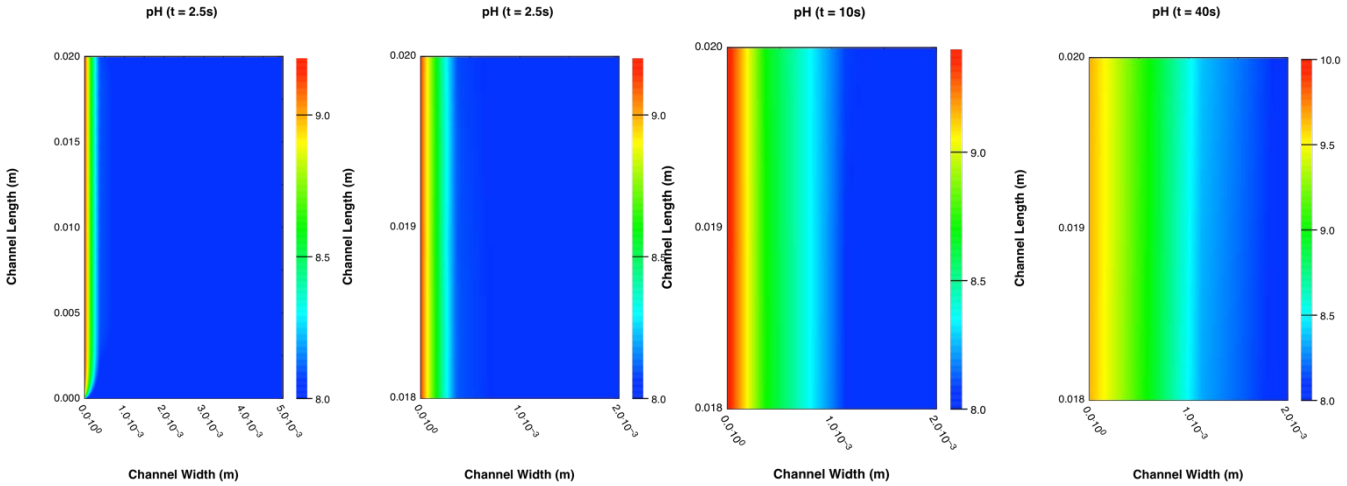

Figure [98]. pH of the effluent at the negative electrode at times 2.5, 2.5, 10 and 40s.

The Phreeqc modelling for the produced water yielded similar results to that of the synthetic produced water. The one difference is in the initial composition of the two effluents, the analysis of the produced water had only cations analysis. This resulted in the anions needing to be added to the effluent to obtain a charge balance. Cl^- is added to make up the charge difference as it is generally an inert ion.

Figure 99 shows the result for gibbsite, $Al(OH)_3$, in solution. This is nearly identical to that for the synthetic produced water, high potential of gibbsite formation near the positive electrode and very low probability of gibbsite formation, as indicated by the negative SI at all times.

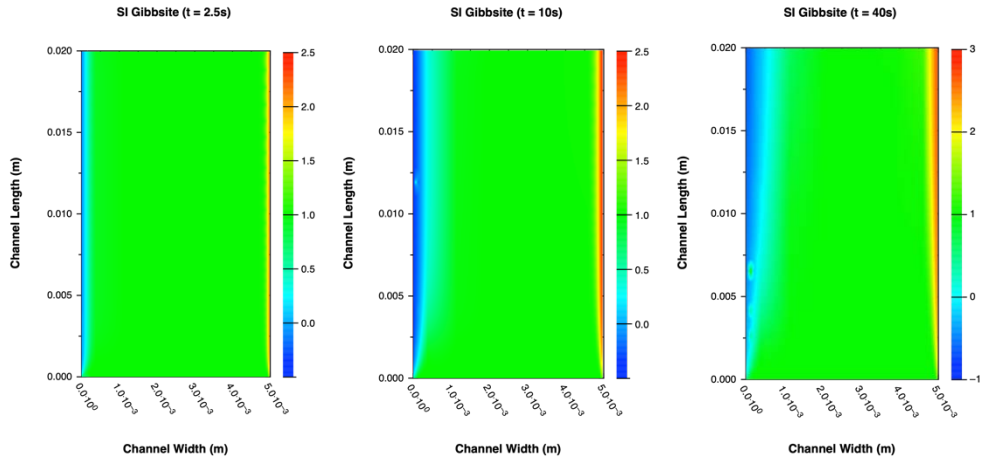

Figure [99]. Saturation Index for gibbsite in the effluent at time 2.5, 10 and 40 s.

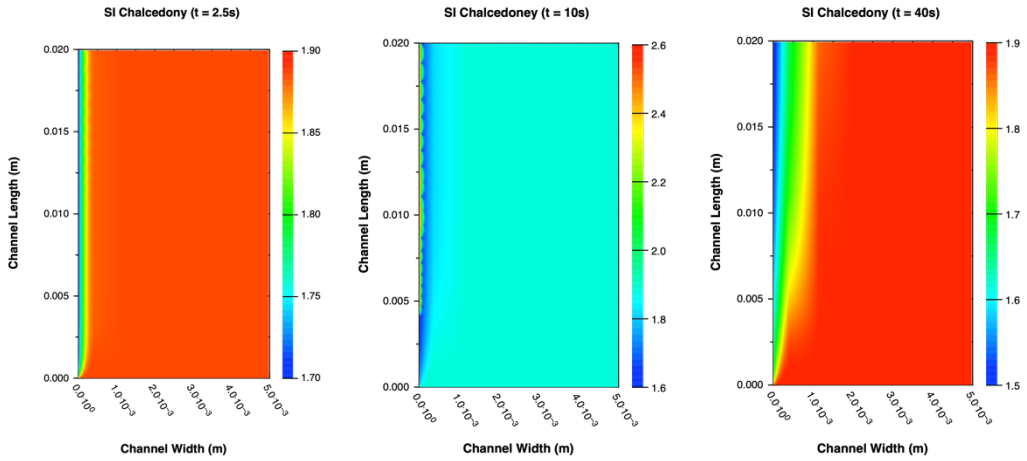

Figure [100]. Saturation Index for chalcedony in the effluent at time 2.5, 10 and 40s.

The evolution of the SI for chalcedony with time is shown in Figure 100. In this case there has been a significant change from the synthetic produced water. In the previous case, the SI for chalcedony were all <0.3, whereas in the produced water, the SI > 1.6 for all time steps. The background SI ~1.9 initially and remains so for all time steps. The SI are lowest adjacent to the negative electrode, ~1.7 for 2.5s and slightly decreasing over time, ~1.6 for 10s and ~1.5 for 40s.

The SI for chrysotile in the produced water is shown in Figure 101. The SI for chrysotile range from ~0 to a high of ~12, which is significantly larger than for the case observed for synthetic produced water which ranges from ~-3 to ~6. While the values of the SI have changes, the shape of the regions of SI higher than the background have not.

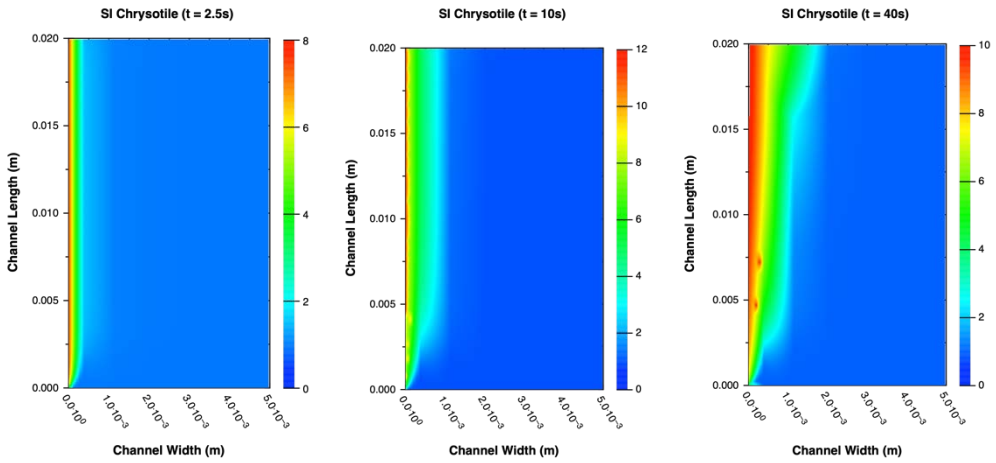

Figure [101]. Saturation Index for chrysotile in the effluent at time 2.5, 10 and 40s.

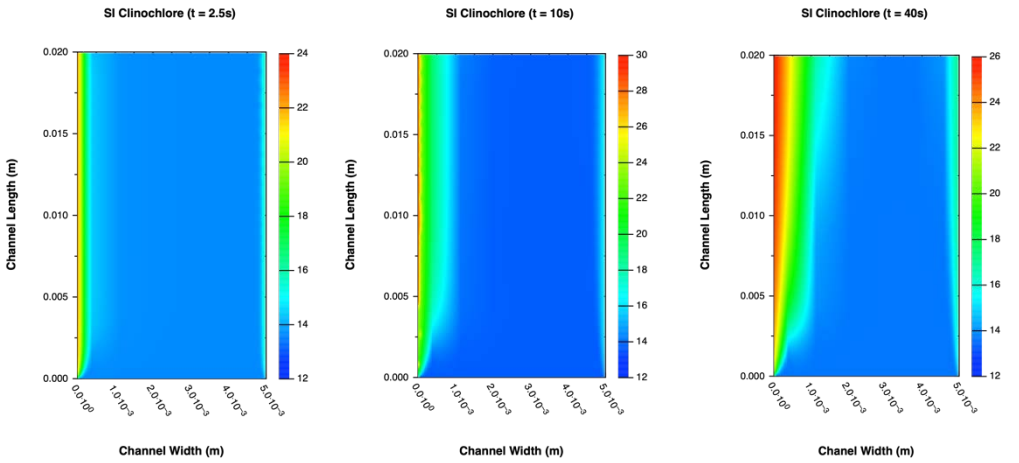

Figure [102]. Saturation Index for clinochlore in the effluent at time 2.5, 10 and 40s.

Figure 102 shows the SI for clinochlore over time. As with other cases, the general shapes of the regions with increased SI are similar to that observed for the synthetic produced water, only the range of the SI have changed, i.e. the SI have increased for each time. The range for the SI in the synthetic produced water is ~+7 to ~+20 whereas for the production brine the range of SI. Is ~+12 to ~+30. The initial SI and background is ~13.5, significantly higher than that of the initial and background SI of ~5.0 for the synthetic produced water.

The SI for laumontite is shown in Figure 103 with an initial and background SI of ~12.3. Again, the shape of the regions of changing SI compared to the background are similar to those found for the synthetic produced water case, i.e. around the negative electrode the SI are lower than the background and around the positive electrode the SI are higher.

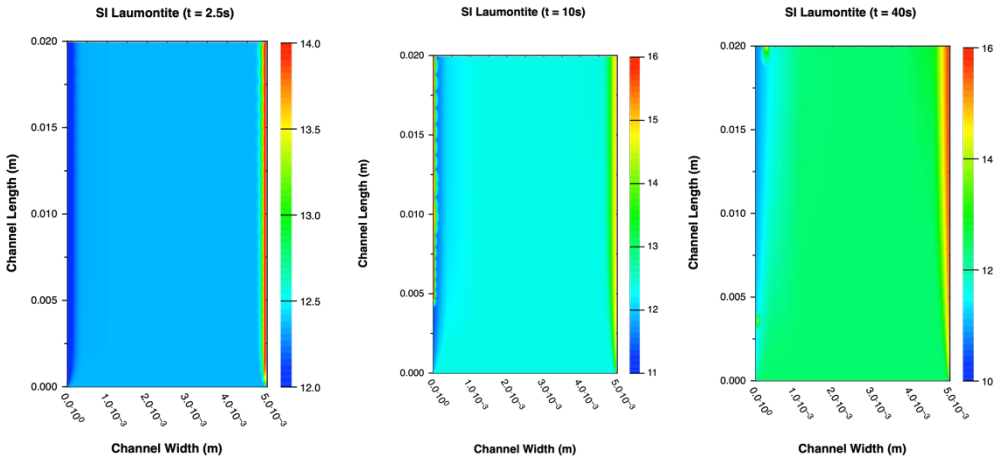

Figure [103]. Saturation Index for laumontite in the effluent at time 2.5, 10 and 40s.

The SI for all of the mineral reactions examined are higher than those for the synthetic brines. The shape of the SI regions is very similar, indicating that the potential for mineral formation in the regions is high. However, there is a difference in the SI, smaller in the synthetic produced water compared to the produced water. When comparing the SI, the larger SI does not mean there is a higher probability of the mineral forming. Equilibrium with the mineral is defined as -0.3<SI<0.3 and SI>0.3 indicate the solution is oversaturated and typically SI>1 indicates the solution is supersaturated.

Consider the SI laumontite at a given cell location, (0.0, 1.073 X 10^{-3}). For the synthetic produced water, the SI is 4.19 and for the produced water the SI is 11.63. According to thermodynamic theory, SI is defined as (Parkhurst and Apello, 2013):

$$SI = log\left[\frac{IAP}{Ksp}\right]$$

Where IAP = ion activity product

Ksp = thermodynamic solubility product

For both cases, the Ksp is identical, log(Ksp) = 11.67 so the difference in the SI is due to the IAP. The IAP's for the solutions are 22.3 and 15.86 for production and synthetic produced waters respectively. This difference is due to the simpler solution chemistry for the produced water versus the synthetic produced water. In the produced water, the only anion given is for SO_4^{2-}, the

solution is charge balanced using Cl^-. The synthetic produced water had an extra anion, HCO_3^-. While this does not seem like a significant difference, the HCO_3^- can be involved in forming other minerals, such as calcite ($CaCO_3$), magnesite ($MgCO_3$) and dolomite ($CaMg(CO_3)_2$). With the potential of forming these minerals, the activity of Ca^{2+} and Mg^{2+} is decreased resulting a lower IAP and thus a lower SI for laumontite. However, the SI for laumontite in the synthetic produced water is still high, 4.19, so it has a strong probability of forming. The SI in the produced water is 11.63 so it to has a strong probability of forming. The difference between the two SI does not represent a difference in the potential, which is high, but rather a difference in the IAP. This comparison indicates why it is important to have as complete water analysis as possible.

Model of H_2 generation at Al^{3+} Positive electrode

At both the positive and negative electrode it is possible to have a number of reactions occurring simultaneously. A recent development found that at the positive electrode a secondary reaction is occurring, in addition to the production of Al^{3+}. Hydrogen is generated via Rxn 7:

$$2H^+ + 2e^- \rightarrow H_2 \qquad (7)$$

It is possible to model the secondary reaction at the positive electrode and results are shown in Figure 104, the concentration of $H_{2(gas)}$ in solution at different times. The rate of the reaction is determined by the Butler Volmer equation, Eqn (v). By varying the secondary current density, the rate of $H_{2(gas)}$ evolution is determined where Figure 104 has i_0 = 10^{-4} A/m^2. By varying $i_{0,}$ the maximum concentration of gas in solution varies, as shown in Table 14. The model found that the varying the current density varies the production rate of $H_{2(gas)}$.

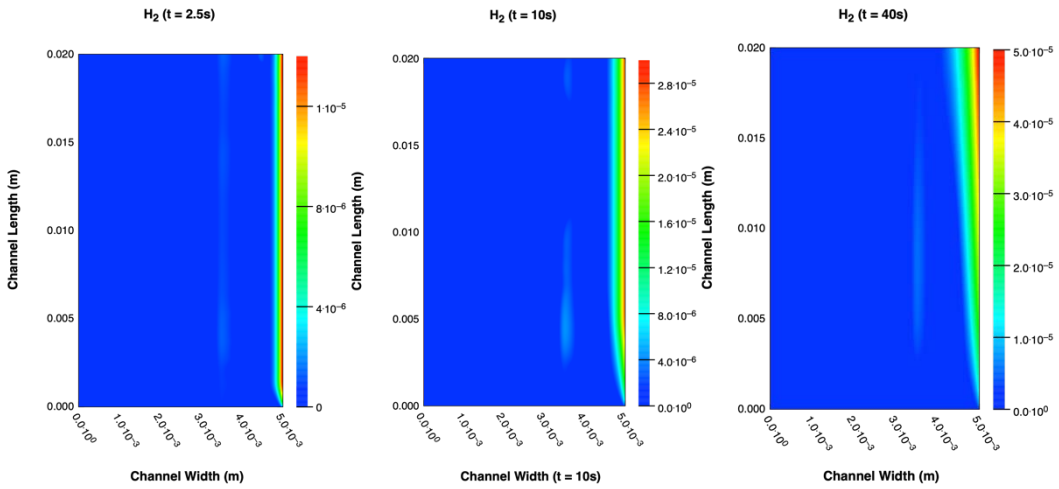

Figure [104]: H_2 generation at the positive electrode, i_0 = 10^{-4} A/m^2

Table 14: Current density and resultant H_2 gas concentration in solution

Current Density (i_0, A/m^2)	Concentration of Gas in Solution (mol/m^3)
10^{-6}	9 X 10^{-7}
10^{-4}	4.9 X 10^{-5}
10^{-2}	4.8 X 10^{-3}

pH at Positive Electrode

Hydrogen gas production did not significantly change the pH of the effluent. Upon closer examination of the system, the significant change in pH would occur with the production of the aluminum hydroxides, i.e. $Al(H_2O)_5(OH)^{2+}$, $Al(H_2O)_4(OH)_2^+$ and $Al(H_2O)_3(OH)_3$.While these species are not formed at the electrochemically at the positive electrode, i.e. Rxns 2-6, they are formed via the following chemical reactions very near the electrode surface:

$$Al^{3+} + 6H_2O \rightarrow Al(H_2O)_6^{3+} \quad (8)$$

$$Al(H_2O)_6^{3+} \rightleftharpoons Al(H_2O)_5(OH)^{2+} + H^+ \quad (9)$$

$$Al(H_2O)_5(OH)^{2+} \rightleftharpoons Al(H_2O)_4(OH)_2^+ + H^+ \quad (10)$$

$$Al(H_2O)_4(OH)_2^+ \rightleftharpoons Al(H_2O)_3(OH)_3 + H^+ \quad (11)$$

As the Al^{3+} is created at the positive electrode, it reacts with the water to form an octahedral ion, $Al(H_2O)_6^{3+}$(Abodi et al., 2012). The $Al(H_2O)_6^{3+}$ ion then undergoes a number of hydrolysis reactions forming the three products, $Al(H_2O)_5(OH)^{2+}$, $Al(H_2O)_4(OH)_2^+$ and $Al(H_2O)_3(OH)_3$ as well as a H^+, resulting in an decrease in the pH around the positive electrode surface (Abodi et al., 2012). The reaction rate constants are given in Table 15.

Table 15: Reaction constants for aluminum hydrolysis reactions

Reaction	k_f	k_r	Ref
$Al(H_2O)_6^{3+} \rightleftharpoons Al(H_2O)_5(OH)^{2+} + H^+$	4.2 X 10^4	4.4 X 10^6	Holmes et al., 1968
$Al(H_2O)_5(OH)^{2+} \rightleftharpoons Al(H_2O)_4(OH)_2^+ + H^+$	4.2 X 10^4	3.6 X 10^6	Foley and Nquyen, 1982
$Al(H_2O)_4(OH)_2^+ \rightleftharpoons Al(H_2O)_3(OH)_3 + H^+$	5.58 X 10^4	2.8 X 10^6	Foley and Nquyen, 1982

The model of the hydrolysis reactions at the positive electrode surface have been carried out using the hydrolysis reactions, Rxns 9 to 11, assuming that the reactions are irreversible. The changes in the pH near the positive electrode surface with time are shown in Figure 105.

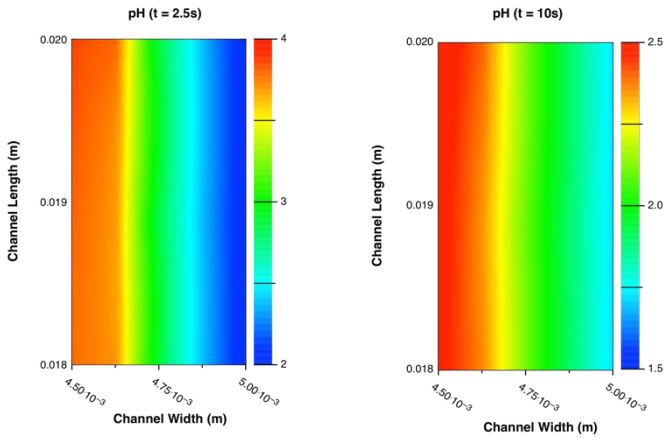

Figure [105]. pH in effluent at 2.5 s and 10s near electrode surface.

The pH at the surface of the electrode decreases very rapidly due to the hydrolysis reactions, Rxns 9 to 11, i.e. the release of the H^+ ion. As time evolves, the pH continues to decrease

due to the hydrolysis reactions with the width of the region decreased pH increasing, as shown in Figure 105 from 2.5s to 10s.

Summary

1. A model has been constructed where Comsol® and Phreeqc have been linked to calculate the saturation indices of minerals indicating regions where potential mineral formation can occur.
2. The pH at the negative and positive electrode surfaces has been successfully modelled in detail. At the positive electrode, the pH decreases with time due to the hydrolysis of $Al(H_2O)_6^{3+}$ to $Al(H_2O)_3(OH)_3$ and H^+. At the negative electrode the reduction of water to $H_{2(gas)}$ and OH^- results in an increase in the pH .
3. Al^{3+} and Fe^{2+} are generated in narrow bands adjacent to the positive electrode. Diffusion and advection do not disperse these cations within the electrocoagulation cell. However reactions may occur downwind of the electrocoagulation system.
4. Calcium and magnesium silicates have a high potential of formation in the region around the negative electrode due to the production of OH^- and due to a high concentration of Ca^{2+} and Mg^{2+} in the effluent.
5. Calcium and magnesium aluminosilicates have a high potential of formation around the positive electrode due to the production of Al^{3+}.The presence of Al^{3+} increases the number of minerals that can form.
6. Iron silicates and iron calcium magnesium silicates have a high potential of formation around the positive electrode.
7. The aluminum electrode gives the largest number of potential minerals when compared to the iron electrode.

References

Abodi, L.C., DeRose,J.A., Van Damme, S., Demeter, A., Suter, T., Deconinck, J., 2012, "Modeling localized aluminum alloy corrosion in chloride solutions under non-equilibrium conditions: Steps towards understanding pitting initiation", Electrochemica Acta, 63, p. 169-178.

Blanc, P., Lassin, A., Piantone, P., Azaroual, M., Jacquemet, N., Fabbri, A., and Gaucher, E. C., **2012**, Thermoddem: "A geochemical database focused on low temperature water/rock interactions and waste materials", Applied Geochemistry, v. 27, p. 2107-2116.

Foley, R.T., and Nguyen, T.H., 1982, "The chemical nature of aluminum corrosion V: Energy transfer in aluminum dissolution", 129(3) p. 464-468.

Hakizimana, J.P., Gourich, B., Chafi, M., Stiriba, Y., Vial, C., Drougi, P. and Naja, J., 2017, "Electrocoagulation process in water treatment: A review of electrocoagulation modeling approaches", Desalination, 404(17), p. 1-21.

Holmes, L.P., Cole, D.L., and Eyring, E.M., 1968, "Kinetics of aluminum ion hydrolysis in dilute solutions", The Journal of Physical Chemistry, 72, p. 301-304.

Lu, J., et al., Modeling of the electrocoagulation process: A study on the mass transfer of electrolysis and hydrolysis products. Chemical Engineering Science, 2017. 165: p. 165-176.

Macdonald, D.D., Real, S and Urquidi-Macdonald, M., 1988, "Evolution of alloy anodes for aluminum-air batteries:: III Mechanism of activation, passivation and hydrogen evolution", Journal of Electrochemical Society, 135(10), -, 2397-2409.

Nightingale, M., Shevalier, M., Humez, P., Osselin, F., Ciszkowski, C., Fagan, R., and Mayer, B., 2017, Boiler Feed Water Limits and Tube Scaling in Once Through Steam Generators, report for COSIA.

Parkhurst, D. L., and Appelo, C. A. J., 2013. Description of input and examples for PHREEQC version 3—a computer program for speciation, batch-reaction, one-dimensional transport, and inverse geochemical calculations. US geological survey techniques and methods, **Book, 6**, 497.

Rumble, J.R., ed., CRC Handbook of Chemistry and Physics, 99th Edition (Internet Version 2018), CRC Press/Taylor & Francis, Boca Raton, FL.

3. RELEVANCE AND IMPACT

The research has demonstrated that EC can offer a new approach for the treatment of in-situ oil sands produced water and blowdown. The application of EC could significantly reduce capital and operating costs of oil-sands operations, as well as reducing environmental impact (through increased water recycle, reduced energy consumption associated with heating of makeup water, and reduced sludge production). The implementation of this technology would increase the attractiveness of new investments in oil sands production. The technology could also be retrofitted to existing operations through blowdown treatment, reducing costs and increasing water recycle.

The target of the treatment process is silica removal, since this is not easily removed by ion exchange processes. While calcium and magnesium removal is slower, they can be removed by ion exchange to enable recycle of the produced water to the once through steam generator. To evaluate the economics of the EC treatment, based on information from Shell / CNRL, the treatment required to reduce the silica concentration by 90% was used. Under these conditions, the partial treatment of calcium and magnesium will reduce the burden on the ion-exchange softening process. A preliminary economic analysis was carried out by estimating the operating cost (CAD) for bench scale EC treatment of synthetic and real produced water using aluminum /or iron electrodes, as shown in Figure 106. The operating costs for electrode replacement and energy consumption were included in the cost estimates. Although the cost of aluminum is significantly higher than iron, the analysis indicates that the use of aluminum has a lower electrical energy cost than iron (as less charge is required) and the overall cost of electrode material and electrical energy were about the same for aluminum and iron. The treatment costs for real produced water were observed to be slightly lower than for the synthetic produced water, due to the higher conductivity of the real produced water which reduced the cell voltage relative to the synthetic produced water.

These treatment costs are low relative to alternative technologies, and although we do not have quantitative figures, it is anticipated that the capital costs of the EC system will also be lower than conventional treatment. Our results also demonstrate that the use of Al-EC would offer a solution with lower capital and operating costs than the more widely used Fe-EC. Fe-EC is more widely used because of the operational challenges of fouling in Al-EC. We have developed novel methods to mitigate the fouling challenges. In addition, investigation of methods to intensify the

treatment process suggest that further reductions in capital and operating costs of 20-50% could be achieved.

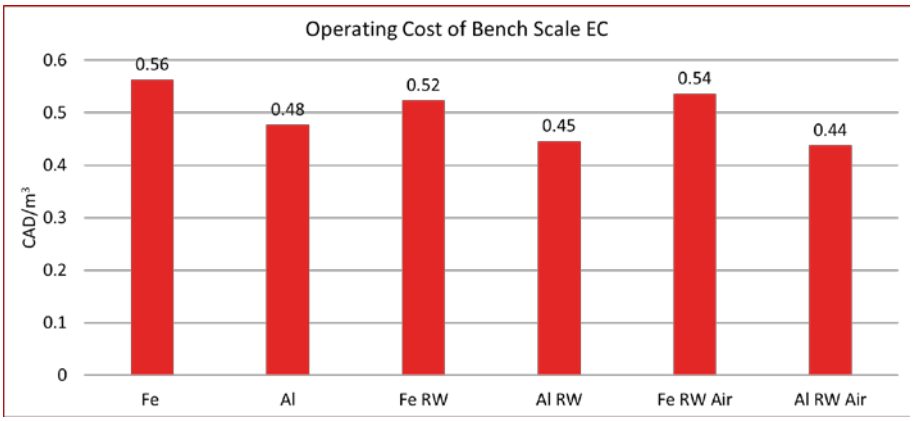

Figure [106] Operating cost of bench scale EC treatment of synthetic and real (RW) produced water by Fe-EC and Al-EC

In addition to reducing treatment costs, EC may enable increased water recycle, reduced consumption of make up water, and reductions in GHG emmissions. t is possible to achieve very low silica concentrations using EC, and this could enable operation of the steam generators at higher steam quality. In addition, treatment and increased recycling of blowdown water should also be possible.

4. OVERALL CONCLUSIONS & NEXT STEPS

The project has demonstrated the potential of the EC process to effectively treat produced water and blowdown. However, detailed techno-economic evaluation has yet to be completed. There also remain significant scientific and fundamental research questions to be answered. The precise nature of the contaminant removal process, the role of flow and transport processes is not fully understood. Further research is on-going funded by an NSERC Strategic Partnership Grant that will help to address these questions. There also remain opportunities to intensify and enhance the process performance that we continue to pursue.

The technology has been evaluated at bench scale, using batch treatment with samples transported to the lab. The next step is to test the technology on-site with continuous treatment using live produced water and blowdown streams. Following on-site testing, scale and pilot scale testing is needed to de-risk the technology and obtain accurate performance and cost data.

The barriers to the these steps will be raising the funding required to pay for these trials. Initially, we plan to apply for an NSERC Idea to Innovation grant that will enable us to perform on-site testing of continuous treatment with live streams of produced water and blowdown.

5. COMMUNICATIONS PLAN:

The findings of the research have been presented at multiple conferences and events (see below). We plan to work with industry stakeholders to perform on site testing, scale up and demonstration of the technology. We are also developing new collaborations with technology companies who can contribute to the implementation of the technology.

6. SCIENTIFIC ACHIEVEMENTS

Journal Papers

1. Paul J.Panikulam, NaelYasri, Edward P.L.Roberts, Electrocoagulation using an oscillating anode for kaolin removal. *Journal of Environmental Chemical Engineering*, Volume 6, Issue 2, April 2018, Pages 2785-2793.

Conferences

1. Tianpei Shu, Behzad Fuladpanjeh-Hojaghan, Nael Yasri, Michael Nightingale, Milana Trifkovic and Edward P.L. Roberts, Performance of Treatment of Oil-Sands Produced Water By Electrocoagulation, Industrial Electrochemistry and Electrochemical Engineering General Session, 233rd Electrochemical Society Meeting, May 2018, Seattle, WA, USA.
2. Tianpei Shu, Behzad Fuladpanjeh-Hojaghan, Nael Yasri, Milana Trifkovic and Edward P.L. Roberts, Electrocoagulation for the Treatment of Oil-Sands Produced Water, World Congress of Congress of Chemical Engineering, Barcleona, Spain, October 2017.
3. Tianpei Shu, Behzad Fuladpanjeh-Hojaghan, Nael Yasri, Michael Nightingale, and Edward P.L. Roberts, Treatment of Oil-Sand Produced Water using Electrocoagulation, 67th Canadian Chemical Engineering Conference, Edmonton, AB, October 2017.
4. B. Fuladpanjeh-Hojaghan, M. Trifkovic, E.P.L. Roberts Visualization of pH Distribution in an Electrocoagulation Cell using Laser Scanning Confocal Microscopy, European Symposium in Electrochemical Eingeering, Prague, Czech Republlic, June 2017.

5. E.P.L. Roberts Development of Electrocoagulation for Oil Sands Water Treatment Applications, , COSIA/AIEES Water Conference, Calgary, AB, March 2016, Keynote presentation.
6. E.P.L. Roberts Electrochemical Treatment of Industrial Wastewater: Challenges & Opportunities, Electrochem 2015, Durham, UK, September 2015, Keynote presentation.
7. Behzad Fuladpanjeh-Hojaghan, Tianpei Shu, Nael Yasri, Milana Trifkovic and Edward P.L. Roberts Removal of Silica from in-Situ Produced Water By Electrocoagulation, AiMES 2018, Cancun, Mexico, September 2018.

Posters

1. Edward Roberts, Nael G. Yasri, Muhammad A. Sabri, Behzad Fuladpanjeh, Tianpei Shu, Milana Trifkovic, Removal of Silica from In-Situ Produced Water by Electrocoagulation, Poster, June 6-8, 2018 COSIA Oil Sands Innovation Summit.
2. Nael Yasri, Aleksandra Goverdarcia, Ishrat Oishee, Rasel Hossain, Edward Roberts, Milana Trifkovic, Sathish Ponnurangam, An Efficient and Low Cost DC Electrocoagulation Technology for Oil Sands Tailings Treatment, Global Petroleum Show, Exhibition organized by North America's Leading Energy Event, Calgary, Canada.

List students or other highly qualified personnel (HQP) being trained as part of this project.

Name HQP name	**Institution Name of institution**	**Level PhD, Masters, etc.**	**Period Insert years**	**Thesis Title/Project If applicable**	**Status Complete, in progress, etc.**
Tianpei Shu	University of Calgary	MSc	2016-2018	Electrocoagulation for produced water treatment	In progress

Behzad Fuladpanjeh-Hojaghan	University of Calgary	PhD	2015-2019	Visualisation of electrocoagulation processes using confocal microscopy	In progress
Muhamed Ashraf Sabri	University of Calgary	PhD	2017 - 2021	Electrocoagulation for applications in the oil sands industry	Withdraw
Muhamed Elsutohy	University of Calgary	Posdoctoral Fellow	2018 - 2020	LSCM of electcoagulation and other electrochemical processes	In progress
Nael Yasri	University of Calgary	Research Associate		N/A	In progress
Michael Nightingale	University of Calgary	Research Associate			In progress
Maurice Shevalier	University of Calgary	Research Associate			In progress
Karen Zhang	University of Calgary	Undergrad.	2017	N/A	Complete (summer internship)